BANGLADESH UNIVERSITY OF ENGINEERING & TECHNOLOGY (BUET), DHAKA
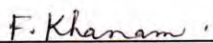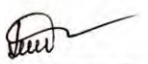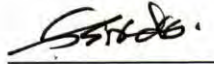**DEPARTMENT OF PHYSICS**

Certification of Thesis work

The thesis titled "SYNTHESIS AND CHARACTERIZATION OF BORON DOPED BISMUTH OXIDE THIN FILM BY SPRAY PYROLYSIS FOR A FUEL CELL APPLICATION" submitted by **Bidhan Chandra Dev**, Roll No-1015142507F, Session: October/2015, has been accepted as satisfactory in partial fulfillment of the requirement for the degree of **Master of Science** (M. Sc.) in Physics on 22 May, 2017.

BOARD OF EXAMINERS

1. **Dr. Jiban Podder (Supervisor)**   Chairman
   Professor
   Department of Physics, BUET, Dhaka

2. **Prof. Fahima Khanam**   Member (Ex-Officio)
   Head
   Department of Physics, BUET, Dhaka

3. **Dr. Md. Abu Hashan Bhuiyan**   Member
   Professor
   Department of Physics, BUET, Dhaka.

4. **Dr. Muhammad Jellur Rahman**   Member
   Assistant Professor
   Department of Physics, BUET, Dhaka.

5. **Dr. Shibendra Sekhar Sikder**   Member (External)
   Professor
   Department of Physics, KUET, Khulna.

CANDIDATE'S DECLARATION

It is hereby declared that this thesis or any part of it has not been submitted elsewhere for the award of any degree or diploma.

Signature of the candidate

Bidhan Chandra Dev

Roll No.: 1015142507F

Session: October/2015

ACKNOWLEDGEMENTS

Abstract

Bismuth oxide (Bi_2O_3) thin films and Boron (B) doped Bismuth oxide thin films with different B concentrations (1.0 at. % ~ 7.0 at. %) have been prepared by spray pyrolysis method on a glass substrate at 350 ^{0}C substrate temperature. The surface morphology, structural, optical and electrical properties of the as-deposited films has been studied in details. The energy dispersive X-ray (EDX) data of the Bi_2O_3 and B doped Bi_2O_3 thin films were taken. From EDX data, atomic weight % of Bismuth and Oxygen in the Bi_2O_3 films is found to be 72.21 at.% and 27.79 at.%, respectively. After B doping, the atomic weight % of boron is increasing on the other hand the atomic percentage of bismuth and oxygen is decreasing.

The Field emission scanning electron microscopy (FESEM) micrographs of the Bi_2O_3 and B doped Bi_2O_3 films have been taken at 350 ^{0}C.The FESEM micrographs of as-deposited films show uniform surface and deposition covers the substrate well. Multigonal or semicircle shaped particles have been observed on the whole substrate of the as-deposited thin films. With Boron concentration the grain size is increasing and after 5 at.% B doped, the surface of the deposited thin films turns into the glassy form. The crystal structure and the crystallite size of the as-deposited Bi_2O_3 and B doped Bi_2O_3 thin films were studied by X-ray diffraction (XRD). From the XRD data it is clear that the Bi_2O_3 and B doped Bi_2O_3 thin films are polycrystalline in nature with mixed phases of monoclinic and tetragonal structures. For pure Bi_2O_3 the crystallite size calculated from (108) plane is found 22.72 nm and for B doping the crystallite size decreases up to 3.0 at.% and then increases. The dislocation density was found for pure Bi_2O_3 is 1.93×10^{-3} line/nm^2 and after B doping the dislocation density increases upto 3.0 at.% and then decreases. The micro strain of the deposited films shows the same nature of dislocation density. The values of inter planer spacing of the thin films are found in good agreement with those adopted in JCPDS card no. 27-1773, 27-0049.

The optical studies were carried out by UV-Vis spectroscopy in the range of 200 to 1100 nm. Various optical constants such as absorption coefficient, extinction coefficient, optical band gap, refractive index and dielectric constant of the films have been measured. The transmittance for pure Bi_2O_3 is found 39% and after 1.0 at.% B doping, the transmittance

drastically decreases but above 1.0 at.% B doping, the transmittance is increased in the visible range (400 - 700) nm. The band gap of the deposited films varies from 3.99 to 3.70 eV. The extinction coefficient and refractive index of the deposited films are increasing with increasing wavelength in the visible range (400 - 700) nm. The dielectric loss of the pure and B doped films shows that the dielectric loss is increasing with increasing wavelength in the visible range to near infrared region (400- 1100) nm.

The electrical studies were carried out using four-probe method. The electrical study of the deposited films confirms that the temperature dependent resistivity of the deposited films is increasing with B doping concentration. The resistivity was found to be of the order of $10^3 \Omega$-m. The activation energy of the deposited films at high temperature (378 - 448) ^{0}K gradually decreases with B doping concentration from 0.2923 eV to 0.2466 eV and at low temperature region the activation energy varies from 0.1655 eV to 0.0447 eV. Form the surface morphology study, we found less porous films and from the electrical study we found that the conductivity of the deposited thin films are decreasing with B doping concentration. This study reveals that B doped Bi_2O_3 thin film could be used in fuel cell applications and other optoelectronic devices more effectively.

CONTENTS   **Page No.**

CHAPTER 1

GENERAL INTRODUCTION   **(2-15)**

CHAPTER 2

THIN FILM DEPOSITION PROCESSES AND ITS FORMATION   **(19-40)**

CHAPTER 3
THIN FILM CHARACTERIZATION TECHNIQUES (43-69)

CHAPTER 4

EXPERIMENTAL DETAILS   **(71-78)**

CHAPTER 5
RESULTS AND DISCUSSION (80-105)

CHAPTER 6
CONCLUSIONS AND SUGGESTIONS FOR FUTURE WORK (108-110)

LIST OF TABLES   **Page No.**

SYMBOLS	LIST OF ABBREVIATIONS
λ	Wavelength
μ	Mobility of charge carrier
θ	Bragg angle
D	Crystallite size
ε	Microstrain
δ	Dislocation density
N	Crystallite per unit area
β	Full width half maximum
A	Absorbance
T	Transmittance
α	Absorption coefficient
n	Refractive index
k	Extinction coefficient
υ	Frequency
h	Plank's constant
ε_r	Real part of dielectric constant
ε_i	Imaginary part of dielectric constant
ρ	Electrical resistivity
σ	Electrical conductivity
k_B	Boltzmann constant
ΔE	Activation energy
t	Thickness
T_s	Substrate temperature

CHAPTER 1

GENERAL INTRODUCTION
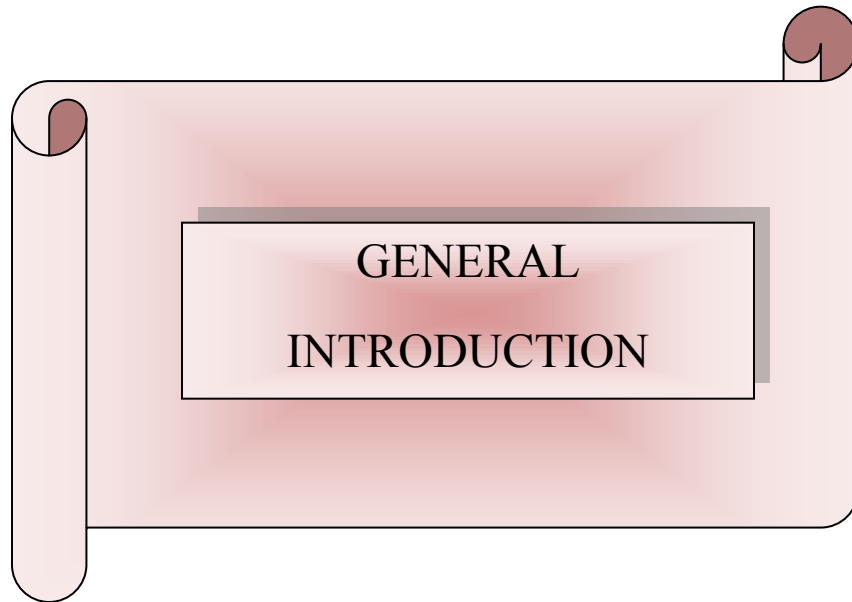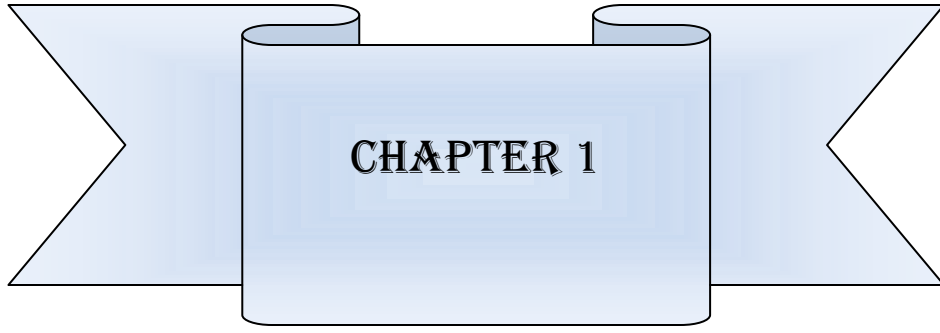
CHAPTER 1
GENERAL INTRODUCTION

1.1 Introduction

In recent years, thin film science has grown world-wide into a major research area. The importance of coatings and the synthesis of new materials for industry have resulted in a tremendous increase of innovative thin film processing technologies. Currently, this development goes hand-in-hand with the explosion of scientific and technological breakthroughs in microelectronics, optics and nanotechnology [1]. A thin film is a layer of material ranging from fractions of a nanometer (monolayer) to several micrometers in thickness. When a thin layer of solid material is formed on a solid substrate and if the layer thickness becomes comparable in magnitude with mean free path of the conduction electrons of solid material then is termed as "thin film". Presently, rapidly changing needs for thin film materials and devices are creating new opportunities for the development of new processes, materials and technologies. The major exploitation of thin film science is still in the field of microelectronics. However, there are growing applications in other areas like thin films for optical and magnetic devices, electrochemistry, protective, and electrolytes for fuel cell, decorative coatings and catalysis. Most features of these thin film activities are represented by a relatively new research area, called surface engineering [2]. Today thin films of metals, semiconductors and dielectric have become an increasing importance for fundamental studies in many fields of science and engineering and are also employed in numerous practical applications. The controlled synthesis of materials as thin films (a process referred to as deposition) is a fundamental step in many applications. Thin film technology is the basis of outstanding development in solid state electronics in modern technology. Experimental work on thin films has been continued in different parts of the world for successful applications of their properties in scientific, engineering and industrial purpose. The increasing demands for microelectronics and micro structural components in different branches of science and technology have greatly expanded the sphere of thin film research [3-4]. Thin film studies have directly or indirectly advanced many new areas of research in solid state physics and chemistry which are based on unique characteristic of the thickness, geometry, and structure of the film [5]. Thin films have very interesting properties that are quite different from those

of the bulk materials which they are made of. As the film become thinner, the surface properties become more important than the bulk. The other cause of interest is the miniaturization of elements such as electronic resistors, the film transistors and capacitors. This is because of the fact that their properties depend on a number of interrelated parameters and also the deposition technique. Thin film may consist of pure material, a composite or a layered structure. Thin film may be thermally stable or unstable. Thin films may also be conductive or non-conductive. Thin films are formed mostly by deposition, either physical or chemical methods. There are some factors which affect the physical, electrical, optical and other properties of a film. The factors are the rate of deposition, the substrate temperature, environment conditions, residual gas and pressure in the system, purity of the material to be deposited [6].

1.2 Characteristics of Thin Films

The thin films are characterized by the thickness, crystalline orientation and multilayer aspects. In addition, uniform crystal structure, nominal stoichoimetry, well oriented crystallites; high film density as well as smooth film surface are necessary properties for high quality thin films. Many factors affect these properties. As for example , the properties of thin film changes significantly when it is cooled to a very low temperature or heated at a higher temperature (above room temperature). This effect of changing properties with temperature provides a better understanding about the properties of thin films. In general the physical properties of thin films depend on a number of factors, such as:

1) The Nature of Substrates

It may be non-crystalline solids e.g., glass of vitreous silica or crystalline such as cleavage plates of rock salt or mica. To select a particular substrate one has to take into consideration of the lattice parameter of the substrate so that it matches to the lattice parameter of the grown film, otherwise structural mismatch may create mechanical fracture in the film. It is also necessary to consider the melting point of the substrate material. It should be comparable with that of the film materials.

2) Substrate Temperature

The temperature of substrate during deposition of film may affect the film properties. At low temperature polycrystalline films with high densities of structural imperfections are formed on both vitreous and crystalline substrate, but at high temperature oriented single crystal films are formed on crystalline substrates.

3) Post- Deposition Annealing of the Films

Heating the film to a higher temperature after deposition and cooling it back to room temperature is known as annealing. Properties of the deposited films are related to the annealing temperature. The post-annealing process removes some defects of the films. It plays an important role in the surface mobility of the atoms.

4) Pressure and Nature of Residual Gas in Deposition Chamber

If the deposition chamber is not evacuated the evaporated atoms cannot reach the surface of the substrate. They interact with the gas molecules within the chamber and scattered inside the chamber. So, sufficient low pressure is necessary for deposition of thin film on substrate.

5) Deposition Rate and Film Thickness

The temperature at which epitaxy occurs is dependent on the deposition rate. Substrate temperature decreases with increasing deposition rate. Film thickness mainly depends on deposition time. If the deposition rate increases, the film thickness also increases having the same deposition time.

6) Temperature of Evaporation Source

If temperature of evaporation source increased uniformly, then the film is likely to be uniform, otherwise it may not be uniform due to sudden increase in temperature.

1.3 Application Area of Thin Films

Thin films are widely used in today''s technology and their applications are expected to be even more widespread in the future. Some application of the thin film in the present time is listed in the table 1.1

Table 1.1: Thin Film Applications

Thin film property category	Typical application
Optical	- Antireflection coatings ("Multicoated Optics"). - Highly reflecting coatings (laser mirrors). - Interference filters. - Beam splitter and thin film polarizers. - Integrated optics - Photosenistive coating of "analog" film for old cameray
Engineering/processing	- Tribological Applications: Protective coatings to reduce wear corrosion and erosion, low lriction coatings. - Hard coatings for cutting tools - Surface passivation - Protection afainst high temperature corrosion - Self-supporting coatings of refractory metals for rocket nozzles, crucibles, pipes. - Decorative coatings - Catalysing coatings
Optoelectronics	- Photo-detectors - Image transmission - Optical memories - LCD/TFT - LED

Electronics	• Passive thin film elements (Resistors, Condensers, Interconnects) • Active thin film elements (Transistors, Diodes) • Integrierted Circuits (VLSI, Very Large Scale Integrated Circuit) • CCD (Charge Coupled Device)
Magnetic Applications	• Audio, video and computer memories • Magnetic read/write heads
Sensor application	• Data acquisition in aggressive environments and media Telemetry • Biological Sensors.
Biomedicine	• Biocompatible implant coatings • Neurological sensors • Claddings for depot pharmacy
Alternative Energies	• Solar collectors and solar cells • Thermal management of architectural glasses and foils • Thermal insulation (metal coated foils)
Cryotechnics	• Superconducting thin films, switches, memories • SQUIDS (Superconducting Quantum Interference Devices)

1.4 Oxide Semiconductors

Oxide semiconductors play an important role in thin film technology. For the preparation of thin film, semiconductor is the key element. The word semiconductor is composed two words-Semi and Conductor. A semiconductor is a material whose electrical resistivity lying between those of an insulator and a conductor. At room temperature this value lies in the range from 10^{-4} Ω-cm to 10^9 Ω-cm. At absolute zero, pure and perfect semiconductors behave like insulators, however, at normal temperatures, in contrasts to metals; semiconductor has a negative temperature co-efficient of resistivity due to the increase in the carrier concentration as the temperature rises. Semiconductors are especially important because varying condition like temperature and impurity content can easily alter their conductivity. Today semiconductor materials widely used in the optoelectronics devices and for their application the search for new semiconductor materials and the improvement of existing materials is an important field of study in materials science. There are different types of semiconductors viz.

- Group IV elemental semiconductors
- Group IV compound semiconductors
- Group VI elemental semiconductors
- III-V semiconductors
- II-VI semiconductors
- I-VII semiconductors
- IV-VI semiconductors
- II-V semiconductors
- Oxides semiconductors
- Magnetic semiconductors etc.

By alloying multiple compounds, some semiconductor materials are tunable. e.g., band gap or lattice constant. Today transition metal oxide is one of the most advanced topics for wide range of device applications. The key components are wide band gap semiconductors, where oxides of different origins play an important role, not only as passive component but also as active component, similar to what is observed in conventional semiconductors like silicon.

The II-VI group compounds semiconductors are very importance due to their applications in various optoelectronics devices. Bismuth oxide (Bi_2O_3) is one of the important transition metal oxides; semiconductors belonging to II-VI group compounds play a significant role in modern solid-state technology due to its physical properties such as band gap, refractive index, dielectric properties, etc. Its band gap varies in the range 2 to 3.96 eV [7]. These properties made it suitable for a wide range of applications such as fuel cell, gas sensor, catalytic materials, optical coatings, photovoltaic cells, microwave integrated circuits [8-10].

1.5 Bismuth Oxide and its Phases

Bismuth oxide has raised much interest for industrial applications over recent years, particularly in the fields of fuel cells and catalysis. The high temperature δ-Bi_2O_3 is the best known oxide ion conductor, with a conductivity of ~1 Ω^{-1} cm^{-1} at 1003 ^0K, approximately two orders of magnitude higher than that of yttria stabilised zirconium, currently the favoured electrolyte in SOFCs. However its use is limited in such devices due to the instability to reduction at the anode.

Bismuth oxide exists as four crystallographic polymorphs [11]. The low temperature α form is monoclinic. It converts at 1002 K into the face-centred cubic δ form, which is stable up to the melting point at 1097 ^0K. On cooling, large thermal hysteresis occurs and the metastable tetragonal β or body-centred cubic γ form can be obtained, depending on the cooling conditions, transforming to the β-phase at 923 ^0K or the γ-phase at 912 ^0K. On cooling, the β-phase transforms to the α-phase at 576 ^0K, and the γ-phase at 773 ^0K, although the γ-phase may persist to room temperature with slow cooling rates. The α-monoclinic and γ-bcc forms are semiconductors, whereas the β-tetragonal and δ-fcc forms are oxide ion conductors, the highest conductivity occurring with the δ-phase.

1.5.1 Properties of Bismuth Oxide (Bi_2O_3)

Bismuth (III) oxide is perhaps the most industrially important compound of bismuth. Bismuth Oxide (Bi_2O_3) is an oxide semiconductor material. Some basic properties of Bi_2O_3 are given below:

❖ Molecular Formula   : Bi_2O_3
❖ Chemical Name   : Bismuth (III) oxide
❖ Molar Mass   : 465.958 g/mol
❖ Color   : White
❖ Odor   : Odorless
❖ Density   : 8.9 g/cm^3
❖ Appearance   : Crystalline solid
❖ Melting Point   : 817 °C
❖ Boiling Point   : 1,890 °C
❖ Solubility in water   : Insoluble
❖ Semiconductor type : n-type
❖ Crystal Structure   : Monoclinic
❖ Refractive index   : 2.5

Bi_2O_3 is an important transition metal oxide. It has excellent thermal stability, good electrical and optical properties. It has also many applications such as catalytic materials, optical coatings, photovoltaic cells, microwave integrated circuits, fuel cells, oxygen sensors and oxygen pumps etc.

1.5.2 Crystal Structure of α-Bi_2O_3

α-Bi_2O_3 has a monoclinic structure and belongs to the $P2_1/C$ space group. In the crystal the bismuth (Bi) atom is coordinated by three oxygen (O) atoms in an approximately square planar configuration is shown in Figure 1. Its lattice parameters a = 5.8499 Å, b = 8.1698 Å , c = 7.5123 Å, β = 112.988˚[12].The structure consists of layers of bismuth ions, parallel to the [100] plane of the monoclinic unit cell, separated by layers of oxide ions, having an ordered defect fluorite structure with one quarter of the oxygen sites vacant[13]. α-Bi_2O_3 has a distorted trigonal bipyramidal structure, where the lone pair of electrons share equatorial positions with two shorter Bi-O bonds, and two larger Bi-O bonds occupy the axial positions.
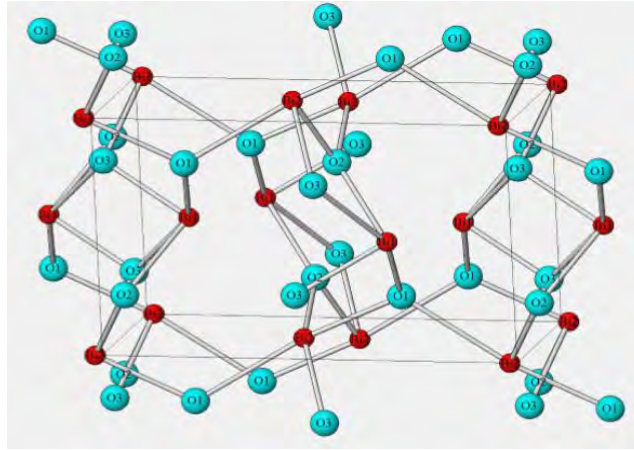
Figure 1: Crystal structure of monoclinic Bi_2O_3

1.6 Properties of Boron

Boron (B) is a metalloid with the atomic number 5. It is the only non-metal in group 13 of the periodic table. B is similar to carbon (C) in its capacity to from stable covalently bonded molecular networks. Amorphous boron contains B_{12} regular icosahedra that are randomly bonded to each other without long range order. Crystalline B is a very hard, black material with a high melting point of above 2000 ^{O}C. It exists in five major polymorphs: α-rhombohedral, β-rhombohedral, β-tetragonal, α-tetragonal, and γ-orthorhombic allotropes. Whereas the β-rhombohedral phase is the most stable and the others are metastable [14]. General properties of B are given below.

❖ Atomic Mass : 10.81
❖ Crystal structure : Rhombohedral
❖ Allotropes : α-, β-rhombohedral, β-, α-tetragonal, and γ- orthorhombic
❖ Appearance : Black-brown
❖ Phase : Solid
❖ Density : 2.08 g-cm^{-3}
❖ Melting point : 2076 ^{o}C
❖ Boiling point : 3927 ^{o}C
❖ Atomic radius : 0.09 nm
❖ Ionic radius : 0.018nm
❖ Electrical resistivity: ~10^6 Ω-m (at 20 ^{o}C)

1.7 A Brief Review of Research Work on Bismuth Oxide Thin Films

Lokhande, C. D. et al. [15] studied the spray pyrolysed bismuth oxide thin films and their characterization. They found mixed phases of monoclinic Bi_2O_3 (predominant), tetragonal β-Bi_2O_3 and nonstiochiometric $Bi_2O_{2.33}$ thin films in XRD data. The surface morphological studies on atomic force micrographs revealed round grain morphology of bismuth oxide crystallites. The films showed direct band gap of 2.90 eV. The electrical resistivity measurements of bismuth oxide films revealed that a semiconducting behavior with the room temperature electrical resistivity of the order of 10^7 Ω-cm. they found n-type electrical conductivity from thermo-emf measurements.

Killedar et al. [16] investigated the Characterization of Spray Deposited Bismuth Oxide Thin Films from Non-Aqueous Medium. They found a well adhered, pin-hole free, uniform yellowish colored film of bismuth oxide. The film thickness was around 0.20 μm. The XRD data revealed that the films were polycrystalline in nature belong to the mixed phases of Bismuth Oxide thin films. They found optical band gap of 2.6 eV. They also found electrical resistivity of the order of 10^6 ohm-cm; and electron carrier concentration and mobility are of the order of 3.8×10^{19} cm^3 and 1.5×10^{-4} cm^2 $V^{-1}s^{-1}$, respectively.

Mallahi et al. [17] Prepared Bismuth oxide nanoparticles via sol-gel method. They prepared homogeneous bismuth oxide nanopowders by sol gel method. The single α-phase was obtained at a temperature lower than that prepared by conventional solid state method. The average size of these nanoparticles ranges was less than 20 nm.

Tezel et al. [18] studied that the Synthesis, surface tension, optical and dielectric properties of bismuth oxide thin film by CBD technique. They found non stoichiometric $Bi_2O_{2.75}$ in XRD analysis. They investigated the grain size (D), dislocation density (δ) and numbers of crystallites per unit area (N), i.e. structural properties of the thin film were determined as16 nm, 39.06×10^{-4} line/nm^2, and 31.25×10^{-3} 1/nm^2, respectively. The optical band gap (Eg) for direct transitions, optical transmission (T %), reflectivity (R %), absorption, refractive index (nr), extinction coefficient (k), dielectric constant of the thin film were found to be 3.77 eV, 25.23 %, 32.25 %, 0.59, 3.62, 0.04 and 2.80, respectively. The thickness of the film was measured by AFM, and was found to be 128 nm.

Behzad et al. [19] studied α-Bismuth (III) oxide catalyzed Biginelli reactions using experimentally designed optimized condition by hydrothermal method. The Synthesized material was characterized by X-ray powder diffraction (XRPD) technique and α-Bi_2O_3 was obtained with small fractions of β-Bi_2O_3. The FE-SEM images showed that the obtained material were multigonal structures in micron dimensions. The optical band gap of Bi_2O_3 was about 4.2 eV.

Ubale et al. [20] studied that the Structural, electrical and optical properties of nanostructured Cu doped Bi_2O_3 thin films deposited by chemical spray pyrolysis technique at 573 K .They investigated that the deposited Cu doped Bi_2O_3 thin films were nanocrystalline in nature with monoclinic and tetragonal lattice. They found that the band gap of the spray deposited Cu doped Bi_2O_3 thin film were 3.1 eV. The electrical resistivity of the Cu doped Bi_2O_3 thin films was of the order of 10^6 Ω-cm. The thermo-emf measurement reveled that n-type conductivity of Cu doped Bi_2O_3 thin films.

Gujar et al. [21] prepared Bismuth oxide thin films by chemical bath deposition (CBD) method: annealing effect. X-ray diffraction patterns revealed that after annealing a non-stoichiometric phase, $Bi_2O_{2.33}$, was removed and pure phase monoclinic Bi_2O_3 was obtained. SEM revealed that Bi_2O_3 was rod-like structure. The optical studies revealed that the band gap decreases by 0.3 eV after annealing. The electrical resistivity variation revealed that semiconductor behavior and from thermo-emf measurements, the electrical conductivity was found to be of n-type.

Gopinath et al. [22] investigated that Influence of Zn doping on nanostructured Bi_2O_3 thin films by spray pyrolysis technique. They found that the deposited film was β-phase tetragonal structure with polycrystalline nature. The grain size was calculated to be around 30 to 40 nm. They found that annealing effect improves the crystallinity and reduces the defect present in the film. They were seen that the surface was like nanoflake, upon annealing an even nanoflake was seen on the film. The optical band gap of the film was found to be 3.25 eV and on annealing the band gap decreases to 2.8eV.They found that the transmittance was varies between 30 % - 35% for as deposited film and 20% - 28% for annealed film. The electrical studies revealed that the semiconducting nature of the film. They also found that the resistance of the annealed film was more than the resistance of the as deposited film.

Patil et al. [23] investigated that the Effect of chopping on the properties of bismuth oxide thin films by thermal oxidation. They found polycrystalline and multiphase bismuth oxide thin films in XRD analysis. They showed at all oxidation temperatures, monoclinic Bi_2O_3 was predominant. They found high transmittance of the deposited thin films in the visible range. The direct band gap of the films obtained was between 2.78 eV and 3.04 eV. The refractive index observed was in the range 1.934 to 2.096.

Waisy et al. [24] studied that the Synthesis of Bi and Bi_2O_3 Polymorphous Structure Using RPLD Method. They employed different laser fluence ranged from (1.8 J/cm^2- 9.8 J/cm^2) to investigated the physical properties. X –Ray diffraction result revealed that the prepared films was monoclinic, tetragonal, and nonstiochiometric phases beside bismuth, while the atomic force microscopic result showed grain size ranged from (33.48nm -131.6 nm) with different laser fluence. They found optical band varies from (1.2-2.9 eV).

Gujar et al. [25] studied the Formation of highly textured (1 1 1) Bi_2O_3 films by anodization of electrodeposited bismuth films. They found uniform and adherent Bi_2O_3 thin films. The X-ray diffraction pattern reveled that Bi_2O_3 films were highly textured along (1 1 1) plane. The room temperature electrical resistivity of the Bi_2O_3 films was 10^5 Ω-cm. Dielectric measurement revealed normal oxide behavior with frequency.

Hicham et al. [26] investigated the Synthesis, characterization and photocatalytic activity of α-Bi_2O_3 nanoparticles from a mixture of oxalate complexes of bismuth $Bi(C_2O_4)OH$ and $Bi_2(C_2O_4)_3 \cdot xH_2O$ obtained by a direct solid-state reaction between a nitrate salt of bismuth and oxalic acid. They found monoclinic structure of Bi_2O_3 with the linear parameters $a = 5.8499$Å, $b = 8.1698$Å, and $c = 7.5123$Å. The crystallite sizes are found in the range of 120 to 170 nm. From the TEM results they found average crystallite size is about 140 nm.

1.8 Aim of the Present Work

The objectives of the present study are to synthesize Bi_2O_3 and Bi_2O_3:B thin films by locally fabricated SP system and to Characterize those thin films by using various experimental techniques. The effect of substrate temperature and dopant concentration on the structural, optical and electrical properties of the thin films is to be studied elaborately. Because the quality of thin films can be controlled by controlling these parameters, the thin films from aqueous solutions might have great advantages on economy and capacity of large area deposition. It is expected that optically transparent and homogeneous thin films can be synthesized by using this low cost technique. These thin films may have expected electrical and optical properties to find applications in sensors, electronic and optoelectronic devices, etc.

1. To synthesize Bi_2O_3: B thin films with different B concentrations.
2. To study the surface morphology of the deposited thin films is to be studied by scanning electron microscopy Field emission SEM (FESEM).
3. To estimate the elemental composition of the prepared thin films by the energy dispersive X-ray (EDX) analysis.
4. To analyze the structure of the deposited films by XRD.
5. To determine transmittance, absorbance, optical absorption coefficient, optical band gap, refractive index, dielectric constants etc. from UV-visible spectroscopy.
6. To measure DC electrical conductivity by liner four point probe method.
7. To calculate activation energies of carriers for electrical conduction of the deposited thin films.

These finding will add new knowledge in spray pyrolyzed Bi_2O_3 and Bi_2O_3: B thin films, which may indicate some suitable application of these materials in the electrical and optoelectronic devices.
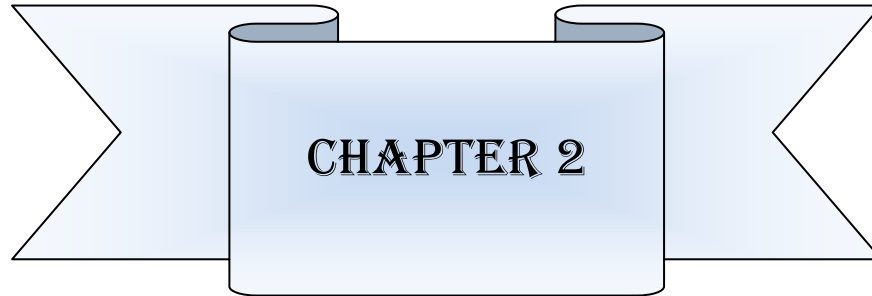
1.9 Outline of This Thesis

This thesis contains six chapters. The general introduction of the thin films and materials with relevant literature survey is given in ***Chapter 01.***Various thin film deposition processes and its formation are discussed in ***Chapter 02***.The theoretical principle of thin film characterization and film thickness measurement are discussed in ***Chapter 03.*** In ***Chapter 04***, the fabrication steps of Bi_2O_3: B thin films by spray pyrolysis technique have been given. Experimental results and their possible discussions are presented in ***Chapter 05.*** Finally the Conclusions of the present work and Suggestion for Future Work are discussed in ***Chapter 06.***
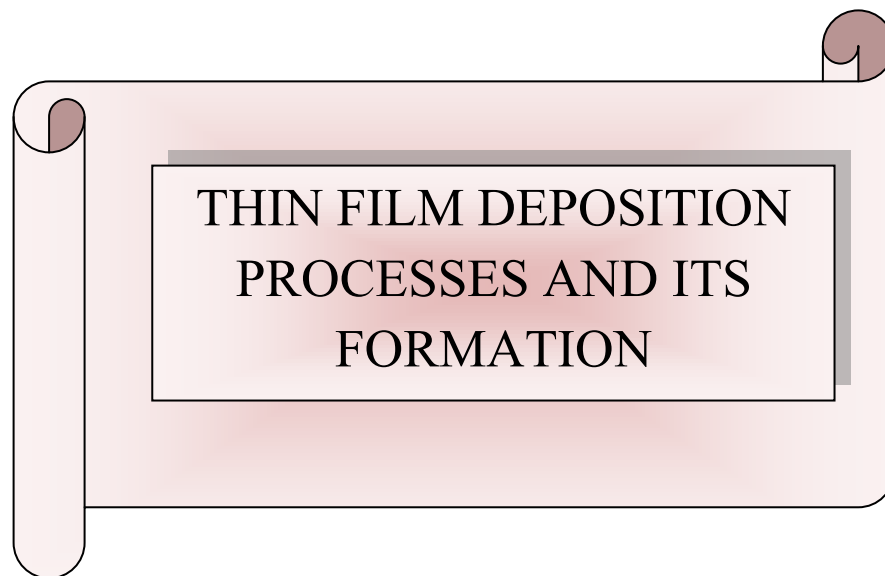
References

[1] Siegel, R. W., Hu, E. H., Roco, W. C., " WTEC Panel Report on R & D Status and Trends in Nanoparticles", J. Nanostructured. Mate, Nanodevices, Workshop, 1997.

[2] Surface Engineering, Science and Technology I, Editors : A. Kumar, Y.-W. Chung, J. J. Moore, J. E. Smugeresky, The Minerals, Metals &Materials Society, Warrendale, 1999.

[3] Kumar, A., Chung, Y. W., Moore, J. J., and Smugeresky, J. E., "Surface Engineering Science and Technology", The Minerals, Metals & Materials Society, Warrendale , 1999.

[4] Gloker, D. A., and Shah, S. I., "Hand Book of thin film process Technology", Instute of Physics Publishing, Bristol and Philadelphia, 1998.

[5] West, A. R., "Solid State Chemistry", John Willey and Sons, Singapore, 2003.

[6] Perednis, D., and Gauckler, L. J., "Thin film deposition using spray pyrolysis", J. Electroceram., Vol. 14, pp. 103-111, 2005.

[7] Hu, Y., Zhou, X., Cao, Q., and Hunag, "Metal Oxide Gas Sensors: Sensitivity and Influencing Factors", Mater. Sci. Eng. B., Vol. 99, pp. 41, 2003.

[8] Fu, J. J., "Optical and phonon properties of Sm-doped α-Bi_2O_3 micro rods", Mater. Sci. Lett., Vol. 16, pp. 1433, 1997.

[9] George, J. B., Pradeep, K. S., Josep, "Preparation of heat mirrors using bismuth oxide films", Phys. Stat. Sol (a). Vol. 100, pp. 513, 1987.

[10] Chopra, K. L., S. R., Das, "Thin Film Solar Cells", Plenum Press, New York, London, 1983.

[11] Carlsson,J. M., Hellsing, B., Domingos, H. S., and Bristowe, P. D., "Equilibrium structure of δ-Bi_2O_3 from first principles", J. Phys. Rev., Vol. 65, pp. 20-120, 2002.

[12] Jun, S., Yuan, G., Chang, H. W., Liang, W., "Enhancing visible-light photocatalytic activity of α-Bi_2O_3 via non-metal N and S doping", J. Chin. Phys., Vol. 23, No.3, 038103, 2014.

[13] Punn, R., Feteira, A. M., Sinclair, D. C., and Greaves, C., "Enhanced Oxide Ion Conductivity in Stabilized δ-Bi_2O_3", J. Am. Chem. Soc., Vol. 128 (48), pp. 15386–15387, 2006.

[14] Oganov, A. R., Chen, J., Gatti, C., Ma, Y. M., Yu, T., Liu, Z., Glass, C. W., Ma, Y. Z., Kurakevych, O. O., Solozhenko, V. L., "Ionic high –pressure form of elemental boron", Nature., Vol. 487, pp. 863-867, 2009.

[15] Gujar,T. P., Shinde, V. R., Lokhande, C. D., "Spray pyrolysed bismuth oxide thin films and their characterization", J. Mate. Res. Bulletin., Vol 41, pp. 1558–1564, 2006.

[16] Killedar, V. V., Bhosale, C. H., "Characterization of Spray Deposited Bismuth Oxide Thin Films from Non-Aqueous Medium", J. of Phys., Vol. 22, pp. 825 – 830, 1998.

[17] Mallahi, M., Shokuhfar, A., Vaez, M. R., Esmaeilirad, A., Mazinani, V., "Synthesis and characterization of Bismuth oxide nanoparticles via sol-gel method", American J. of Eng. Res., Vol. 03, pp. 162-165, 2014.

[18] Tezel, F. M., Kariper, I. A., "Synthesis, surface tension, optical and dielectr properties of bismuth oxide thin film", J. Mate. Phys., Vol. 20. pp. 30-36, 2017

[19] Sabaghiana, M., Behzada, M., Jahromib, H. S., "Alfa-Bismuth(III)oxide catalyzed Biginelli reactions using experimentally designed optimized condition", J. Adv. Mate. Proc, Vol. 3, pp. 61-69, 2016.

[20] Ubale, A. U., Ibrahim, S. G., Choudhary, A. R., "Structural, electrical and optical properties of nanostructured Cu doped Bi2O3 thin films deposited by chemical spray pyrolysis technique", Vidarbha .J. of Science., Vol. 9, pp. 202- 230, 2014.

[21] Gujar,T. P., Shinde, V. R., Lokhande, C. D., Mane, R. S., Han, S. H., "Bismuth oxide thin films prepared by chemical bath deposition (CBD) method: annealing effect", J. Appl Surf.Sci., Vol. 250, pp.161–167, 2005.

[22] Gopinath, P., Sriram, S., and Chandiramouli, R., "Influence of Zn doping on nanostructured Bi_2O_3 thin films", Inter. J. Chem.Tech Research., Vol. 5, pp. 2534-2539, 2013.

[23] Patil, R. B., Puri, R. K., Puri, V., "Effect of chopping on the properties of bismuth oxide thin films", J. Mater. Lett., Vol. 62, pp. 198-201, 2008.

[24] Waisy, E. T. A., Wazny, M. A. S., "Synthesis of Bi and Bi2O3 Polymorphous Structure Using RPLD Method", J. Eng. & Tech., Vol. 32, PP. 4, 2014.

[25] Gujar,T. P., Shinde,V. R., Lokhande, C. D., Mane, R. S., Han' S. H.,"Formation of highly textured (1 1 1) Bi_2O_3 films by anodization of electrodeposited bismuth films", J. Appl. Surf. Sci.,Vol. 252, pp. 2747–2751, 2006.

[26] Hicham, O. H., Souad, R., Fahd, T., Khalaf, J., Ahmed, O., Mouslim, M., Mostafa, A., "Synthesis, characterization and photo catalytic activity of α-Bi_2O_3 nanoparticles" J.Taibah University Sci. Vol. 9, Issue 4, pp. 508–512, 2015.

CHAPTER 2

THIN FILM DEPOSITION PROCESSES AND ITS FORMATION

CHAPTER 2

THIN FILM DEPOSITION PROCESSES AND ITS FORMATION

2.1 Introduction

Thin film science has grown world-wide into a major research area. During the last few decades a number of experimental techniques have been developed for the preparation of thin films of different types of materials, mainly due to the increase in the application of thin films. Thin film deposition techniques are essential to the development of material structure forming the core of semiconductor devices such as microprocessors and memory units. Requirements for thin solid films of wide variety of materials deposited from the gas, liquid or solid phase with improved quality, purity and versatile applicability as well as improved understanding of the physics and chemistry of films, interfaces, surfaces and microstructures has fueled the rapid evolution of technology in this field. Thin films are applied to modify the surface of a material or to build functional devices. The properties of a thin film and thereby its area of application is mainly determined by the choice of material. But the structure of the film on a nanometer or micrometer scale can also affect the film properties [1]. Thin film deposition process of insulating, conducting and dielectric materials plays an important role in manufacturing, production, research and application.

2.2 Classification of Thin Films Deposition Processes

Thin Film Deposition is the technology of applying a very thin film of material – between a few nanometers to about 100 micrometers. The methods employed for thin film deposition can be divided into mainly two broad categories based on the nature of the deposition process such as physical and chemical [2]. The different types of deposition techniques are given in table 2.

Table 2.1: Thin film deposition processes

```
                    ┌─────────────────────────┐
                    │   Thin film deposition  │
                    └─────────────────────────┘
                       │                    │
              ┌──────────────┐        ┌──────────────┐
              │   Physical   │        │   Chemical   │
              └──────────────┘        └──────────────┘
              │            │          │            │
        ┌─────────┐  ┌───────────┐  ┌───────────┐  ┌──────────────┐
        │ Vacuum  │  │ Sputtering│  │ Gas Phase │  │ Liquid Phase │
        └─────────┘  └───────────┘  └───────────┘  └──────────────┘
```

Vacuum	Sputtering	Gas Phase	Liquid Phase
• .Electron beam evaporation • Pulsed laser deposition • Arc evaporation • Thermal evaporation	• Dc • Rf • AC • Ion beam	• Chemical vapor • Thermal oxidation • Chemical beam epitaxy • Atomic layer epitaxy	• Spray pyrolysis • Sol-gel • Dip coating • Spin-coating • Chemical bath
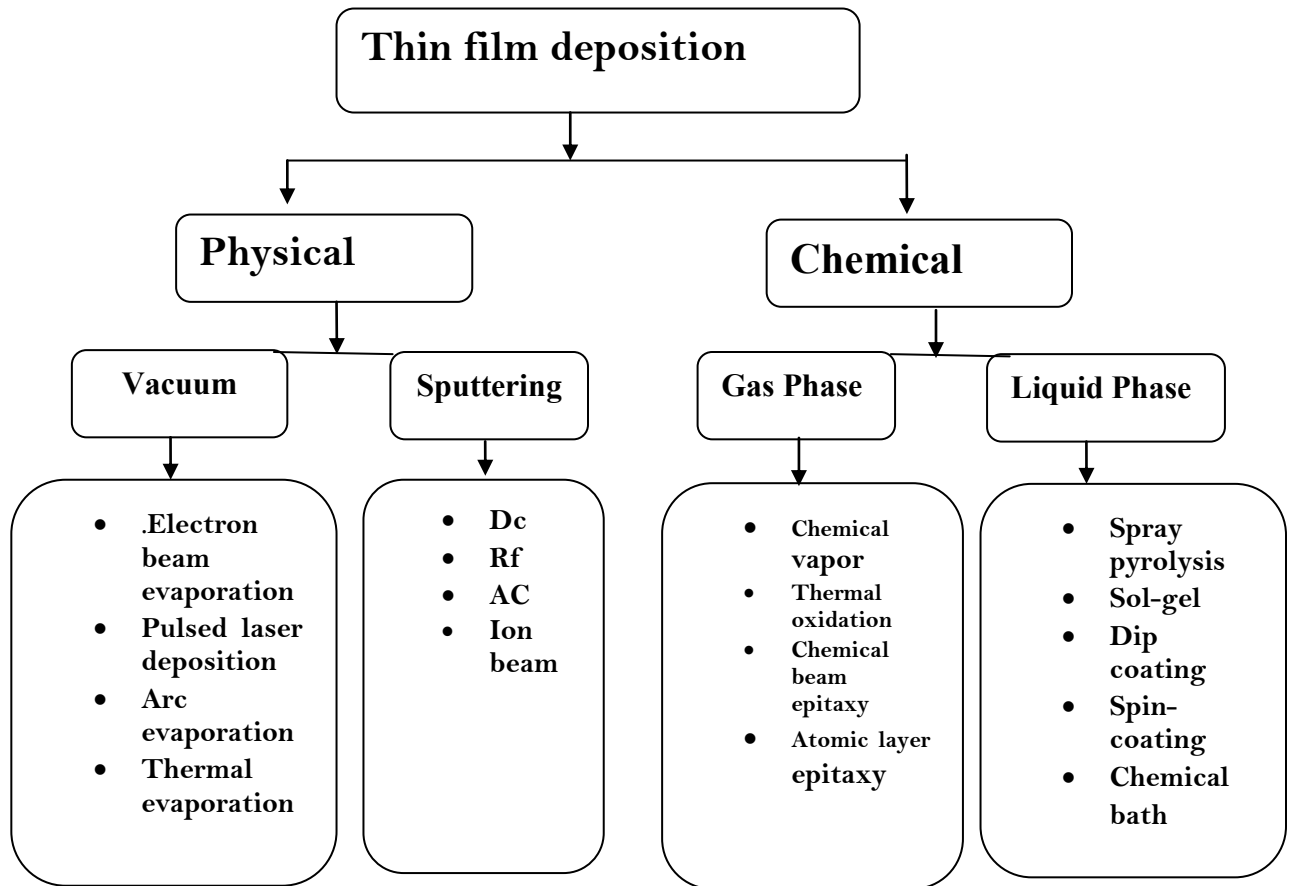
2.3 Overview of Various Thin Film Deposition Techniques

Among various types of thin film deposition techniques some of the commonly used techniques are described briefly in the following subsections.

2.3.1 Physical Deposition Processes

Physical deposition processes conduct mechanical, electromechanical or thermodynamic means to produce a thin film of solid.

The material to be deposited is placed is an energetic, entropic environment, so that particles of material escape its surface. Facing this source is a cooler surface which draws energy from these particle as they arrive, allowing them to from a solid layer. The whole system is kept in

a vacuum deposition chamber, to allow the particles to travel as freely as possible. Since particles tend to follow a straight path, films deposited by physical means are commonly directional, rather than conformal.

2.3.1.1 Thermal Evaporation

Thermal Evaporation is one of the simplest of the Physical Vapor Deposition (PVD) techniques. Basically, material is heated in a vacuum chamber until its surface atoms have sufficient energy to leave the surface. At this point they will traverse the vacuum chamber, at thermal energy (less than 1 eV), and coat a substrate positioned above the evaporating material (average working distances are 200 mm to 1 meter).

Thermal evaporation is a resistive heated boat. Evaporation is a common method of thin-film deposition. The source material is evaporated in a vacuum. The vacuum allows vapor particles to travel directly to the target object (substrate), where they condense back to a solid state.

Although one of the oldest methods used for depositing thin films, thermal evaporation or vacuum evaporation, is still widely used in the laboratory and in industry for deposition metal and metal alloys [3]. Figure 2.1 shows the diagram of thermal evaporation system. The material to be deposited is loaded into a heated container called a crucible. The crucible is resistively heated by applying a large current. As the material in the crucible becomes hot it gives of a vapor which atoms travel in straight lines until they strike a surface where they accumulate as a film.
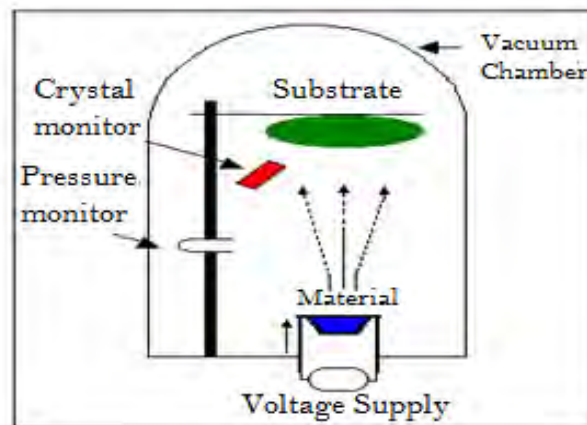
Figure 2.1: A schematic diagram of thermal evaporation system

2.3.1.2 Sputtering

Sputtering is a process whereby particles are ejected from a solid target material due to bombardment of the target by energetic particles, particularly, in the laboratory, gas ions. It only happens when the kinetic energy of the incoming particles is much higher than conventional thermal energies ($\gg$ 1eV).The ejected atoms can be condensed on to a substrate to from a thin film. This method has various advantages over normal evaporation technique in which no container contamination will occur. It is also possible to deposit alloy films which retain the composition of the parent target material. Figure 2.2 shows the diagram of sputtering system. DC sputtering, radio frequency (RF) sputtering and magnetron sputtering methods are the oldest types of sputtering used [4]. High pressure oxygen sputtering and facing target sputtering are the two new methods introduced for deposition of thin films for application in superconducting and magnetic films.
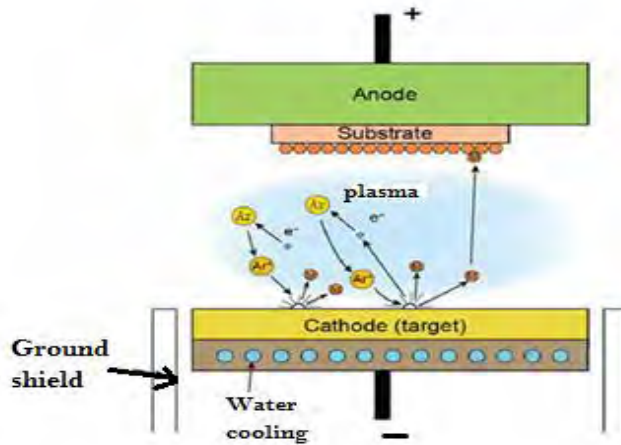
Figure 2.2: A diagram of a sputtering system

2.3.1.3 Physical Vapor Deposition

Physical vapor deposition (PVD) describes a variety of vacuum deposition methods which can be used to produce thin films and coatings. Physical Vapor Deposition (PVD) is a collective set of processes used to deposit thin layers of material, typically in the range of few nanometers to several micrometers.
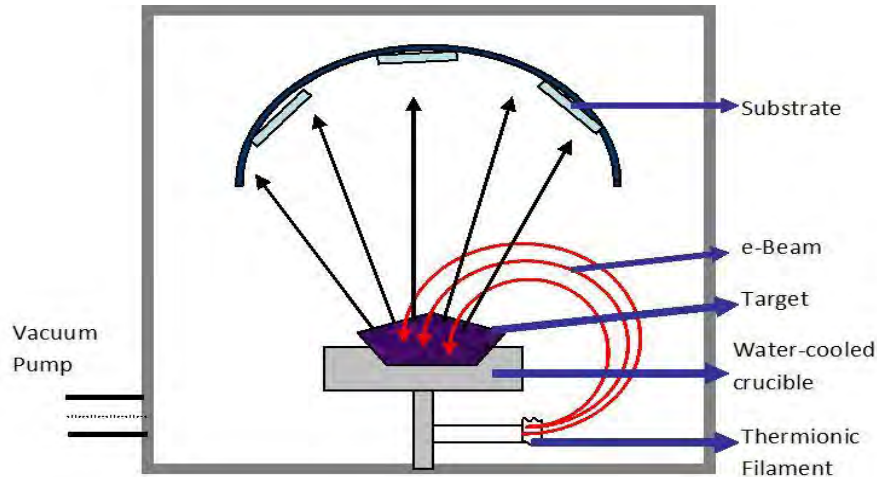
Figure 2.3: A diagram of physical vapor deposition

PVD processes are environmentally friendly vacuum deposition techniques consisting of three fundamental steps:

a) The solid material to be deposited is physically converted to vapor phase;
b) The vapor phase is transported across a region of reduced pressure from the source to the substrate;
c) The vapor condenses on the substrate to from the thin films;

2.3.1.4 Pulsed Laser Deposition

Pulsed laser deposition (PLD) is a physical vapor deposition (PVD) technique where a high-power pulsed laser beam is focused inside a vacuum chamber to strike a target of the material that is to be deposited. This material is vaporized from the target (in a plasma plume) which deposits it as a thin film on a substrate. This process can occur in ultra high vacuum or in the presence of a background gas, such as oxygen which is commonly used when depositing oxides to fully oxygenate the deposited films. In laser deposition, a high- power pulsed laser (1 J/shot) is irradiated onto the target of source materials through a quartz window. A quartz lens is used to increase the energy density of the laser power on the target source. Atoms that are ablated or evaporated from the surface are collected on nearby substrate surfaces to form thin films [5].
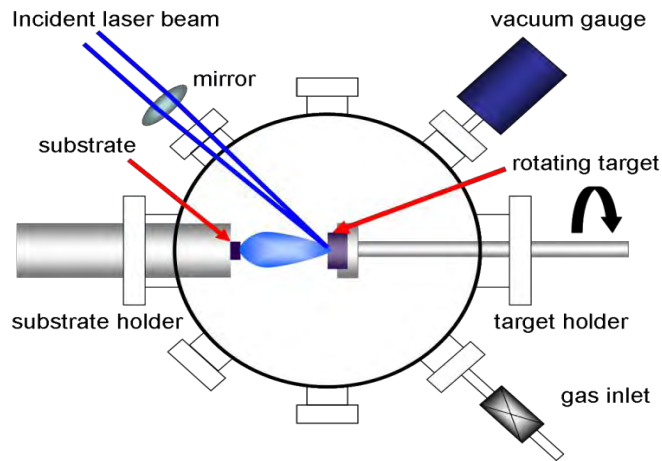
Figure 2.4: A diagram of pulsed laser deposition system

The target material is locally heated to the melting point, melted, and vaporized in a vacuum. The laser pulse may also provide photo-emitted electrons from the target to make a plasma plume and the evaporation mechanism may be complex since the process includes the thermal process and the plasma process. By optimizing various parameters such as ablation energy, base vacuum level, background oxygen pressure, distance between target and substrate and the temperature of substrates, one can have desired deposition rate and structure quality. A diagram of PLD system is shown in figure 2.4.

2.3.2 Chemical Deposition Processes

Chemical deposition processes are mainly classified into two types viz: gas phase techniques and liquid or solution phase techniques. Here, a fluid precursor undergoes a chemical change at a solid surface, leaving a solid layer. An everyday example is the formation of soot on a cool object when it is placed inside a flame. Since the fluid surrounds the solid object, deposition happens on every surface, with little regard to direction; thin films from chemical deposition techniques tend to be conformal, rather than directional.

2.3.2.1 Chemical Vapor Deposition

Chemical vapor deposition (CVD) is a chemical process used to produce high quality, high-performance, solid materials. The process is often used in the semiconductor industry to produce thin films. On the other hand Chemical vapor deposition (CVD) can be defined as a material synthesis method in which the constituents of vapor phase react together to form a solid film at a surface [6]. In typical CVD, the wafer (substrate) is exposed to one or more volatile precursors, which react and/or decompose on the substrate surface to produce the desired deposit.
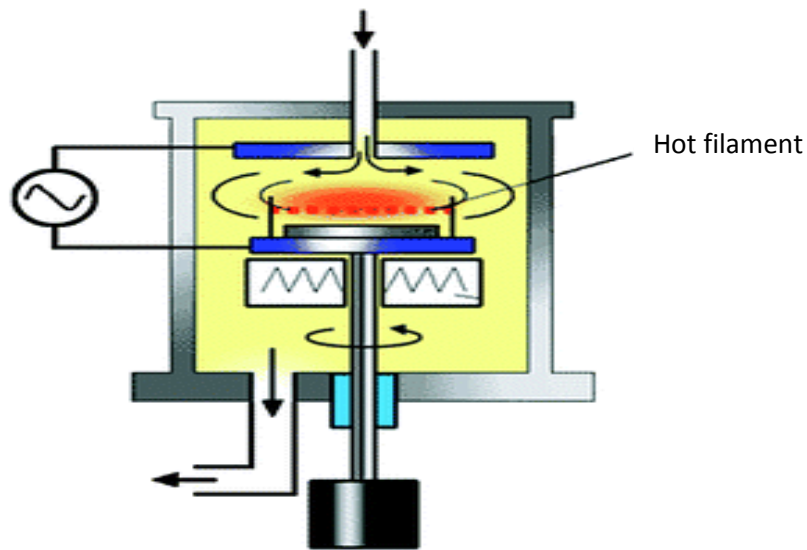
Figure 2.5: A diagram of CVD process

Frequently, volatile by-products are also produced, which are removed by gas flow through the reaction chamber. Various types of chemical reactions are utilized in CVD for the formation of solids is pyrolysis, reduction, oxidation, hydrolysis, synthetic chemical transport reactions etc. It has emerged one of the powerful techniques of thin film growth. Among the reasons for the growing adoption of CVD method is the ability to produce a large variety of films and coatings of metals, semiconductors, and compounds in a crystalline or amorphous form, possessing high purity and desirable properties. Figure 2.5 shows the diagram of a CVD process. CVD has numerous other names and adjective associated with it such as Vapor Phase Epitaxy (VPE) when CVD is used to deposit single crystal films, Metal-organic

CVD (MOCVD) when the precursor gas is a metal-organic species, Plasma Enhanced CVD (PECVD) when a plasma is used to induce or enhance decomposition and reaction, and Low Pressure CVD (LPCVD) when the pressure is less than ambient.

2.3.2.2 Chemical Bath Deposition

Chemical bath deposition (CBD) is a method to deposit thin films and nonmaterials; it can be employed for large-area batch processing or continuous deposition. It is also known as Chemical Solution Deposition (CSD). It is not a new technique as early as in 1835 Liebig reported the first deposition of Silver, the silver mirror deposition using a chemical solution technique.
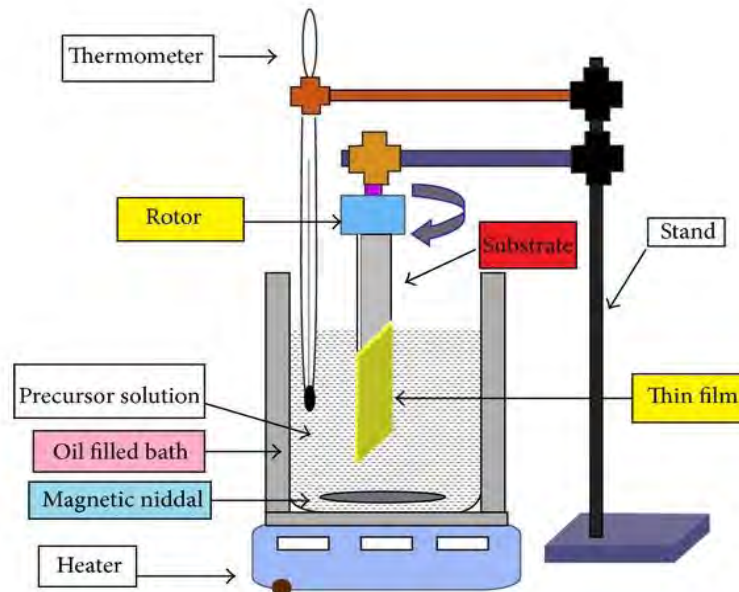
Figure 2.6: A diagram of CBD method**.**

The only requirements of these methods are a vessel to contain the solution (usually an aqueous solution of chemicals) and the substrate on which deposition is to be carried out. In addition to this various complications such as some mechanism for stirring and a thermo started bath to maintain a specific and constant temperature are options that they may be useful [7,8]. CBD is a method of growing thin film of certain materials on a substrate immersed in an aqueous bath containing appropriate reagents at temperature ranging from

room temperature to 100 ^{0}C. Figure 2.6 shows the diagram of a CBD process. CBD involves two steps, nucleation and particle growth. It also involves the controlled precipitation from solution of a compound on a suitable substrate. The technique offers many advantages over the more established vapor phase synthetic routes to semiconductor materials, such as CVD and MBE etc. varying the solution pH , temperature and reagent concentration allies factors such as control of film thickness and deposition rate with the ability of CBD to coat large areas in a reproducible and low cost process. In CBD two processes are traditionally used for growth: single dip, where the substrate is immersed in the reaction both only once, and multiple dips, where the same substrate is repeatedly coated to obtain thicker film.

2.3.2.3 Sol – gel Technique

The sol-gel process is a method for producing solid materials from small molecules. The method is used for the fabrication of metal oxides. The process involves conversion of monomers into a colloidal solution (sol) that acts as the precursor for an integrated network (or gel) of either discrete particles or network polymers. On the other hand sol- gel technique is a wet chemical route for the synthesis of colloidal dispersions of oxides which can be altered to powders, fibers, thin films and monoliths [9]. Sol- gel coating is a process of preparation of single or multi-component oxide coating which may be glass, glass ceramic or crystalline ceramic depending on the process. Also, the nano-materials used in modern ceramic and device technology require high purity and facilitate to control over composition and structure. Figure 2.7 shows the diagram of sol-gel technique. The sol-gel method is one of the interesting methods because it has many advantages [10]. Examples are as the followings:

❖ The chemical reactants for sol-gel process can be conveniently purified by distillation and crystallization

❖ Organic and inorganic salts can be added to adjust he microstructure or to improve the structural, optical and electrical properties of oxide films.

❖ All strong materials are mixed at the molecular level in the solution so that a high degree of homogeneity of films can be expected.

❖ The sol-gel method is almost exclusively applied for fabrication of transparent layers with a high degree of planarity and surface quality.
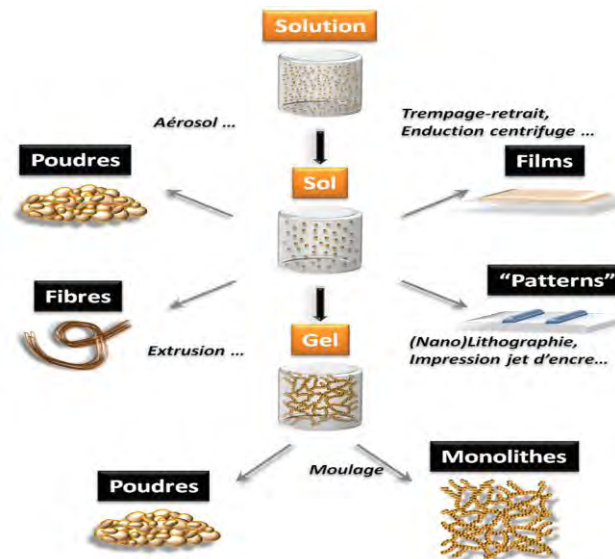
Figure 2.7: The diagram of sol-gel technique

2.3.2.4 Spray Pyrolysis Technique

Spray pyrolysisis a technique which uses a liquid source for thin film coating. Spray pyrolysis is a process in which a thin film is deposited by spraying a solution on a heated surface, where the constituents react to form a chemical compound. The chemical reactants are selected such that the products other than the desired compound are volatile at the temperature of deposition. The chemical reactants are selected such that the products other than the desired. Unlike many other film deposition techniques, spray pyrolysis represents a very simple and relatively cost effective processing method especially with regard to equipment costs. It offers an extremely easy technique for preparing films of any composition. SPT does not require high quality substrate or chemicals. The method has been employed for the deposition of dense films, porous films and for powder production. Even

multi-layered films can be easily prepared using this versatile technique [12]. Thereafter, due to the simplicity of the apparatus and good productivity of this technique on a large scale it offered a most attractive way for the formation of thin films of noble metals, metal oxides, calcogenides and superconducting compounds. In SPT process, the quality and properties of thin films depend largely on the preparation conditions. Recently, emphasis given to two aspects: (1) atomization techniques to control the droplet size and their distribution more precisely and (2) use of starting compounds such as organ tin to obtain highly oriented thin films seems more promising. Viguie & Spitz classified chemical spray deposition processes according to the type of reaction. In process A, the droplet resides on the surface as the solvent evaporates, leaving behind a solid that may further react in the dry state.
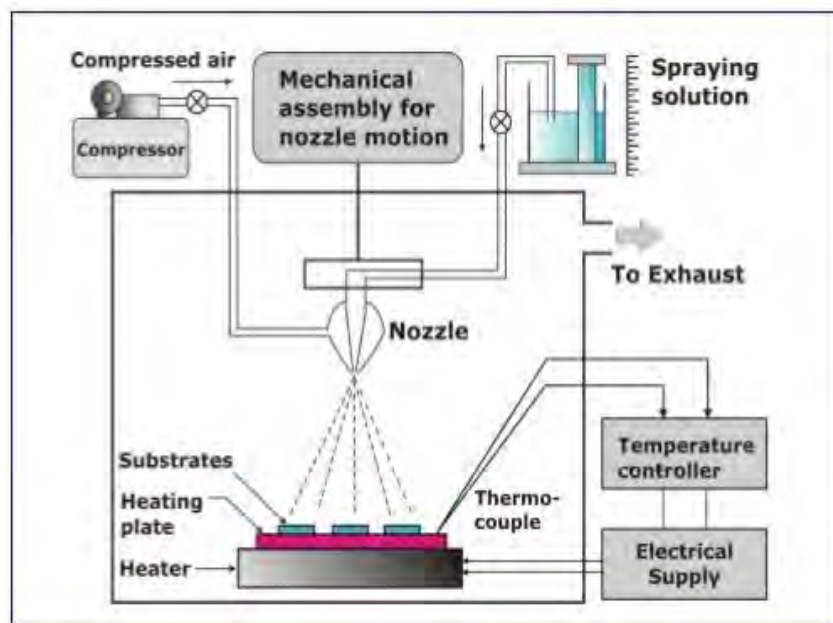
Figure 2.8: A diagram of spray pyrolysis technique

In process B, the solvent evaporates before the droplet reaches the surface and the dry solid impinges on the surface, where decomposition occurs. In process C, the solvent vaporizes as the droplet approaches the substrate; the solid then melts and vaporizes, and the vapor diffuses to the substrate, there to undergo a heterogeneous reaction. (They identify this process as true chemical vapor deposition.) In process D, the entire reaction takes place in the vapor state. In all processes, the significant variables are the ambient temperature, carrier gas

flow rate, nozzle-to-substrate distance, droplet radius, solution concentration, solution flow rate, and-for continuous processes substrate motion. To this list one should add the chemical composition of the carrier gas and/or environment, and, most importantly, substrate temperature. Most spray pyrolysis depositions are type A or B.

2.3.2.5 Spin coating

Spin coating is a procedure used to apply uniform thin films to flat substrates. A typical process involves depositing a small puddle of a fluid resin onto the center of a substrate and then spinning the substrate at high speed (typically around 3000 rpm) (Mitzi et al. 2004).Centrifugal force will cause the resin to spread to, and eventually off, the edge of the substrate leaving a thin film of resin on the surface.
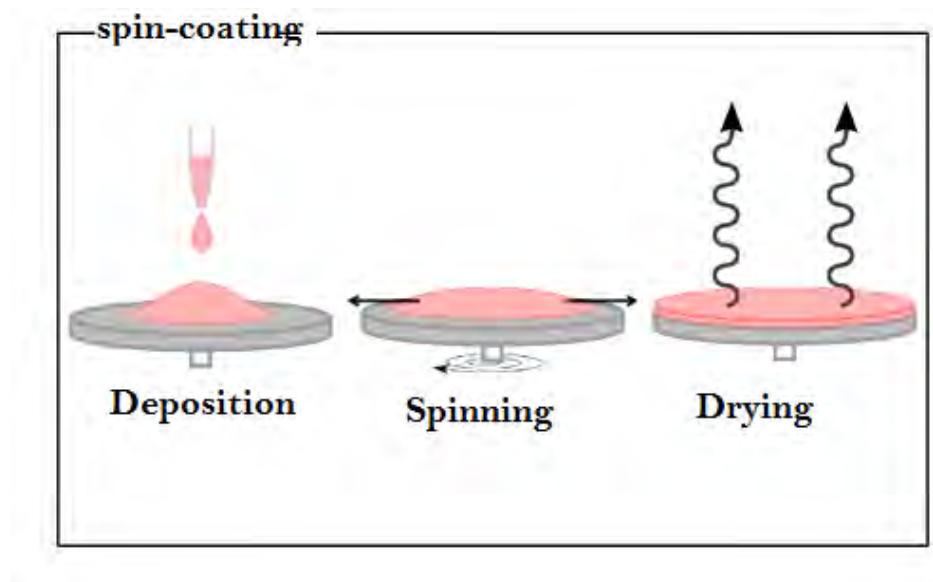
Figure 2.9: A diagram of spin coating technique

Final film thickness and other properties will depend on the nature of the resin (viscosity, drying rate, percent solids, surface tension, etc.) and the parameters chosen for the spin

process. A machine used for spin coating is called a spin coater, or simply spinner. Rotation is continued while the fluid spins off the edges of the substrate, until the desired thickness of the film is achieved. The applied solvent is usually volatile, and simultaneously evaporates. So, the higher the angular speed of spinning, the thinner the film. The thickness of the film also depends on the concentration of the solution and the solvent (Hellstrom 2007). Spin coating is widely used in micro-fabrication, where it can be used to create thin films with thicknesses below 10 nm.

2.4 Thin Film Formation

The growth of epitaxial (homogeneous or heterogeneous) thin films on a single crystal surface depends critically on the interaction strength between adatoms and the surface. While, it is possible to grow epilayers from a liquid solution. Three major steps that constitute a typical thin-film deposition process are [13]:

  i. Production of the appropriate atomic, molecular, or ionic species.
  ii. Transport of these species to the substrate through a medium.
  iii. Condensation on the substrate, either directly or via a chemical and/or electrochemical reaction, to form a solid deposit.
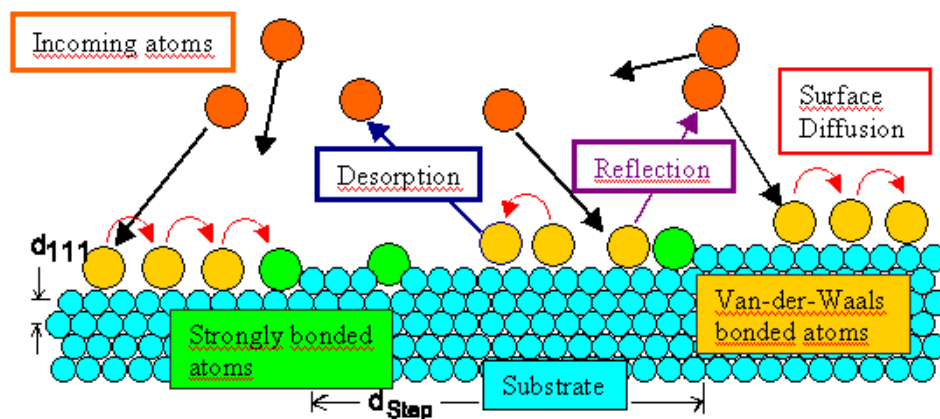
Figure 2.10.Schematic diagram of thin film formation process.

Thin film is prepared by deposition of the film materials (metals, semiconductors, insulators, dielectric etc.) atom by atom on a substrate through a phase transformation. Sufficient time interval between the two successive deposition of atoms and also layers are required so that these can occupy the minimum potential energy configuration.

2.4.1 Different Stages of Film Formation

There are three mechanisms of thin film condensation which can be distinguished, depending on the strength of interaction between the atoms of the growing film and between the atoms of the film and substrate. These are:

I. Layer by layer growth (Frank-van-der Merwe mechanism): during Frank–van der Merwe (FM) growth, adatoms attach preferentially to surface sites resulting in atomically smooth, fully formed layers. This layer-by-layer growth is two-dimensional, indicating that complete films form prior to growth of subsequent layers.

II. Island growth (Vollmer-Weber mechanism): In Vollmer–Weber (VW) growth, adatom–adatom interactions are stronger than those of the adatom with the surface, leading to the formation of three-dimensional adatom clusters or islands. Growth of these clusters, along with coarsening, will cause rough multi-layer films to grow on the substrate surface

III. Layer-plus-island growth (Stranski-Krastanov mechanism): Stranski–Krastanov growth is an intermediary process characterized by both 2D layer and 3D island growth. Transition from the layer-by-layer to island-based growth occurs at a critical layer thickness which is highly dependent on the chemical and physical properties, such as surface energies and lattice parameters, of the substrate and film.
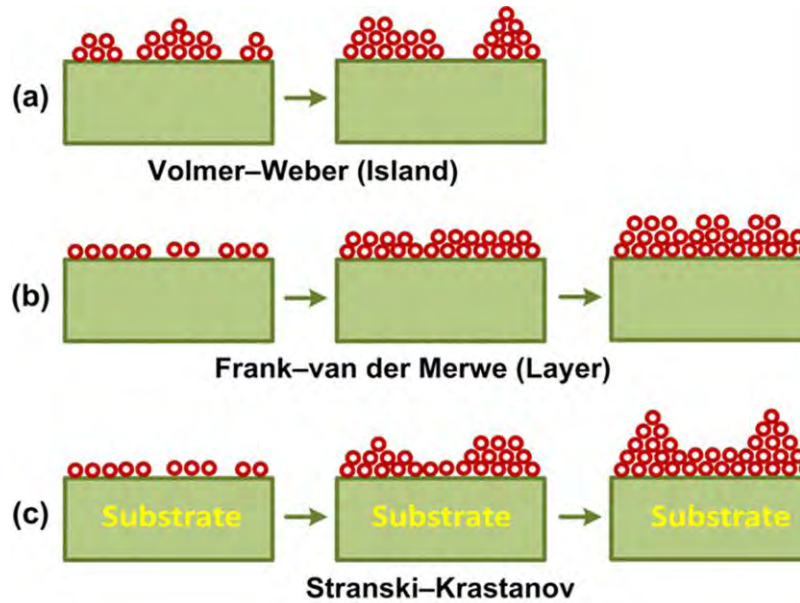
Figure 2.11: Schematic illustration of the three different modes of growth.

2.4.2   Condensation

Condensation is the change of the physical state of matter from gas phase into liquid phase, and is the reverse of evaporation. Thermodynamically, for condensation to occur on a substrate, the partial vapour pressure in the gaseous phase should be equal to or greater than its vapour pressure in the condensed phase at the same temperature. If the substrate material is different from the vapour material, the impinging vapour atoms are first adsorbed on the surface of the substrate and the condensation is initiated by the formation of small clusters of the adsorbed atoms. These small clusters then act as the initial centre"s of condensation. The process of adsorption and formation of small clusters may be visualized as follows. The impinging vapour atoms on approaching the substrate surface within a few atomic diameters, come under the influence of the field of force of the surface atoms of the substrate, and then several interactions may follow. These interactions are (l) An impinging atom may be reflected almost instantly retaining most of its kinetic energy; (2) there may be physical

33

adsorption of a vapour atom under the influence of van der Waals force of substrate atoms; (3) there may be chemical adsorption due to force of the type forming chemical bond between a vapour atom and a substrate atom; (4) an impinging atom may form immediate association with other atom or atoms already adsorbed on the surface. An adsorbed atom may also be desorbed after a finite stay time, or it may stick to the surface of the substrate and then migrate laterally to join a cluster of adsorbed atoms. 4 Adsorption of incident vapour atoms is possible only when there is thermal accommodation with the substrate atoms. If the kinetic energy of an incident atom is less than the energy of desorption, thermal accommodation is easily attained. Usually, an incident atom attains thermal accommodation by giving up its excess kinetic energy through lattice vibrations of the substrate, and except for light incident atoms or for atoms with very high incident kinetic energy; the incident vapour atoms attain thermal equilibrium with the substrate within a very short time, facilitating adsorption. Under appropriate conditions, when the rate of adsorption becomes greater than the rate of desorption, the small clusters of adsorbed atoms begin to enlarge, leading to stable nucleation and growth. [14-15].

2.4.3 Nucleation

The first stage in the process of depositing thin films on substrates is the formation of adsorbed monomers of one or more atoms which in the second phase, under the action of forces similar to surface tension, or capillarity combine to form small clusters. These clusters are called nuclei and the process of cluster formation is called nucleation. There are two types of nucleation occurs during the formation of a thin film: (1) homogeneous nucleation and (2) heterogeneous nucleation.

Homogeneous nucleation: Homogeneous nucleation refers to the spontaneous creation of a new phase from a metastable phase. The phase change can be from the vapor to a condensed phase (condensation), from a condensed phase to the vapor phase (cavitations), or from a solution phase to solid phase. Here the total free energy is used in the formation of a cluster of adatoms [16].

Heterogeneous nucleation: Heterogeneous nucleation occurs much more often than homogeneous nucleation. Phase changes which occurs due to impurities is called the

heterogeneous nucleation.[17] Heterogeneous nucleation applies to the phase transformation between any two phases of gas, liquid, or solid, typically for example, condensation of gas/vapor, solidification from liquid, bubble formation from liquid, etc.
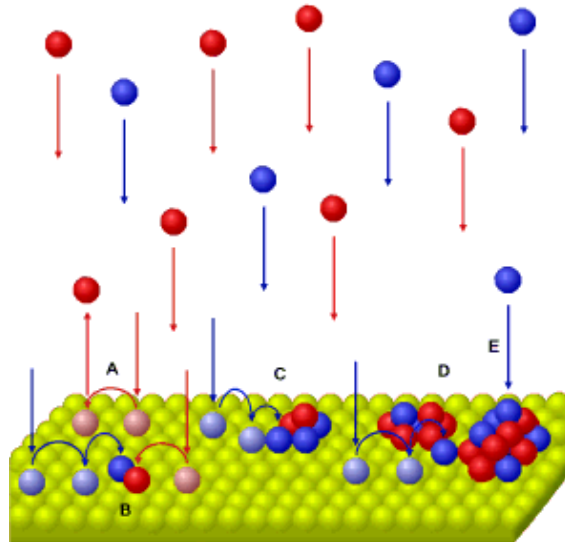
Figure 2.12: Adatom processes (sort red and blue) during heterogeneous condensation.

2.4.4 Growth

Growth is the final and completion stage of thin film formation. Growth refers to a positive change in size, or maturation, often over a period of time. The predictions of the nucleation theories in general have been found to be true even through relatively crude experimentations, but for quantitative comparison sophisticated techniques are needed. However, the observations have revealed distinct stages of film growth leading to a continuous film [18]. These stages are:

(l) Nucleation and island formation
(2) Coalescence of islands
(3) Channel formation, and
(4) Formation of continuous film.

2.4.4.1 Nucleation and Island Formation

When a substrate under impingement of condenses monomers is observed in the electron microscope, the first evidence of condensation is a sudden burst of nuclei of fairly uniform size. Smallest nuclei detected have a size of 2.0 to 3.0 nm. Growth of nuclei is three dimensional, but the growth parallel to the substrate is greater than that normal to it. This is probably because growth occurs largely by the surface diffusion of monomers on the substrate, rather by direct impingement from the vapor phase. The tendency to form an island structure is increased by,

- At high substrate temperature
- At low boiling point of film material
- At low deposition rate
- At weak binding energy between film material and substrate
- At high surface energy of the film material and
- At low surface energy of the substrate
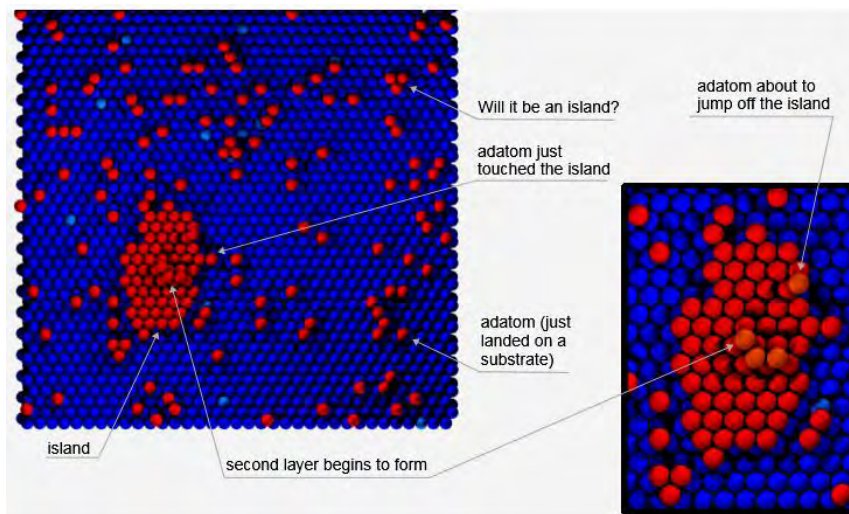
Figure 2.13.The mechanism of formation of island stage during thin film growth.

2.4.4.2 Coalescence of Islands

As, island increases their size by further deposition and come closer to each other. The larger ones appear to grow by coalescence of the smaller ones. The coalescence occurs in less than 0.1s for the small nuclei. After coalescence has taken place, the island assumes a more hexagonal profile is often faulted. In addition , nuclei having well –defined crystallographic shapes before coalescence become rounded during the event [19].A sequence of micrographs illustrating the effects as shown in Fig.2.14 where island which eventually becomes cryptographically shaped.
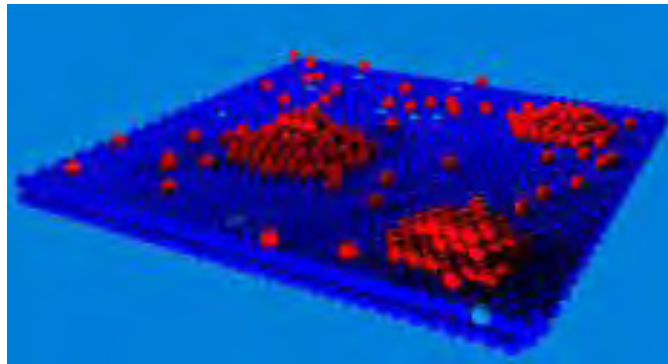
Figure 2.14. Schematic diagram of coalescence stage.

2.4.4.3 The Channel Stage

When larger islands grow together they have channels of interconnected holes of exposed substrate in the form of a network structure on the substrate. As deposition continues, secondary nucleation occurs in these channels and forms the last stage of nucleation.
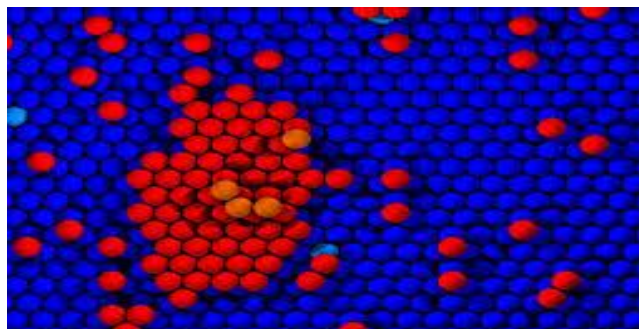
Figure 2.15.Schematic diagram of channel stage.

2.4.4.4 The Continuous Film Stage

This is the final stage of the film growth. This is slow and filing the empty channels which requires a considerable amount of deposits. These empty channels are filed by secondary nucleation, growth and coalescence and in this way a continuous film are formed.
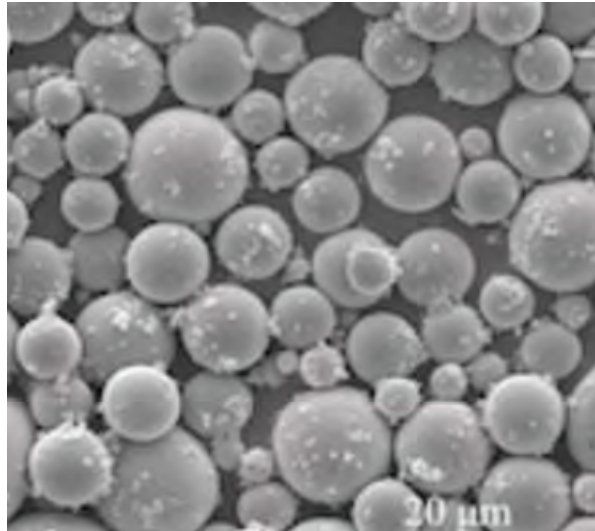
Figure 2.16: Schematic diagram of a continuous film stages.
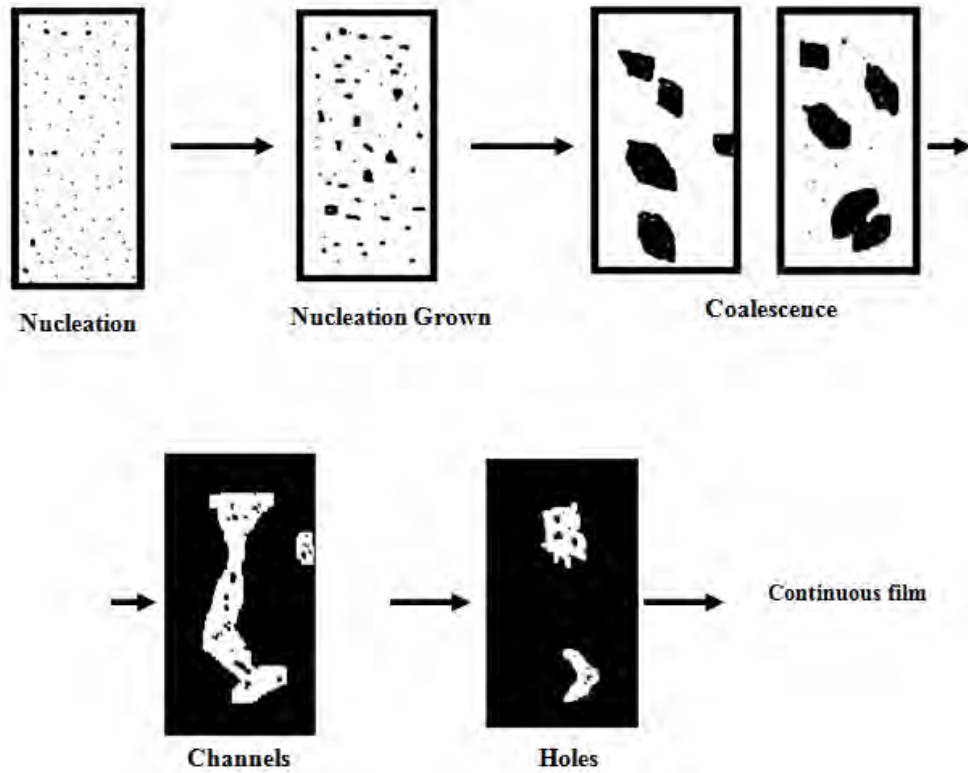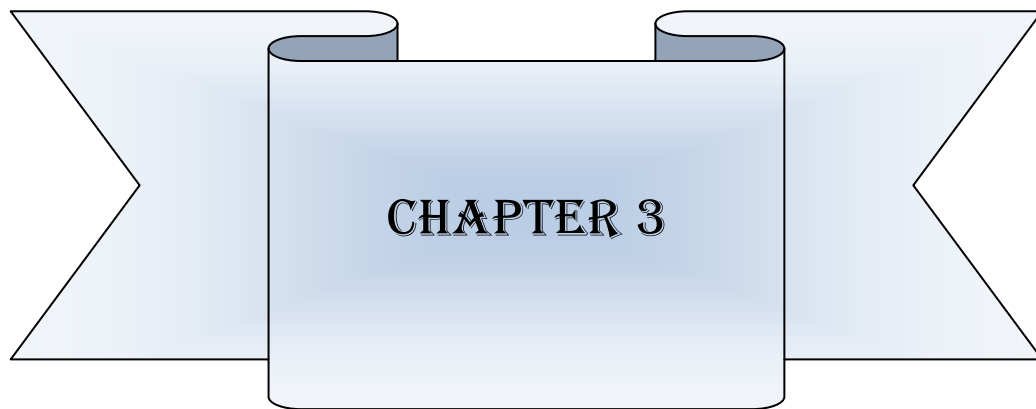
Figure 2.17: Different   stages of film growth
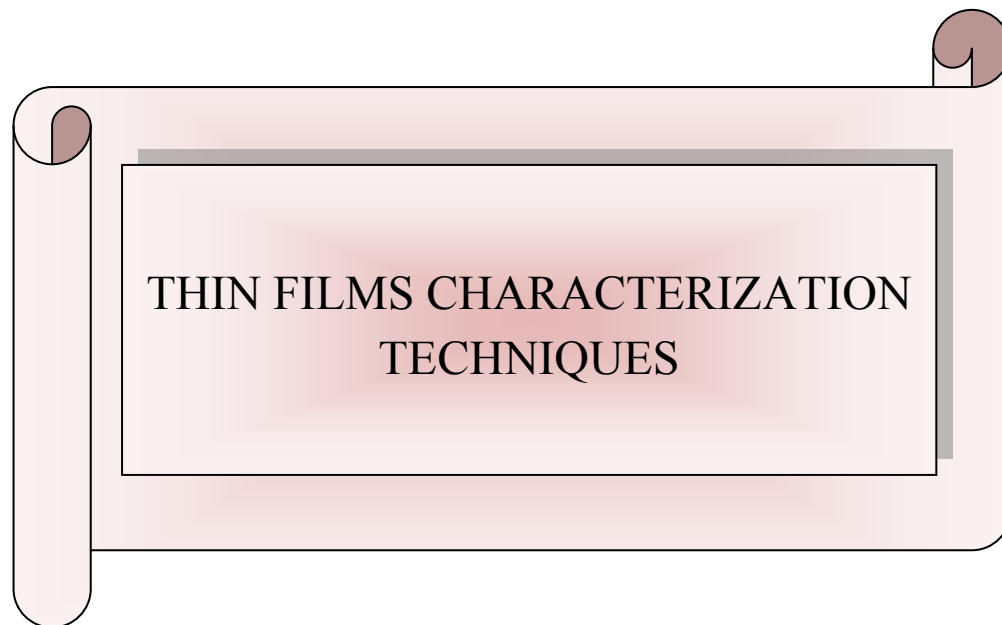
References

[1]   Ohring, M., "Materials Science of thin films", Academic Press, San Diego, CA, 2nd edition, 2002.

[2]   Chopra, K. L., "Thin Film Phenomena", McGraw Hill, New York, 1969.

[3]   Brown, R., Maissel, L. I. and Glang, R., "Handbook of Thin Film Technology", McGraw Hill, NewYork, 1970.

[4]   Behrisch, R., "Sputtering by Particle Bombardment", Springer, Berlin, 1981.

[5]   Aziz, M. J., "Film growth mechanism in pulsed laser depositon", Appl. Phys. A: Matter. Sci. Proc., Vol. 93(3), pp. 579-587, 2008.

[6]   Dobkin, D. and Zuraw, M. K., "Principles of Chemical Vapor Deposition", Springer, Science and Business Media, 2003.

[7]   Chopra, K. L., Kainthla, R. C., Pandya, D. K., and Thakoor, A.P., "In: Physics of Thin Films", Vol. 12, Academic Press, London, 1982.

[8]   Lokhande, C. D., "A chemical method for preparation of metal sulfide thin films", Mater. Chem. Phys., Vol. 28(1), pp. 145-149, 1991.

[9]   Hench, L. L. and West, J.K., "The sol-gel process", Chem. Rev., Vol. 90(1), pp. 33-72, 1990.

[10]   Ilican, Caglar, M. and Caglar, Y., "The effect of deposition parameters on the physical properties of CdxZn1-xs fims deposited by spray pyrolysis method", J. Optoelectr. and Adv. Mater., Vol. 9, pp.1414-1417, 2007.

[11]   Chamberlin, R. R.and Skarman, J. S., "Chemical spray deposition process for inorganic films", J. Electrochem. Soc., Vol. 113(1), pp. 86-89, 1966.

[12]   Perednis, D. and Gauckler, L. J., "Thin film deposition using spray   pyrolysis", J. Electroceram., Vol. 14, pp.103-111, 2005.

[13]   Hartnagle, H. L., Dawar, A. L., Jain, A. K., and Jagadis, C., "Semiconducting Transparent Thin Films", CRC Press, Bristol, 1995.

[14]   Zhang, Z. and Lagally, M. G., "Atomistic processes in the early stages of thin film growth", Science, Vol. 276, pp. 377-383, 1997.

[15]   Chopra, K. L., "Nucleation, growth and structure of films", Thin Film Phenomena, McGraw Hill, New York, pp. 110-137, 1969.

[16]   Waugh, M. R., "Characterization of Transparent Conducting Thin Films", University College, London, 2011.

[17]   Tolman, R. C., "The Effect of Droplet Size on Surface Tension", J. Chem. Phys., Vol. 17, pp.118, 1949.

[18]   Jensen, Havlin, P., "A fractal model for the first stage of thin film growth", Fractels, Vol. 4(3), pp. 321-329, 1996

[19] Ratsch, C. and Venables, J.A., "Nucleation theory and the early stages of   thin   Films
       growth", J. Vac. Sci. Technol. A, Vol. 21(5), pp. 96-109, 2003.

CHAPTER 3

THIN FILMS CHARACTERIZATION TECHNIQUES

CHAPTER 3
THIN FILM CHARACTERIZATION TECHNIQUES

3. Introduction

The deposited Bi_2O_3 and B doped Bi_2O_3 thin films are characterized for their structural, surface morphological, electrical and optical properties. X-ray diffraction (XRD) is used for studying the nature and structure, scanning electron microscopy (SEM) is used to identify the surface morphology and energy dispersive X-ray (EDX) spectroscopy is used to compositional study of the prepared films,. The optical parameters were analyzed from the transmittance and absorbance spectra obtained using UV- Visible spectrophotometer. The Four point probe technique is employed to measure electrical resistivity of the films. The principle, functioning and importance of each technique are briefly outlined in this chapter with related theory.

3.1 Structural Characterization

A rapidly increasing number of research topics and applications in science and engineering rely on thin films, superlative growth, and pattering down to the sub micrometer scale. In order to understand the structural properties of such nanostructures, a through and detailed structure characterization is required. XRD techniques allow us to probe the internal structure of the layers and the quality of the interfaces between the different materials in a multilayer. XRD provides most definitive structural information.

3.1.1 X-ray Diffraction

X-ray scattering techniques are a family of non-destructive analytical techniques which reveal information about the crystallographic structure, chemical composition, and physical properties of materials and thin films. These techniques are based on observing the scattered intensity of an X-ray beam hitting a sample as a function of incident and scattered angle, polarization, and wavelength or energy-ray diffraction (XRD) is a rapid analytical technique primarily used for phase identification of a crystalline material and can provide information on unit cell dimensions. The analyzed material is finely ground, homogenized, and average bulk composition is determined. XRD has been used in two main areas, for the fingerprint

characterization of crystalline materials and the determination of their structure [1]. Easy crystalline solid has its unique characteristic X –ray powder pattern which may be used as a "fingerprint "for its identification. Once the material has been identified, X –ray crystallography may be used to determine its structure, i.e. how the atoms pack together in the crystalline state and what the inter–atomic distance and angle are etc.

The size and the shape of the unit cell for any compound and can be determined most easily using XRD. X-rays are the electromagnetic waves of wavelength about $1A^0$. When X-rays are incident on a crystal surface, they are reflected from it.
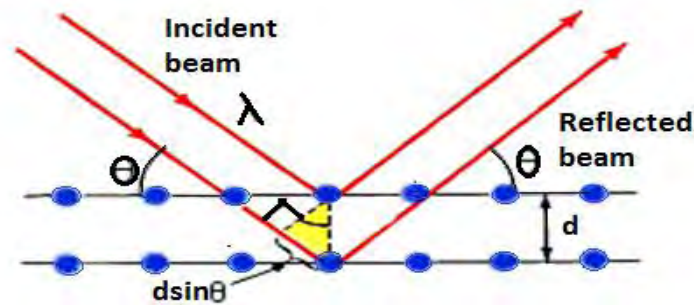
Figure 3.1: Reflection of X-rays from two planes of atoms in a solid.

The reflection obeys the following Bragg"s law,

$$2dsin\theta = n \hspace{5cm} (3.1)$$

Where d is the distance between crystal planes, θ is the incident angle of X-ray, λ is the wavelength of the X–ray and n is a positive integer. Bragg"s law also suggests that the diffraction is only possible when $\lambda < 2d$.

From the width of the diffraction line, it is possible to estimate the average grain size of the thin film [2].

Surface thickness in thin films are about 3000 A^0, can be investigated using XRD [3]. Thicker films can be characterized by reflection high-energy electron diffraction (RHEED). Analysis of the diffraction patterns obtained by these techniques and composition with standard ASTM data can reveal the existence of different crystallographic phases in the film, their relative abundance, the lattice parameters and any preferred orientations.

Using" values the set of lattice planes (h k l) are identified from the standard data and the lattice parameters are calculated using the relations. For a monoclinic crystal structure the lattice parameters can be determined using the relation,

$$\frac{1}{d^2} = \frac{1}{\sin^2\beta}\left(\frac{h^2}{a^2} + \frac{k^2\sin^2\beta}{b^2} + \frac{l^2}{c^2} - \frac{2hl\cos\beta}{ac}\right)$$

(3.2)

Where h, k and l are the indices of the crystal planes; d is the interplanar spacing and β is the full-width half maximum.

Crystallite size (D) is the of the effective crystal domain. It contributes to the peak broadening and as crystallite size decreases, the full width increases. The average D of the film is determined by using Debye Scherrer formula [4].

$$D = \frac{K\lambda}{\beta\cos\theta}$$

(3.3)

Where k is a constant known as shape factor and taken as 0.94, λ is the wavelength of X-rays.

The origin of micro strain (ε) is calculated using the relation [5],

$$\varepsilon = \frac{\beta\cos\theta}{4}$$

(3.4)

The dislocation density (δ) is the dislocation lines per unit area of the crystal, can also be evaluated from the crystalline size „D" using the formula [6],

$$\delta = \frac{1}{D^2}$$

(3.5)

3.2 Surface Morphology

Surface morphology is a subset of analytical imaging, which is an advanced form of high spatial resolution imaging that uses sophisticated microscopes to produce images of samples, objects and products that cannot be seen with the naked eye. Such images originate from the exposed surface of the sample or product.

3.2.1 Electron Microscope

An electron microscope is a microscope that uses a beam of accelerated electrons as a source of illumination. As the wavelength of an electron can be up to 100,000 times shorter than that of visible light photons, electron microscopes have a higher resolving power than light microscopes and can reveal the structure of smaller objects. There are four fundamental types of electron microscopes such as scanning electron microscope (SEM), transmission electron microscope (TEM), refection electron microscope (REM), and scanning transmission electron microscope (STEM). Figure 3.2 shows the basic steps involved in all electron microscopes. Electron microscope use signals, arising from the interaction of an electron beam with the sample to obtain information about structure, morphology and composition. Electrons are such small particles that, like photons in light, they act as waves. A beam of electrons passes through the specimen, then through a series of lenses that magnify the image. The image results from a scattering of electrons by atoms in the specimen. A heavy atom is more effective in scattering than one of two atomic numbers, and the presence of heavy atoms will increase the image contrast. The above procedures are followed by all types of electron microscope.
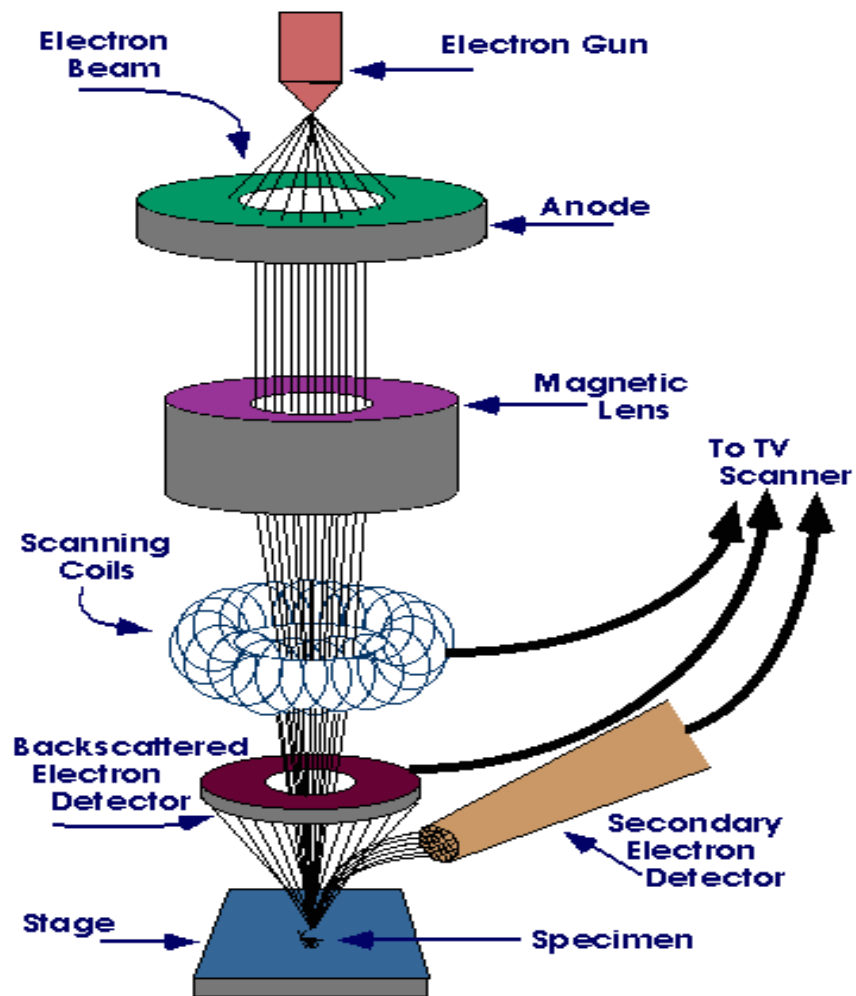
Figure 3.2: Schematic diagram of an electron microscope.

3.2.2 Scanning electron microscopy

The scanning electron microscope (SEM) is a type of microscope that uses a focused beam of high-energy electrons to generate a variety of signals at the surface of solid specimens. The signals that derive from electron-sample interactions reveal information about the sample including external morphology (texture), chemical composition, and crystalline structure and orientation of materials making up the sample. The SEM is a powerful and oftentimes used microscope in both academia and industry. In 1965 Stewart and Snelling at first designed the commercial version of a SEM. SEM uses electrons rather than light to form an image of various objects such as fractured metal components, foreign particles and residues, polymers, thin films electronic component , biological samples and countless others. The shorter wavelength of electrons permits image magnification 0 up to 100,000X, as compared to about 2,000X for conventional light microscopy.

In SEM, an electron beam is scanned across a sample‟s surface. The electrons is produced by a thermal emission source, such as a heated tungsten filament, or by a field emission cathode. The energy of the incident electrons can be as low as 100 eV or as high as 30 keV depending on the evaluation objectives. This electron beam generates a number of different types of signals include secondary electrons(SE), back –scattered electrons (BSE), characteristic X-rays, light emitted from the area of the specimen where the electron beam is impinging. The electrons are focused into a small beam by a series of electromagnetic lenses in the SEM column. The beam passes through pairs of scanning coils or pairs of deflector plates in electron column. The beam passes through pairs of scanning coils or pairs of deflector plates in electron column, typically in the final lens, which deflect the beam in the x and y axes so that it scans in a raster fashion over a rectangular area of the sample surface. When the primary electron beam interacts with the sample, the electrons lose energy by repeated random scattering and absorption within a teardrop-shaped volume of the specimen known as the interaction volume, which extends from less than 100 nm to approximately 5 μm into the surface. The size of the interaction volume depends on the electron‟s landing energy, the atomic number of the specimen and the specimen‟s density. The energy exchange between the electron beam and the sample, results in the reflection of high-energy electrons by inelastic scattering and the emission of electromagnetic radiation, each of which can be

detected by specialized detectors. The beam current absorbed by the specimen can also be detected and used to create images of the distribution of specimen current. Electronic amplifiers of various types are used to amplify the signals, which are displayed as variations in brightness on a cathode ray tube. The raster scanning of the CRT display is synchronized with the position of the beam on the specimen in the microscope, and the resulting image is therefore a distribution map of the intensity of the signal being emitted from the scanned area of the specimen. The image may be captured by photography from a high –resolution cathode ray tube, but in modern machines is digitally captured and displayed on a computer monitor and also saved to a computer"s hard disc.

Figure 3.3 represents a thermal field emission gun scanning electron microscope of model JEOL JSM-7600F. This field emission scanning microscope (FESEM) is used in this research work.

Figure 3.3: A field emission scanning electron microscope set up

3.3 Elemental Analysis

Elemental analysis is a process where a sample of some material (e.g., soil, waste or drinking water, bodily fluids, minerals, chemical compounds) is analyzed for its elemental and sometimes isotopic composition. Elemental analysis is a process where a sample of some

material (e.g., soil, waste or drinking water, bodily fluids, minerals, chemical compounds) is analyzed for its elemental and sometimes isotopic composition.

3.3.1 Energy Dispersive X-ray Spectroscopy

Energy dispersive X-ray spectroscopy (EDX, EDX, or XEDS), sometimes called energy dispersive X-ray analysis (EDXA) or energy dispersive X-ray microanalysis (EDXMA), is a analytical technique used for the elemental analysis or chemical characterization of a sample.
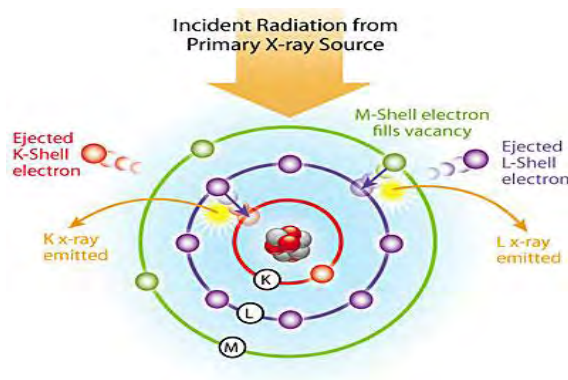
Figure 3.4: Schematic of X-ray excitations in EDX analysis.

It relies on an interaction of some source of X-ray excitation and a sample. Its characterization capabilities are due in large part to the fundamental principle that each element has a unique atomic structure allowing a unique set of peaks on its electromagnetic emission spectrum. To stimulate the emission of characteristic X-rays from a specimen, a high-energy beam of charged particles such as electrons or protons or a beam of X-rays, is focused into the sample being studied. At rest, an atom within the sample contains ground state (or unexcited) electrons in discrete energy levels or electron shells bound to the nucleus. The incident beam may excite an electron in an inner shell, ejecting it from the shell while creating an electron hole where the electron was. An electron from an outer, higher-energy shell then fills the hole, and the difference in energy between the higher-energy shell and the lower energy shell may be released in the form of an X-ray.

An EDX spectrum not only identifies the element corresponding to each of its peaks, but also the type of X-ray to which it corresponds as well. For example, a peak corresponding to the amount of energy possessed by X-rays emitted by an electron in the L-shell going to the K-shell is identified as a K-alpha peak. The peak corresponding to X-rays emitted by M-shell electrons going to the K-shell is identified as K-beta peak (figure: 3. 4).

3.4 Optical Characterization

The optical behaviors of a semiconductor are investigated in term of these phenomena namely transmission, reflection, absorption, reflection, refraction, polarization, interference and etc.

Figure 3.5: A UV-visible spectrophotometer

From these properties it is possible to calculate the optical constants such as : absorption coefficient (α), direct and indirect band gap, refractive index (n), extinction coefficient (k), optical conductivity (σ_{opt}), real and imaginary part of dielectric constant etc. For optical property studies of pure and Boron doped Bismuth Oxide thin films transmittance and

absorbance were measured by using a double beam UV-Vis spectrophotometer (SHIMADZU UV-1601) in the wavelength range of 200-1100 nm at room temperature (Figure 3.5). Measurements were made by placing the sample in the incident beam and another empty glass substrate in the reference beam of the instrument. The transmission spectra were recorded both for the Bi_2O_3 and Bi_2O_3: B at Ts of 350 ^{o}C thin films of concentration 1at%-7at%.   The optical properties of films have been studied extensively primarily because of their applications in various optical and electro-optical devices. Optical properties of a solid emanate from its interactions with electromagnetic waves and are manifested in optical frequencies. The effect of such interactions in the audio frequency region results in the dielectric behavior and in the optical frequencies, optical behavior.

3.4.1 Beer-Lambert law

The Beer-Lambert law (or Beer's law) [7] is the linear relationship between absorbance and concentration of an absorbing species. The general Beer-Lambert law is usually written as:

$$A=abc \qquad (3.6)$$

Where A is the measured absorbance, $\alpha(\lambda)$ is a wavelength-dependent absorbance coefficient, b is the path length, and c is the analyzed concentration. When working in concentration units of morality, the Beer-Lambert law is written as

$$A = \varepsilon bc \qquad (3.7)$$

Where ε is the wavelength-dependent molar absorptivity coefficient with units of $M^{-1}cm^{-1}$. Experimental measurements are usually made in terms of transmittance (T), which is defined as:

$$T = I / Io \qquad (3.8)$$

Where I is the light intensity after it passes through the sample and Io is the initial light intensity. The relation between A and T is:

$$A = -\log T = - \log (I / Io) \qquad (3.9)$$

Modern absorption instruments can usually display the data as transmittance, %transmittance, or absorbance. An unknown concentration of an analytic can be determined by measuring the amount of light that a sample absorbs and applying Beer's law. If the absorptive coefficient is not known, the unknown concentration can be determined using a working curve of absorbance versus concentration derived from standards.

3.4.2 Derivation of the Beer-Lambert law

The Beer-Lambert law can be derived from an approximation for the absorption coefficient for a molecule by approximating the molecule by an opaque disk whose cross-sectional area σ represents the effective area seen by a photon of frequency υ .If the frequency of the light is far from resonance, the area is approximately 0, and if υ is close to resonance the area is a maximum. Taking an infinitesimal slab, dz, of sample (Figure 3.6)
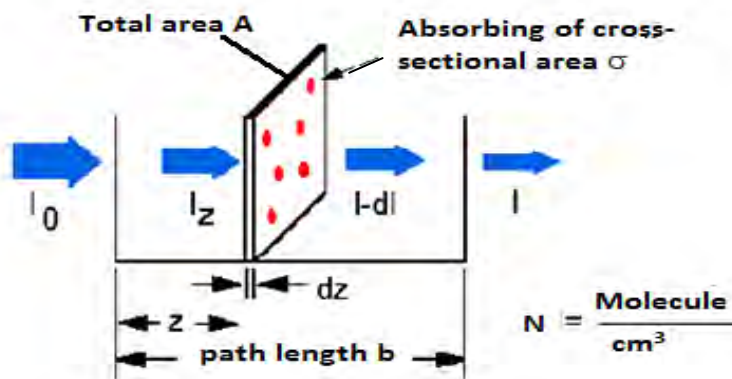
Figure 3.6: Absorption of light by a sample.

I_o is the intensity entering the sample at z = 0, I_z is the intensity entering the infinitesimal slab at z, dI is the intensity absorbed in the slab, and I is the intensity of light leaving the sample. Then, the total opaque area on the slab due to the absorbers will be σNA dz. Then, the fraction of photons absorbed will be σNA dz /A so,

$$\frac{dI}{Iz} = -\sigma Ndz \qquad (3.10)$$

Integrating this equation from z = 0 to z = b gives:

$$\ln(I) - \ln(Io) = -\sigma Nb$$

$$\text{or} - \ln(I / Io) = \sigma Nb.$$

Since N (molecules/cm3)×(1 mole / 6.023x1023 molecules)×1000 cm3 / liter = c (moles/liter) and 2.30 log(x) = ln(x) then,

$$- \log(I / Io) = \sigma (6.023\text{x}1020 / 2.303) \, cb$$

$$\text{or, } A = \varepsilon bc = -\log(I / Io) \tag{3.11}$$

Where $\varepsilon = \sigma \times (6.023\text{x}1020 / 2.303) = \sigma \times 2.61\text{x}1020$, and ε is called absorptivity. Thus the intensity of the transmitted light can be expressed as $I = Io \, e^{-\alpha d}$ where d is the path length through the sample and α is the absorbance coefficient. This equation can be written as,

$$\alpha = 2.303\left(\frac{A}{d}\right) \tag{3.12}$$

3.4.3 Electronic Transitions

The absorption of UV or visible radiation corresponds to the excitation of outer electrons. There are three types of electronic transition which can be considered;

1. Transitions involving π, σ, and n electrons
2. Transitions involving charge-transfer electrons
3. Transitions involving d and f electrons (not covered in this Unit).

When an atom or molecule absorbs energy, electrons are promoted from their ground state to an excited state. In a molecule, the atoms can rotate and vibrate with respect to each other. These vibrations and rotations also have discrete energy levels, which can be considered as being packed on top of each electronic level (Figure3.7).
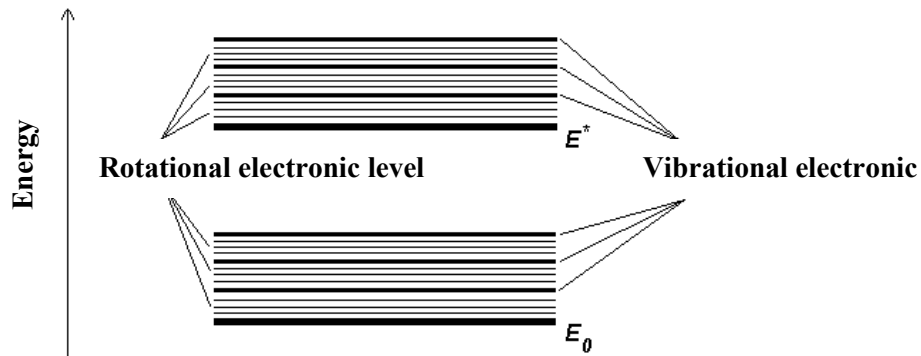
Figure 3.7: Vibrational and rotational energy

Absorbing species containing π, σ, and n electrons

Absorption of ultraviolet and visible radiation in organic molecules is restricted to certain functional groups (chromophores) that contain valence electrons of low excitation energy. The spectrum of a molecule containing these chromospheres is complex. This is because the superposition of rotational and Vibrational transitions on the electronic transitions gives a combination of overlapping lines. This appears as continuous absorption band. Possible electronic transitions of π, ζ, and n electrons are discussed below in figure 3.8
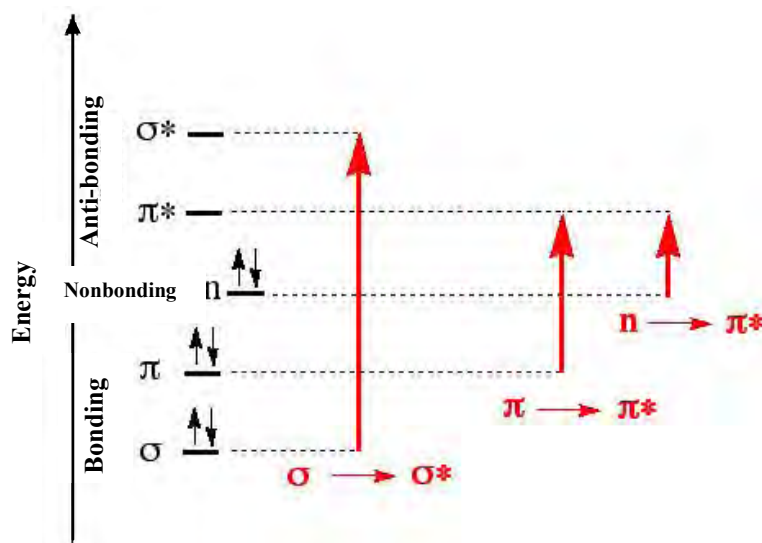
Figure 3.8: Possible electronic transitions

σ → σ* Transitions

An electron in a bonding ζ orbital is excited to the corresponding antibonding orbital. The energy required is large. For example, methane (which has only C-H bonds, and can only undergo ζ → ζ* transitions) shows an absorbance maximum at 125 nm. Absorption maxima due to ζ → ζ* transitions are not seen in typical UV-Vis. spectra (200 - 700 nm)

n →σ* Transitions

Saturated compounds containing atoms with lone pairs (non-bonding electrons) are capable of n →ζ* transitions. These transitions usually need less energy than n →ζ* * transitions. They can be initiated by light whose wavelength is in the range 150 - 250 nm. The number of organic functional groups with n →ζ* peaks in the UV region is small.

n →σ* and π→π* Transitions

Most absorption spectroscopy of organic compounds is based on transitions of n or π electrons to the π* excited state. This is because the absorption peaks for these transitions fall in an experimentally convenient region of the spectrum (200 - 700 nm). These transitions need an unsaturated group in the molecule to provide the π electrons.

Molar absorbtivities from n →ζ* transitions are relatively low, and range from 10 to100 L mol-1 cm-1. π→π* transitions normally give molar absorbtivities between 1000 and 10,000 L mol-1 cm-1. The solvent in which the absorbing species is dissolved also has an effect on the spectrum of the species. Peaks resulting from n →ζ* transitions are shifted to shorter wavelengths (blue shift) with increasing solvent polarity. This arises from increased solvation of the lone pair, which lowers the energy of the n orbital. Often (but not always), the reverse (i.e. red shift) is seen for π→π* transitions. This is caused by attractive polarisation forces between the solvent and the absorber, which lower the energy levels of both the excited and unexcited states. This effect is greater for the excited state, and so the energy difference between the excited and unexcited states is slightly reduced - resulting in a small red shift. This effect also influences n →ζ * transitions but is overshadowed by the blue shift resulting from solvation of lone pairs.

3.4.4 Direct and Indirect Optical Transition

In solid state physics, a band gap, also called an energy gap or band gap, is an energy range in a solid where no electron states exist. For insulators and semiconductors, the band gap generally refers to the energy difference (in electron volts) between the top of the valence band and the bottom of the conduction band. It is the amount of energy required to free an outer shell electron from its orbit about the nucleus to become a mobile charge carrier, able to move freely within the solid material.
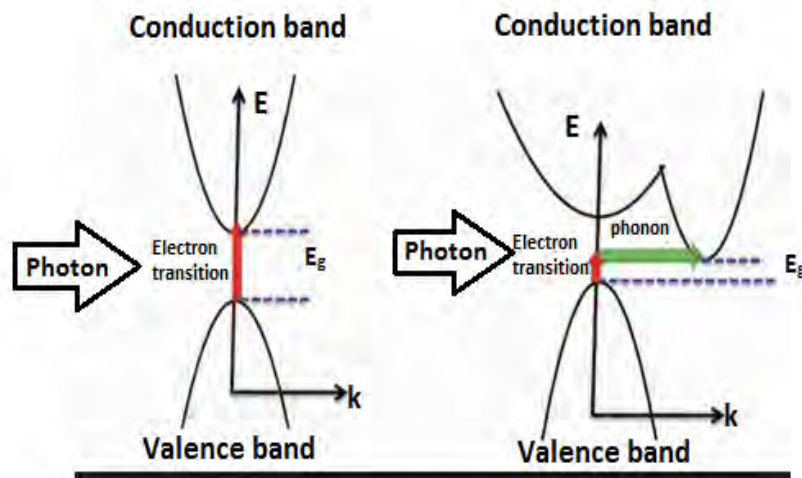
Figure 3.9: Schematic presentation of direct and indirect transitions between valence and conduction band.

In semiconductor physics, the band gap of a semiconductor is always one of two types, a direct band gap or an indirect band gap. The minimal-energy state in the conduction band, and the maximal-energy state in the valence band, are each characterized by a certain k-vector in the Brillouin zone. If the k-vectors are the same, it is called a "direct band gap". If they are different, it is called an "indirect band gap".

The direct and indirect band gap of the material can be obtained from the tauc relation. The tauc relation is given below.

$$\alpha h v = A \, (h v - E_g)^n \qquad\qquad 3.13$$

Where A is a constant or Tauc parameter depending upon the transition probability for direct transitions, n = 1/2 and n = for indirect transitions [8]. E_g is the optical gap.

3.4.5 Refractive Index and Extinction Coefficient

One of the most important optical constants of a material is its refractive index, which in general depends on the wavelength of the electromagnetic wave, through a relationship called dispersion. In materials where an electromagnetic wave, can be lose its energy during its propagation, the refractive index become complex. Refraction of light at the interface between two media of different refractive indices n1 and n2 are shown in figure 3.10
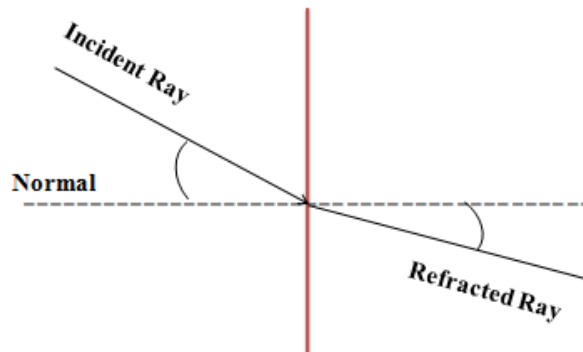
Figure 3.10: Refraction of light at the interface between two different refractive indices media.

The real part is usually the refractive index (n) and the imaginary part is called the extinction coefficient (k). In this section, n and k will be presented in detail along with some common dispersion relations. N of an optical or dielectric medium, is the ratio of the velocity of light (c) in vacuum to its velocity v in the medium, n= c/v. Using the Maxwell"s equations, one obtains the well known Maxwell"s formula for the refractive index of substance as n=√εμr where ε is the static dielectric constant or relative permittivity and μ_r the relative permeability. As μ_r = 1 for nonmagnetic substrate, one gets, n=√ε, which is very useful in relating the dielectric property to optical properties of materials at any particular frequency of interest. As ε depends on the wavelength of light, n also depends on the wavelength of light,

and this dependence is called dispersion. In addition to dispersion, an electromagnetic wave propagating through a medium, which means it, loses its energy, due to various loss mechanisms such as the generation of phonons (lattice wave), photo generation, free carrier absorption, scattering, etc. In such materials, the refractive index becomes a complex function of the frequency of light wave. The complex refractive index, denoted by n*, with real part n, and imaginary part k, called the extinction coefficient, is related to the complex relative permittivity (ε) by:

$$n* = n - jk = \sqrt{\varepsilon} = \sqrt{(\varepsilon r - j\varepsilon i)} \tag{3.14}$$

Where ε_r and ε_i are, respectively, the real and imagination parts of ε. Equation gives

$$n^2 - k^2 = \varepsilon_r \text{ and } 2nk = \varepsilon_i \tag{3.15}$$

In explicit terms, n and k can be obtained as:

$$n = \sqrt{1/2} \left[\sqrt{(\varepsilon_r{}^2 + \varepsilon_i{}^2)} + \varepsilon_r \right]^{1/2} \tag{3.16}$$

$$k = \sqrt{1/2} \left[\sqrt{(\varepsilon_r{}^2 + \varepsilon_i{}^2)} - \varepsilon_r \right]^{1/2} \tag{3.17}$$

the optical constants n and k can be determined by measuring the reflectance from the surface of a material as a function of polarization and the angle of incidence. For normal incidence, the reflective coefficient, r, is obtained as

$$r = (1-n^*)/(1+n^*) = (1-n+jk)/(1+n+jk) \tag{3.18}$$

The reflectance R is then defined by:

$$R = |r|^2 = |1-n+jk/1+n+jk|^2 = \{(1-n)^2+k^2\}/\{(1+n)^2+k^2\} \tag{3.19}$$

And refractive index can be calculated by using following equation

$$n = \left(\frac{1+R}{1-R}\right) + \sqrt{\left(\frac{4R}{(1-R)^2} - k^2\right)} \tag{3.20}$$

Notice that whenever k is large, for example over a range of wavelength, the absorption is strong, and the reflectance is almost unity. The light is then reflected, and any light in the

medium is highly attenuated. Extinction coefficient can be determined from the relation as follows

$$k = \frac{\alpha\lambda}{4\pi}$$
(3.21)

Optical conductivity of thin films is calculated by using the following equation

$$\sigma_{opt} = \frac{\alpha n c}{4\pi}$$
(3.22)

3.4.6 Absorption Coefficient

When a semiconductor is illuminated by a light, a photon strikes the surface, a fraction of photons are reflected and the remaining photons enter the semiconductor. Some of these are absorbed within the semiconductor and the remainder transmitted into the semiconductor. The absorption of radiation by any medium occurs through the excitation of electrons and photons. For semiconductor, it is convection to consider several types of absorption arising from

I.   Electronic transition between different energy bands.
II. Electronic transitions within energy band
III. Electronic transitions to localized states of impurity atoms
IV. Lattice Vibrations
V.   Vibrations of impurity atoms

In the fundamental absorption region the transmission T is given by

$$T = A \exp\left(\frac{4\pi\kappa t}{\lambda}\right)$$
(3.23)

Where „A" is a constant, „k" is the extinction co-efficient and„t"is the thickness. For $k^2 \ll n^2$, the principle variation of T occurs in the exponential term and pre-exponential term A. Therefore

$$T \approx \exp(-\alpha t)$$
(3.24)

60

Where $\alpha = \dfrac{4\pi\kappa}{\lambda}$ is the absorption co-efficient of the film. Thus the value of absorption co-efficient may be calculated from the relation

$$\alpha = -\frac{\ln T}{t} \tag{3.25}$$

3.5 Thickness Measurement of Thin Film

Film thickness is defined as the perpendicular distance from any point on a surface to the other end of the film. It plays an important role on the properties of thin film and also it is one of the most significant film parameter. Therefore the thickness should be measured with great care as far as possible to have an accurate value. There are several methods for thin film thickness measurement, for instance, weighing, X-ray fluorescence, stylus profiler technique and multiple-beam interferometer technique [9]. Multiple-beam interferometer technique is employed for the measurement of thickness of the thin films. In this method two reflecting surface are brought into close proximity to produce interference fringes. Nowadays it is a well-developed and standard method [10]. When two reflecting surfaces are brought into close proximity, interference fringes are produced, the measurement of which makes possible a direct determination of film thickness and surface topography with high accuracy. In this method, two types of fringes are utilized for thickness measurement. The first produces Fizeau fringes of equal thickness, using a monochromatic light source. The second uses a light source and produces fringes of equal chromatic order. The second method is prepared for thinner films. The Fizeau fringes method is used in the present work for the measurement of film thickness. For the experimental set up a low power microscope, a monochromatic source of light, a glass plate and an interferometer are required. To make the Fizeau fringes of equal thickness visible in a multiple beam interferometer formed by a thin absorbing film on a glass substrate, generally and auxiliary reflecting Coating on the film surface is required. But if the experimental sample is transparent with a very smooth surface no such auxiliary coating is necessary. The film whose thickness is to be measured is required to form a step on a glass substrate and over it another plane glass plate is placed. This illuminated with a parallel monochromatic beam of light a fringe system is produced and is viewed with low power microscope.
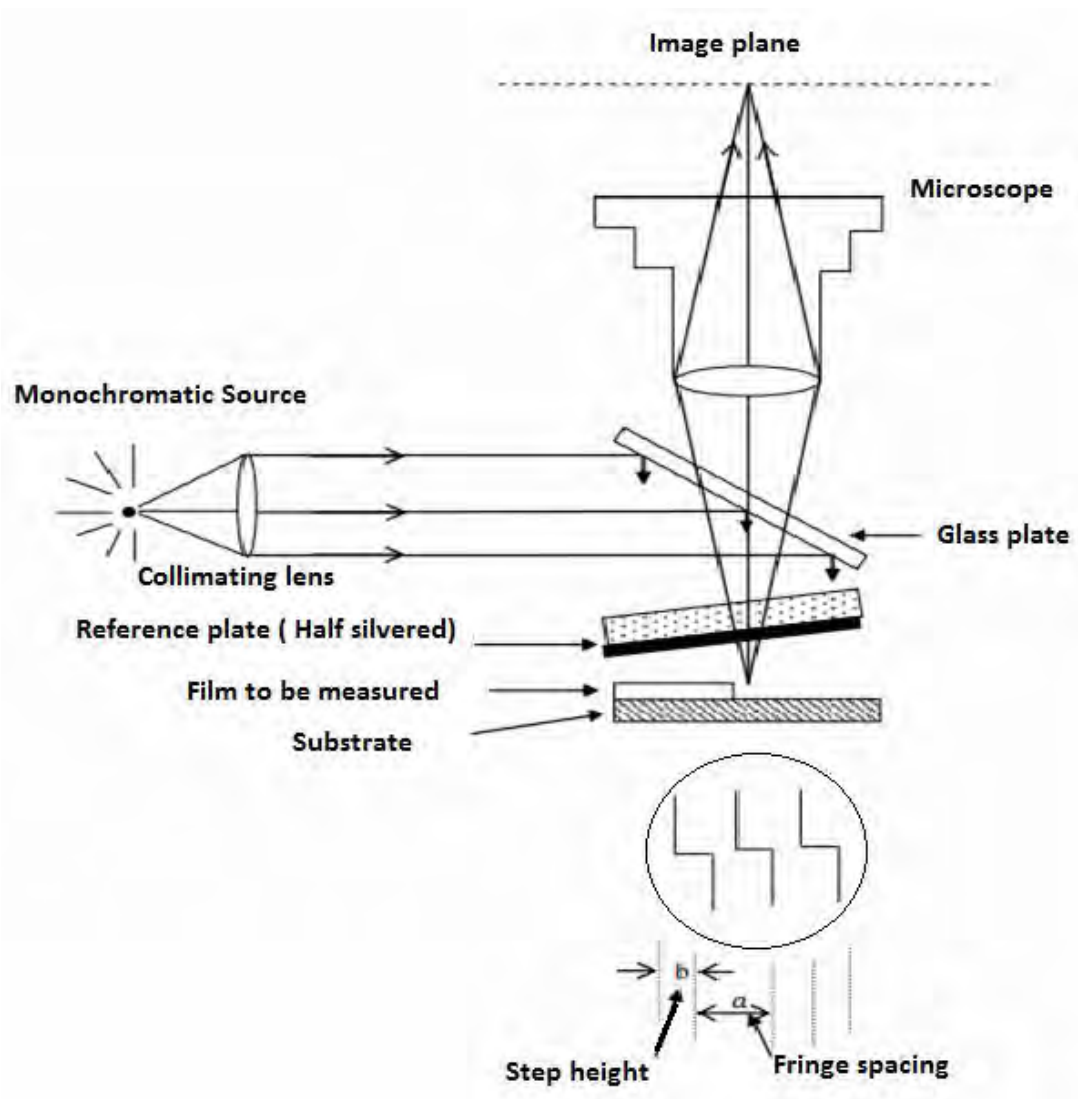
Figure 3.11: Interferometer arrangement for producing refection Fizeau fringes of equal thickness.

The fringe spacing and fringe displacement (step height) across the step are measured and used to calculate the film thickness. The thickness of film "d" can then be determined by the relation,

$$d = \frac{\lambda}{2} \times \frac{b}{a} \qquad (3.26)$$

Where,

λ = wavelength

b = step height

a = fringe spacing

In general, the sodium light is used, for which λ = 5893 A^0. Figure 3.5 shows the diagram of multiple –beam interferometer thickness measurement method.

3.6 Electrical Characterization

Electrical characterization methods for the analysis of thin films include the measurement of the electrical resistivity (ρ). ρ Is a key physical property of all materials. It is often necessary to accurately measure the value of ρ of a given material. There are four methods commonly used for the measurement of resistivity such as:

   I.   Direct method

  II.   Two point probe method

 III.   Four point probe method

 IV.   Van der pauw method

3.6.1 Direct Method

The resistivity of a thin film can be measured easily by direct method using the relation

$$\rho = R \frac{wt}{L} \qquad (3.27)$$

Where, w and t are the breath and thickness of the sample. For simplicity, if we consider w = L, the above equation becomes

$$\rho = Rt \tag{3.28}$$

Electrical conductivity of a material is reciprocal of resistivity of the material. Conductivity is denoted by a σ and defined as

$$\sigma = \frac{1}{\rho} \tag{3.29}$$

Measuring the resistance, R and thickness, t one can easily determine the resistivity and the conductivity.

3.6.2 Two Point Probe Method

It is simple method of measuring resistivity and is illustrated in figure 3.8.

In this method, voltage drop V across the sample and current through the sample I are measured. Then the resistivity is given as

$$\rho = \frac{VA}{IL} \tag{3.30}$$

Where, L is the specimen length and A is the cross- sectional area of the specimen. This method is useful when the sample has large resistance
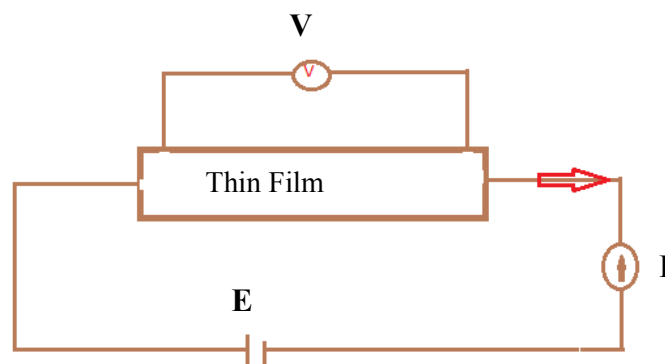
Figure 3.12: Electrical resistivity measurement by two point probe method.

3.6.3 Four Point Probe Method

Four probe apparatus is one of the standard and most widely used apparatus for the measurement of resistivity of semiconductors. This method is employed when the sample is in the form of a thin wafer, such as a thin semiconductor material deposited on a substrate. The sample is millimeter in size and having a thickness w. It consists of four probe arranged linearly in a straight line at equal distance S from each other. A constant current is passed through the two probes and the potential drop V across the middle two probes is measured. An oven is provided with a heater to heat the sample so that behavior of the sample is studied with increase in temperature.
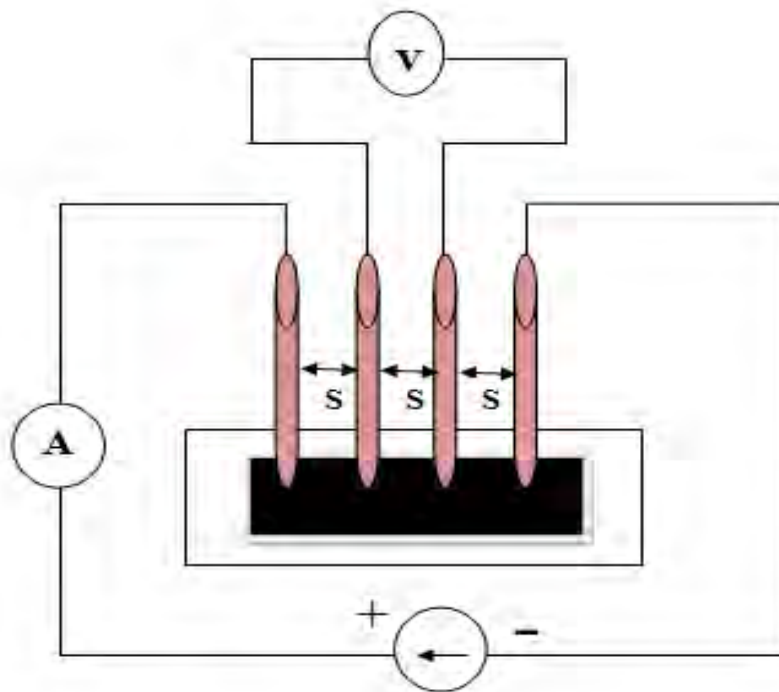
Figure 3.13: The arrangements of four probes that measure voltage (V) and supply current (I) to the surface of the crystal.

In the case of a four point probe on a sheet, the two outside current points represent the dipole. Therefore, the resistivity in this case can be given by [11]

$$\rho = 2\pi S \left(\frac{V}{I}\right) \qquad (3.31)$$

Here, the distance between all the four points is equal. I is the current flowing through the sample, V_D is produced voltage across two inner points and S is the distance between the adjacent points. If the distance between contact points is not equal and it is given as S_1, S_2 and S_3 respectively, then the resistivity is given as

$$\rho = \frac{V}{I}\left[\frac{2\pi}{\left(\frac{1}{S_1}+\frac{1}{S_2}-\frac{1}{S_1+S_2}-\frac{1}{S_2+S_3}\right)}\right] \qquad (3.32)$$

Where V is the floating potential difference between the inner probes, and I is the current through outer pair of probes.

3.6.4 Van der pauw Method

The van der pauw method, due to its convenience, is widely used in the semiconductor industry to determine the resistivity of sample [12]. The van der pauw method can be used to measure samples of arbitrary shape, although several basic sample condition must be satisfied to obtain accurate measurements, such as the thickness of the sample must be constant, point contacts placed at the edges of the samples must be used for the measurements, and the sample quality has to be homogeneous. Most semiconductor samples satisfy these conditions, so that this convenient measurement method has been widely utilized.
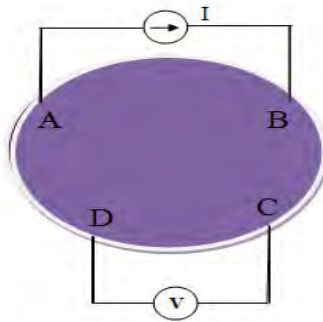
Figure 3.14: experimental arrangements for measuring resistivity by using Van der Pauw method.

At first we select a region on the sample where four electrical contacts were made at four corners, say A, B, C and D as shown in figure 3.10. Silver paste or indium was used to the contact. If a current I_{AB} entering the specimen through the contact A and leaving through the contact, B produces a potential difference V_{DC} between the points C and D then the resistance $R_{AB,CD}$ is defined as

$$R_{AB,CD} = \frac{V_{DC}}{I_{AB}} \tag{3.33}$$

Similarly, we have

$$R_{CD,AB} = \frac{V_{BA}}{I_{CD}} \tag{3.34}$$

$$R_{BC,DA} = \frac{V_{AD}}{I_{BC}} \tag{3.35}$$

$$R_{DA,BC} = \frac{V_{CB}}{I_{DA}} \tag{3.36}$$

The resistivity of a thin film can be expressed by the equation

$$\rho = \frac{\pi d}{\ln 2}\left[\frac{R_{AB,CD} + R_{BC,DA}}{2}\right] f\left(\frac{R_{AB,CD}}{R_{BC,DA}}\right) \tag{3.37}$$

$$\rho = 4.53d\left[\frac{R_{AB,CD} + R_{BC,DA}}{2}\right] f\left(\frac{R_{AB,CD}}{R_{BC,DA}}\right) \tag{3.38}$$

Where d is the thickness of the film and the function f can be evaluated from the equation

$$[R_{AB,CD} - R_{BC,DA}/R_{AB,CD} + R_{BC,AD}] = f/\ln2 \ arc \ cosh \ exp \ (\ln2/f)/2 \tag{3.39}$$

If $R_{AB,CD}$ and $R_{BC,DA}$ is almost equal, f may be approximately equal to unity and then the equation 3.42 takes the form.

$$\rho = 2.265d\ (R_{AB,CD} + R_{BC,DA})\ \Omega\text{-cm.} \tag{3.40}$$

3.6.5 Activation Energy

The energy required to transfer charge from one initially neutral island to another is known as activation energy and denoted by ΔE. This is equivalent to the electrostatic binding energy of the charge of the island. When these charge carriers are excited to a least this energy from the Fermi-level, there will be tunneling from one island to another. These islands or small particles are called crystalline. The activation energy is related with film conductivity and given by the relation

$$\sigma = \sigma_0 \exp(-\Delta E / 2KT) \tag{3.41}$$

Where σ_0 is the conductivity at 273 K, k is the Boltzmann constant and T is the absolute temperature. Equation (3.41) can be written as
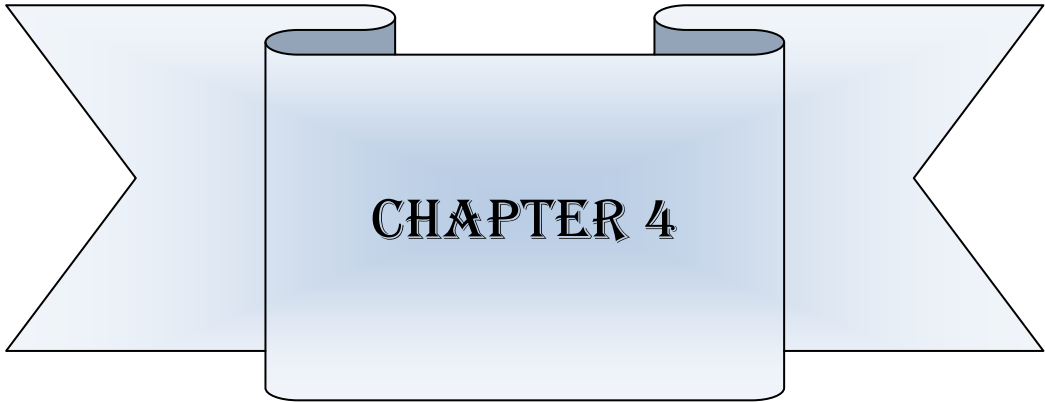
$$\ln \sigma = -\frac{\Delta E}{2KT} + \ln \sigma_0 \tag{3.42}$$

Equation (3.44) is equivalent to a straight line equation, $y = mx + c$. So that ΔE can be determined from the slope of the straight line. From the graph of $\ln\sigma$ vs. $\frac{1}{T}$, ΔE can be calculated by using the relation
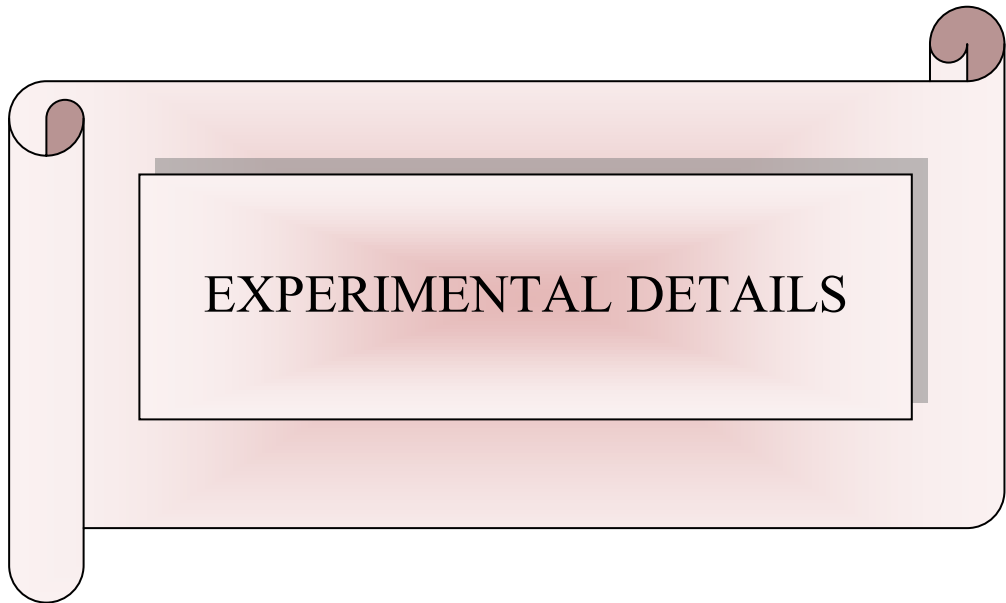
$$\Delta E = -\frac{\ln \sigma}{\frac{1}{T}} \times 2k\ (eV) \tag{3.43}$$

References

[1] Knag, S. J., Joung, Y. H., and Yoon, Y. S., "Effect of substrate temperature on structural, optical and electrical properties of ZnO thin films deposited by pulsed laser deposition", J. Matter. Sci.:Mater. Electron, Vol. 1, pp. 1073-1078, 2008.

[2] Raviprakash, Y., Kasturi, Bangera, V., Shivakumar, G. k., "Preparation and characterization of $CdZn_{1-x}S$ thin films by spray pyrolysis technique for photovoltaic applications", Solar Energy., Vol. 83, pp. 1645-1651, 2009.

[3] Gupta, B. k. and Agnihoti, O. P., "Structural investigations of spray –deposited CdS films doped with Cu, In, and Ga", Philos. Mag. (b), Vol. 37, pp. 631-633, 1978.

[4] Warren, B. E., "X-ray Diffraction", Addision Wesely Publishing Co.: London, 1969.

[5] Zhao, Y. and Zhang, J., "Microstrain and grain-size analysis form diffraction peak width and graphical derivation of high –pressure thermomechanics", J. Appl. Cryst., Vol. 41, pp. `1095-1108, 2008.

[6] Szekely, F., Groma, I., and Lendvai, J., "Characterization of self-similar dislocation structures by X-ray diffraction", Mater. Sci, Engn., A, Vol. 324, pp.179-182, 2002.

[7] Swinehart, D. F., "The Beer-lambert law", J. Chem. Edu., Vol. 39(7), pp. 333-335, 1962.

[8] Davies, E. A., and Mott, N. F., "Conduction in non-crystalline system, optical absorption and photoconductivity in amorphous semiconductor", Philos. Mag.,Vol. 22, pp. 903-922, 1970.

[9] Singh, Y., "Electrical resistivity measurement: a review", Int. J. Mod. Phys.: Conf. Series, Vol. 22, pp. 745-756, 2013.

[10] Van der Pauw, L. J., "A method of measuring specific resistivity and hall effect of discs of arbitrary shape", Philips. Res. Report., Vol. 13(1), pp. 1-9, 1958.

[11] Pliskin, W. A., and Stelvio, J. Z., "Thin Film Technology", McGraw Hill New York, 1970.

[12] Tolanasky, S., "Multiple Beam Interferometry", Oxford University Press, London, 1948.

CHAPTER 4

EXPERIMENTAL DETAILS

CHAPTER FOUR

EXPERIMENTAL DETAILS

4.1 Introduction

A thin film can be defined as a quasi-two-dimensional material created by condensing, atomic/molecular/ionic species of mater. Thin film preparation is a sequential process. Spray pyrolysis is the most commonly used technique adopted for the synthesis of thin film of transparent, conducting, etc. compounds. In this chapter, the details about design and construction of different experimental apparatus and preparation of Bi_2O_3 and Bi_2O_3: B thin films onto glass substrate by SPT are discussed briefly.

Thin film preparation consists of four sequential steps (Figure 4.1). A source of film material is supplied. The material is transported and deposition takes place. The films are characterized by various experimental techniques and finally the results are analyzed to evaluate the process.
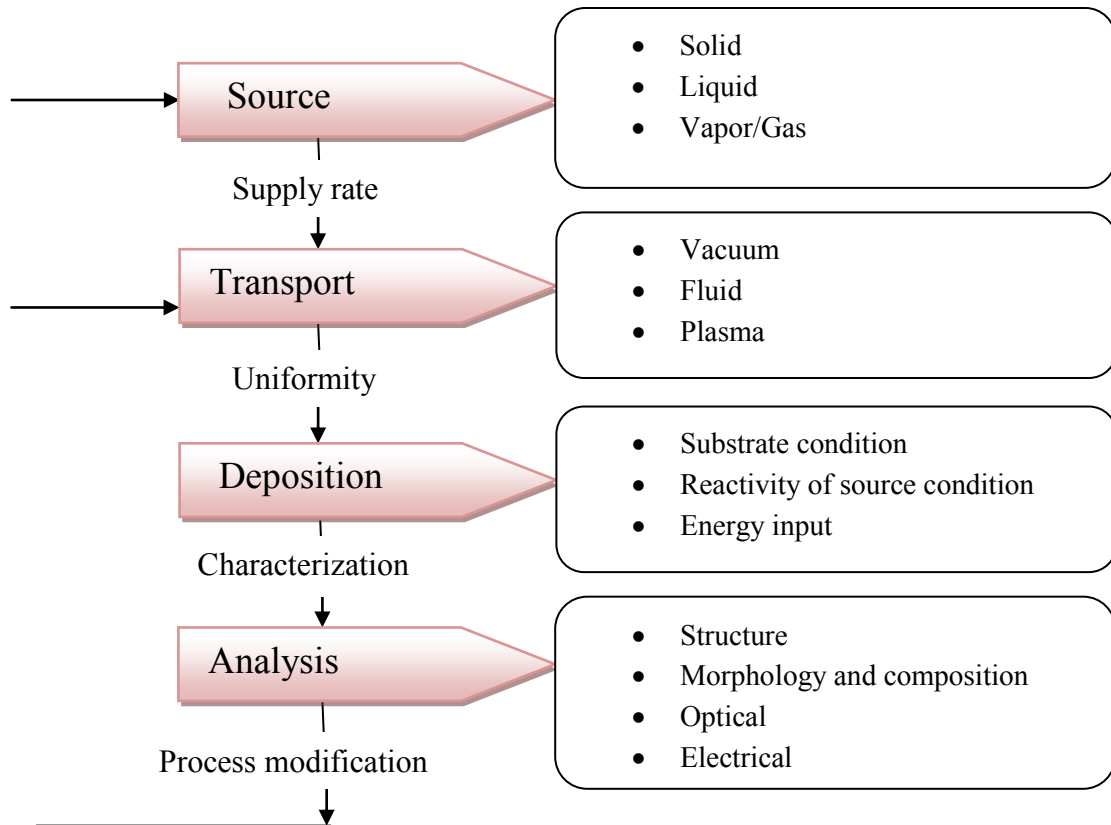

Figure 4.1: Steps of thin film processes

Spray pyrolysis (SP) is one of the most common techniques used for deposition of thin films. In this work, Bi_2O_3 and Bi_2O: B thin films are prepared by using a locally fabricated SP deposition (SPD) unit. This chapter includes a brief discussion of the SPD unit and v arious steps of preparation of $Bi_2O_{3:B}$ thin films on glass substrate by SPD technique.

4.2. Experimental Details

4.2.1. Preparation of Masks

The direct deposition of thin film pattern requires a suitably shaped aperture, commonly referred to as a mask. For the purpose of various experimental studies, film of specific size and shape are required. Mask is made from stainless steel plate with the desired pattern cut into it. The aperture is made in a bath machine.

Figure 4.2: Mask for the sample

The mask is placed in proximity to the substrate, thereby allowing condensation of the evaporated only in the exposed substrate areas. The mask is prepared in such a way that the edge of the mask is smooth so that it is helpful for determining the film thickness accurately. Mask used for film are shown in (Figure 4.2).

4.2.2 Heater

The heater "H" is an ordinary hot plate 2kW michrome wire heater. The top of the plate is covered with a piece of asbestos sheet having a small open area at the center where a mica sheet is attached. A thick stainless steel plate "G" (Figure 4.3) is placed on this mica sheet. Substrate is placed on this susceptor plate „G" to have a uniform temperature throughout the

substrate surface. An electrical voltage variac controls the heater power. The temperature of the heater was measured by copper constantan thermocouple tightly attached to the substrate surface placed on the heater susceptor.

4.2.3 The Design of the Reactor

The design of the reactor is shown in Figure 4.3. It is a vertical batch type reactor composed of a galvanized iron enclosure „E‟, heater „H‟ and heat susceptor „G‟. For the rapid expulsion of the by-product gases there are opening at the side and at the top of the reactor. It helps focusing the incoming sprayed solution towards the substrate „S‟ and also provides a chimney action to the exhaust gas upwards.
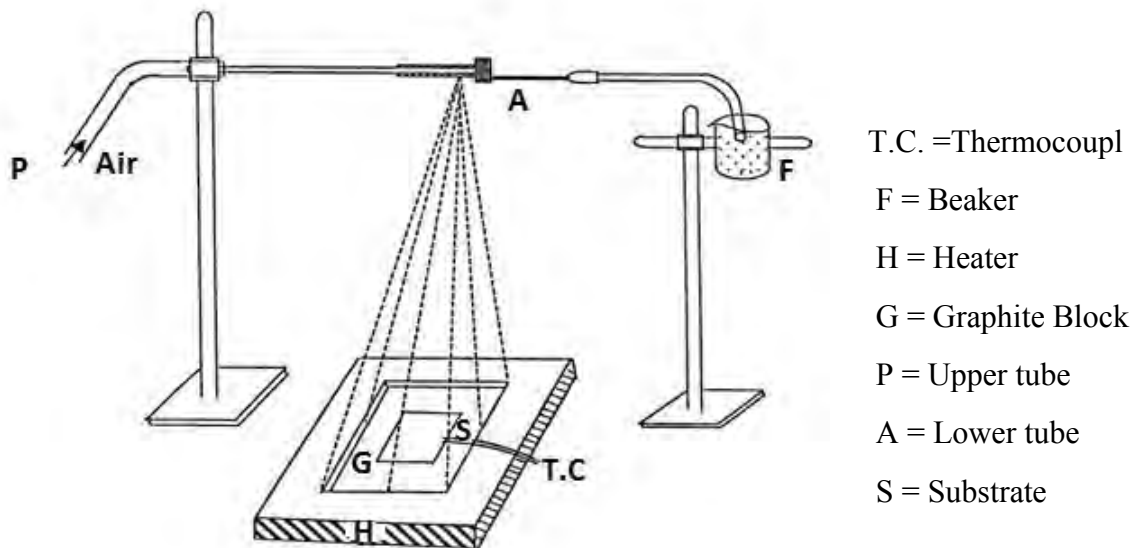

T.C. =Thermocoupl

F = Beaker

H = Heater

G = Graphite Block

P = Upper tube

A = Lower tube

S = Substrate

Fig. 4.3: Experimental setup of spray pyrolysis technique

4.2.4 The Fume Chamber

It is a large type chamber with a slanting top and is provided with a chimney. There is an exhaust fan fitted at the mouth of the chimney to remove the unused gases from the chamber. The slanting top and the sidewalls are made of glass and wood. There are airtight doors in the front side. The chamber has purging facilities. The whole spray system and the reactor are kept inside the fume chamber at the time of film deposition because of the safety grounds and to check air current disturbances at the deposition site. These two points just stated are very important for the spray process when deposition is carried out in open air atmosphere.

4.2.5 Air Compressor

An air compressor is a device that converts power usually from an electric engine into kinetic energy by pressurizing and compressing air, which is then released in quick bursts. It is reservoir type electrical air compressor. A rotary pump in this section mode draws atmospheric air and keeps it reserved in a large capacity air tank. At the outlet of the tank a pressure gauge is attached which records the pressure of the air at the time of supplying it from the tank. There is a bypass control valve which can keep the output pressure constant.

4.2.6 Spray Nozzle

The single spray nozzle consists of capillary tubes (stainless steels) fitted perpendicular to the other tube as shown in Figure 4.3. When compressed air is passed rapidly through the upper tube „P"in direction tangential to the mouth of the lower tube „A" a partial vacuum is created at the front part of the tube „A" whose other end is kept immersed in the spray liquid. Due to this partial vacuum the liquid rises up through the tube „A" and the compressed air drives it away in the form of fine spray particles. The thinner spray nozzle would give the finer spray particles. A very fine needle shaped capillary tube was used for the spray nozzle and it may vary from nozzle to nozzle.

4.3 Substrate and Substrate Cleaning

Several types of substrates are used for thin film deposition. Substrate may influence various the properties of thin films [1]. Generally, glass, quartz, plastic and ceramic substrates are used for polycrystalline films. However, in the present work, thin films are deposited on glass substrates. The most commonly microscope glass slides having 5 cm long, 2 cm wide and 0.1 cm thickness are used. These are fine smooth high quality microscope glass slides. The cleaning of substrate has a major influence on the properties of the thin film deposited onto them. Surface contaminations manifest it in pinholes, which can cause open resister or localized high resistance. The following procedures are used for substrate cleaning. The gross contamination of each of the substrate are first removed by warm aqueous solution carbonate and then washed with distilled water. After washing in distilled water, the substrate was washing by ultrasonic bath. Finally these are dried in hot air and preserved for use. During the whole process the substrates are always held by slide holding forceps.

4.4 Working Solution

The working solution is prepared by taking bismuth nitrate pentahydrade [Bi $(NO_3)_3.5H_2O$] as a source precursor material for pure Bi_2O_3 and boric acid (H_3BO_3) precursor used for dopant. For solvent distilled water and little amount of acetic acid are used. 94ml H_2O and 6 ml acetic acid are used for 100 ml solution. The precursor materials are dissolves in water at room temperature. Since the spray system used in the present experiment operates via a partial vacuum path as the mouth of the spray nozzle, the concentration of the solution prepared by the solvent is made in such a way that it could be at least be drawn by the nozzle. If the solution is high the spray rate will be low. A typical value of solution concentration 0.1 M is used in this work. In order to prepare the Bi_2O_3: B thin films, the aqueous solution of Bismuth nitrate and Boric acid are used as the precursor solution.

4.5 Deposition Parameters

In the spray pyrolysis technique the structure, composition and other characteristics of the deposited thin films depend on a number of process variables (deposition parameters). The deposition parameters such as the substrate temperature (T_S), type and concentration of the solution (C), flow rate of the solution (S_r), deposition time (t_d), quality of the substrate

material, size of atomized particles, carrier air pressure (P_a) and substrate to spray outlet distance (d_s), etc. affect the properties of the thin films. It is obvious that T_s is the most important deposition parameter and it must be controlled with great care.

The deposition parameters t_d, S_r, d_s, p_a, and C are kept constant when Bi_2O_3 and Bi_2O_3:B thin films are deposited onto glass substrates. Bi_2O_3 and Bi_2O_3: B thin films are deposited at various substrate temperatures (T_s) 350 ^{o}C. Bi_2O_3: B thin films are prepared by changing the B doping concentration from 1.0 at. % to 7.0 at.% at constant values of T_s. The effect of these two film parameters on the structural, optical and electrical properties of Bi_2O_3 and Bi_2O_3: B thin films are studied in this work.

4.6 Thickness Control

Thickness plays an important role in the properties of thin films unlike a bulk material [2-4].In the present spray deposition process, the deposition time is the main factor for the thickness control, provided the other parameters, remain constant. Since the deposition is carried out in normal atmosphere a direct and inside control of thickness is not so easy. To control the film thickness therefore calibration chart may be used. These charts are generally plots of deposition time vs. thickness, and can be prepared at different constant substrate temperatures prior to the preparation of particular experimental samples using the same solution and deposition variables.

4.7 Sample Deposition

It has been stated earlier that spray pyrolysis method for preparing bismuth oxide thin films is an economically attractive method [5-7], which consist basically of spraying solution on a heated glass substrate. The apparatus needed to carry out the chemical spray process consists of a device to atomize the spray solution and a substrate heater. Figure 4.3 shows a schematic diagram of SPD unit and Figure 4.4 shows a typical experimental setup for SPD used in this work. A considerable amount of 100 ml solution taken in the container „F" fitted with the spray nozzle „A". The clean substrate with a suitable mask was put on the susceptor of the heater „H". The distance between the tip of the nozzle and the surface of the glass substrate was kept 25 cm. Before supplying the compressed air the substrate temperature „T_s" was to be kept at a level slightly higher than the required substrate temperature because at the onset

of spraying a slight fall of temperature is likely. The temperature of a substrate was controlled by controlling the heater power using a variac. The substrate temperature was measured by placing a copper constantant thermocouple on the substrate. When compressed air is passed through „P‟ at constant pressure (0.5 bar), a fine Bi_2O_3 was produced and automatically carried to the reactor zone where film was deposited on the heated substrate [8-10]. The solution is adjusted such that about 10 minutes of spray produces Bi_2O_3 and Bi_2O_3: B thin films of thickness about 200-300 nm. The possible chemical reaction that takes place on the heated substrate to produce Bi_2O_3 may be as follows:
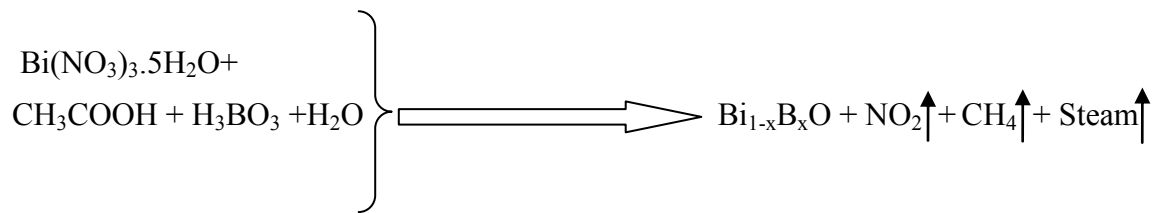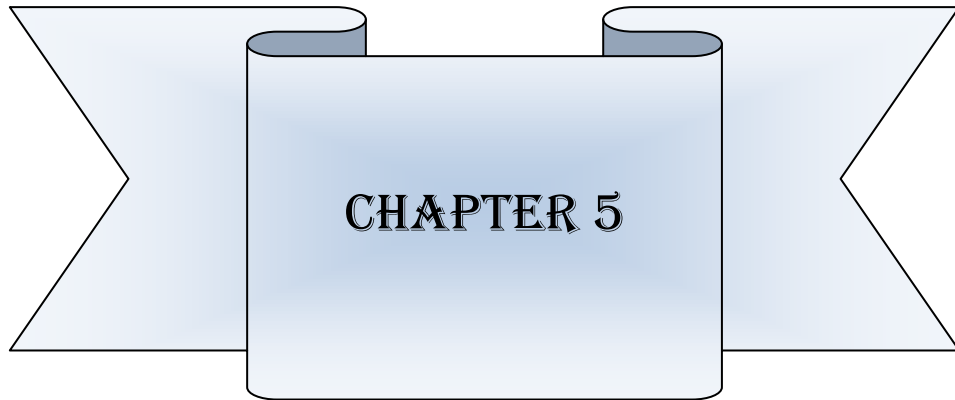
$$Bi(NO_3)_3.5H_2O + CH_3COOH + H_3BO_3 + H_2O \longrightarrow Bi_{1-x}B_xO + NO_2\uparrow + CH_4\uparrow + Steam\uparrow$$

Figure 4.4: Experimental set up of Spray Pyrolysis unit at the Department of Physics, BUET

References

[1]   Choudhury, C., Sehgal H. K., "Properties of spray deposited cobalt oxide selective coating on aluminum and galvanized iron substrate", Appl. Energy, 10, 313-324, 1982.

[2]   Kadam, L. D., Patil P. S., "Thickness dependent properties of sprayed cobalt oxide thin films" Mat. Chem. Phys., 68, 225-232, 2001.

[3]   Islam, M. R., Podder j., "Optical properties of ZnO nanofiber thin films grown by spray pyrolysis of zinc acetate precursor, Cryst. Res. Technol., 44(3), 286- 292, 2009.

[4]   Affreen, S., Balamurugan D., Jeyaprakash B.G., "Thickness dependent physical property of spray deposited $ZnFe_2O_4$ thin film" J. Appl. Sci., 12: 1636-1640, 2012.

[5]   Chamberlin, R.R., Skarman J. S., "Chemical spray deposition process for inorganic films", J. Electrochem. Soc., 113(1), 86-89, 1996.

[6]   Altiokka, B., Akasy S., "Optical properties of CulnS2 films produced by spray pyrolysis method," J. Phys., 36(3B), 1042-1045, 2006.

[7]   Riveros R., Romero E., Gordillo G., "Synthesis and characterization of highly transparent and conductive SnO_2:F and In_2O_3:Sn thin films deposited by spray pyrolysis," Braz. J. Phys., 36(3B), 1042-1045, 2006.

[8]   Elangovan, E., Rsmamurthi K., "Studies on optical properties of polycrystalline SnO_2:Sb thin films prepared using $SnCl_2$ precursor," Cryst. Res. Technol. 38(9), 779-784, 2003.

[9]   Anuar, K., Ho S. M., Tan W. T., Atan M. S., Kuang D., Jelas H. M., Saravanan N., "Effects of solution concentration on the properties of Cu_4SnS_4 thin films," Mater. Sci., 14(2), 101-105, 2008.

[10]   Yadav, S. C., Uplane M. D., "Synthesis and properties of boron doped ZnO thin films by spray CVD technique at low substrate temperature," Int. J. Engr. Sci. Technol., 4(12), 4893-4898, 2012.

CHAPTER 5

RESULTS & DISCUSSION

CHAPTER 5

RESULTS AND DISCUSSION

5.1 Introduction

The synthesized Boron doped Bismuth oxide thin films by spray pyrolysis method have been characterized structurally, optically and electrically by employing various experimental tools. In this chapter the results and possible explanations and discussion of the various experimental studies namely surface morphology, structural, optical and electrical properties of as deposited Boron doped Bismuth oxide thin films are presented and discussed in details.

5.2 Surface Morphology

The surface morphology of Bi_2O_3 thin film and Boron (B) doped Bi_2O_3 thin films deposited at the substrate temperature T_S of 350 ^{0}C is shown in Figures 5.1 and 5.2. FESEM images are taken at X 30k and X 50k magnifications. The FESEM micrographs reveal that sprayed particles are covered the whole substrate uniformly. From the FESEM micrographs it is clear that the deposited thin films have low porosity. Nano particles are observed in both Bi_2O_3 and Bi_2O_3: B thin films. Figure 5.1 shows that the uniform nature grains covered the entire surface of the film and well-defined grain boundaries are observed. The films are crack free with nano-sized particles agglomerate the doped films exhibit that the grain sizes are increasing with increasing of B concentrations. Since the radius of B^{3+} (0.023 nm) is much smaller than that of Bi^{3+} (0.117 nm), it is difficult for B^{3+} to replace the Bi^{3+} site. Thus it is estimated that most boron ions are doped in the interstitial of Bi_2O_3 matrix. Boron ions may enter the interstitial site of Bi_2O_3 and leads to the swell of the grain size see Figure. 5.2(d). Further increase of the B may cause a decrease in crystallite size and transition to the amorphous glassy structure see Fig 5.2(e) which is consistent with literature [1].
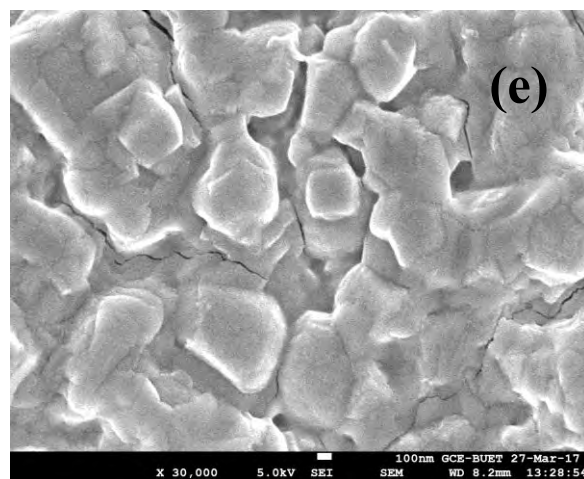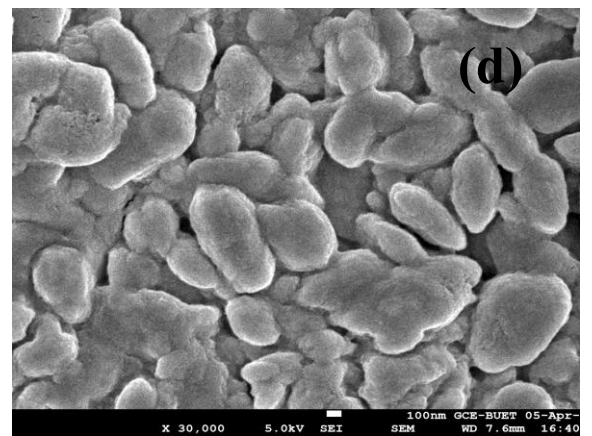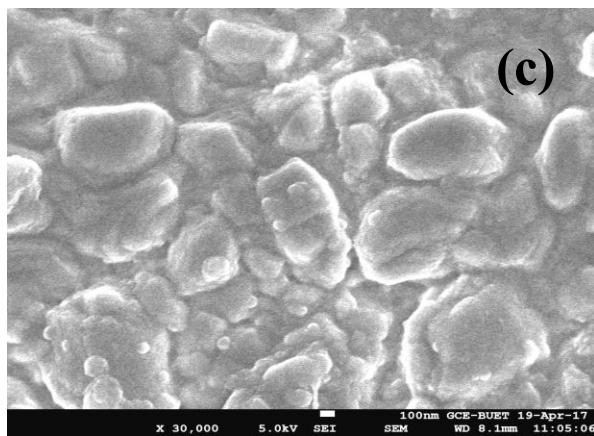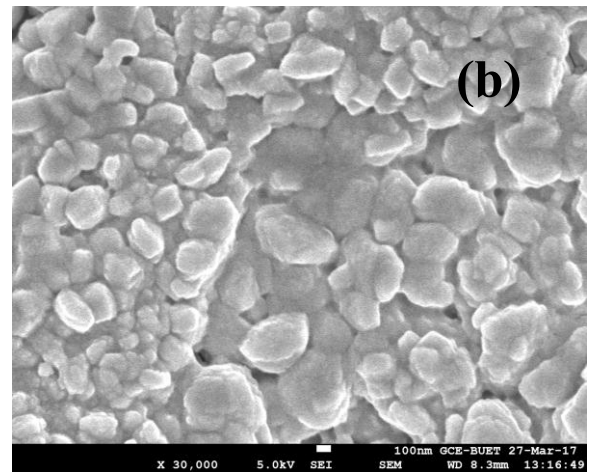
Figure 5.1: SEM images of B doped Bi_2O_3 thin films at $\times 30K$ magnifications, a) Pure Bi_2O_3, b) 1.0 at.% B doped Bi_2O_3 ,c) 3.0 at.% B doped Bi_2O_3, d) 5.0 at.% B doped Bi_2O_3, e) 7.0 at.% B doped Bi_2O_3.
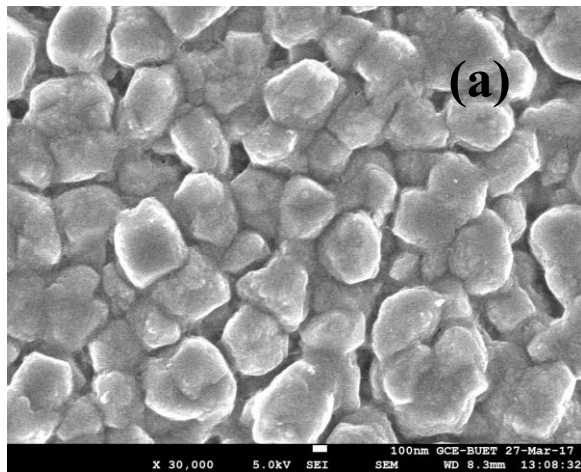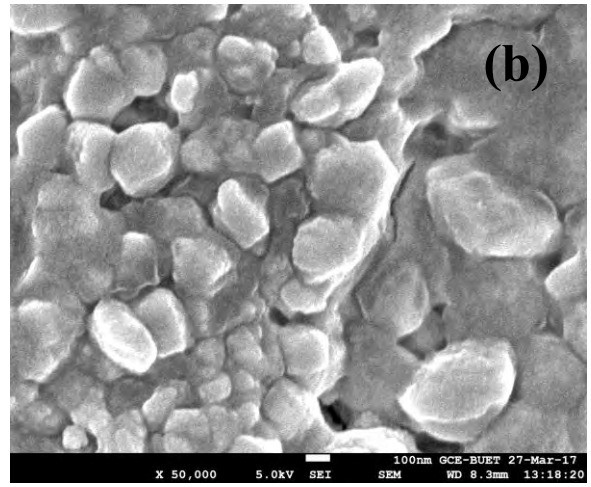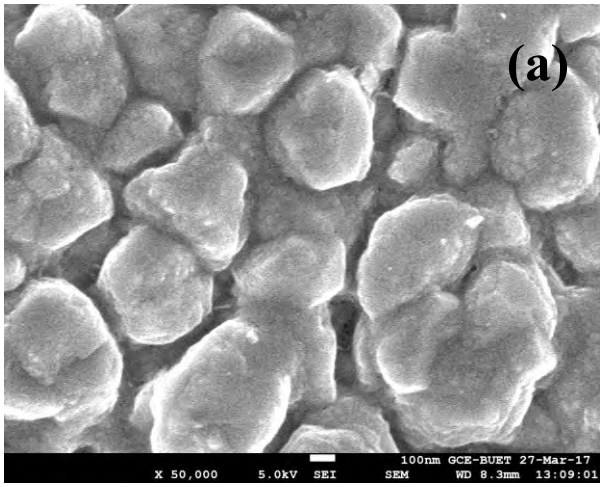
Figure 5.2: SEM images of B doped Bi_2O_3 thin films at ×50K magnifications, a) Pure Bi_2O_3, b) 1.0 at.% B doped Bi_2O_3 c) 3.0 at.% B doped Bi_2O_3, d) 5.0 at.% B doped Bi_2O_3, e) 7.0 at.% B doped Bi_2O_3.
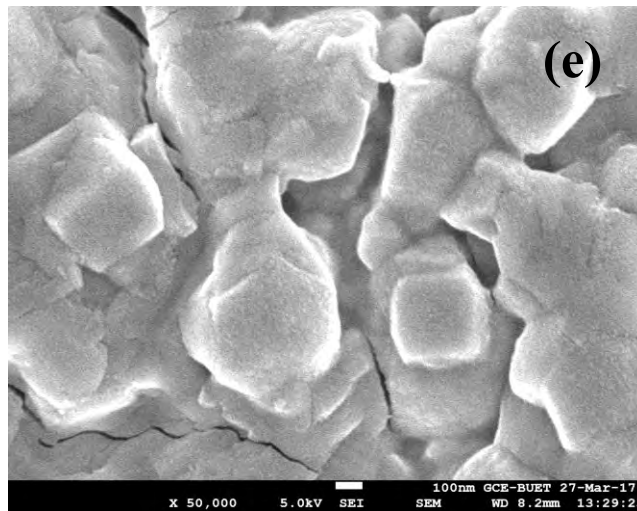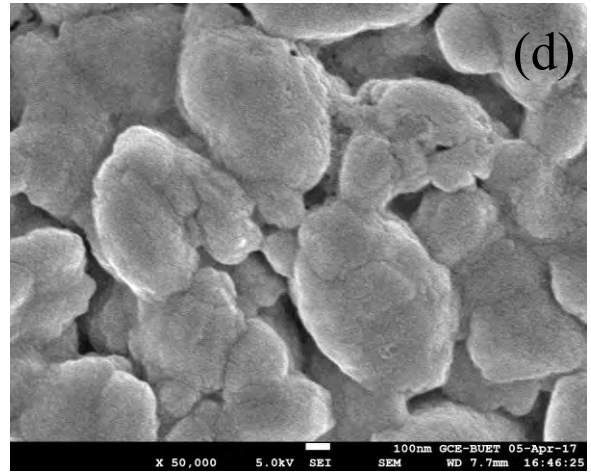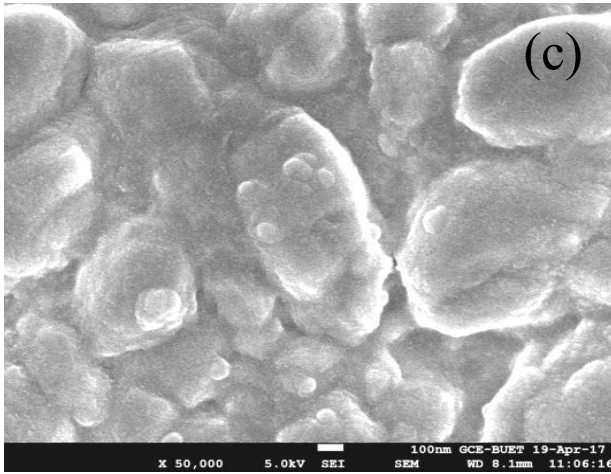
5.3 Elemental Analysis

The elements in Bi_2O_3 and Bi_2O_3: B thin films are confirmed by EDX analysis and are shown in Figure 5.3. Two strong peaks corresponding to Bi and O are found in the EDX spectrum that confirms the purity of Bi_2O_3 thin films. There are small peaks found for doped samples. Data of elemental analysis for prepared thin films are reported in table 5.1. From this table it is seen that the deposited thin films are highly stoichiometric. The atomic percentage of Bi is decreased with B concentration up to 5.0 at.% and then it is increased for 7.0 at.%. The EDX report reveals that the highest value of B atomic percentage is 22.65 for 7.0 at.% B concentration. The prominent presence of O is observed in the synthesized films which play a major role in changing the structure and properties of these thin films.

Figure 5.3: EDAX images of Bi_2O_3 thin films

Figure 5.4: EDAX images of B doped Bi_2O_3 thin films: a) Pure Bi_2O_3, b) 1.0 at.% B doped Bi_2O_3, c) 3.0 at.% doped Bi_2O_3, d) 5.0 at.% doped Bi_2O_3, e) 7.0 at.% doped Bi_2O_3.
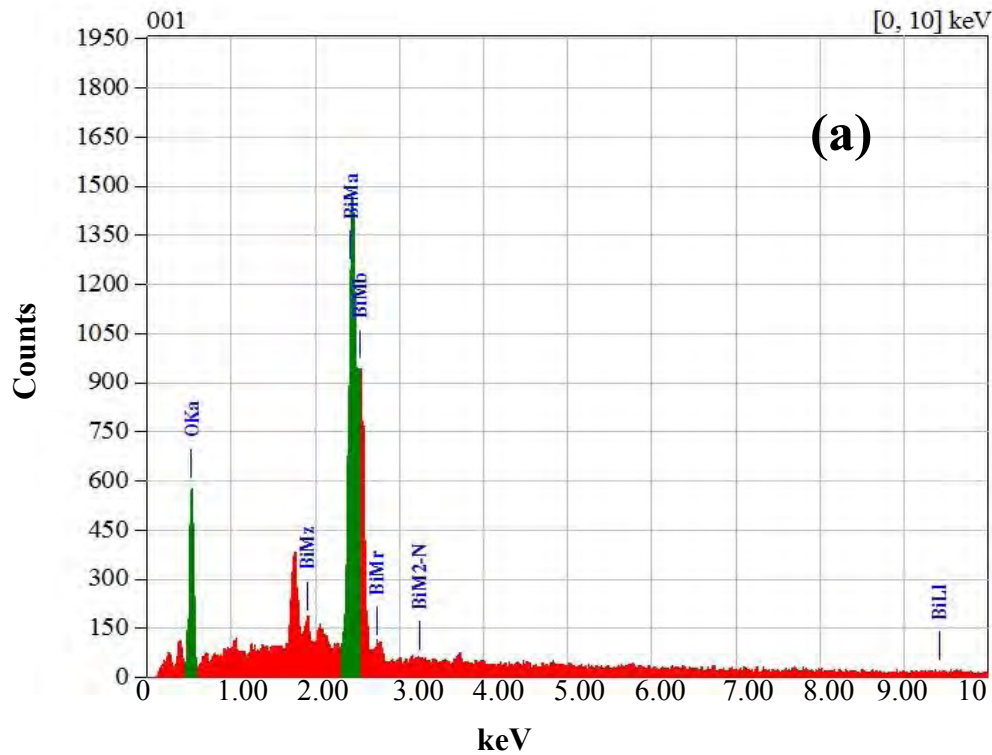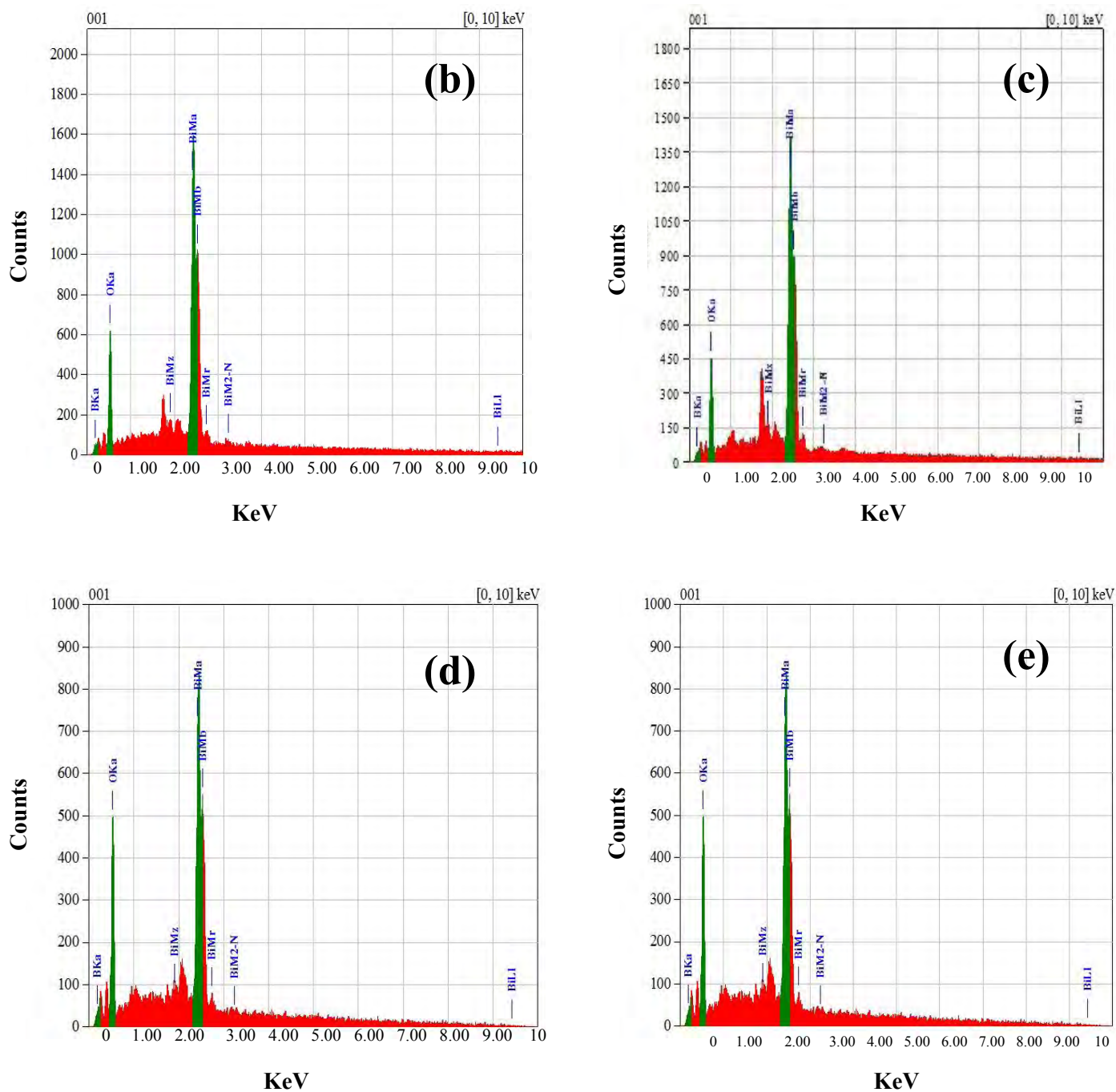
Table 5.1: Data of elemental analysis for different compositions of B doped Bi_2O_3 thin films

Sample	Atomic percentage of elements		
	Bi	O	B
Bi_2O_3	72.21	27.79	-----
1 at.% Bi_2O_3:B	57.85	35.86	6.29
3 at.% Bi_2O_3:B	35.62	55.18	9.20
5 at.% Bi_2O_3:B	42.47	40.83	16.70
7 at.% Bi_2O_3:B	50.66	26.68	22.65

5.4 X-ray Diffraction Analysis

The XRD pattern of Bi_2O_3 thin films deposited at the $T_s = 350$ ^{0}C is shown in Figure 5.4. The XRD patterns of Bi_2O_3: B thin films with B concentration of 1.0, 3.0, 5.0 and 7.0 at.% deposited at the T_s of 350 ^{0}C are shown in Figure 5.4. In XRD spectra the characteristic peaks are identified from the JCPDS card no. 27-1773, 27-0049 for Bi_2O_3. The fundamental peaks are identified as (111), (120), (121), (200), and (321), etc., planes for Bi_2O_3 and Bi_2O_3:B thin films which indicates the monoclinic structure of Bi_2O_3. From the XRD patterns it is confirmed that the deposited films are mixed phases. Leontie et al. [2] also reported the formation of mixed phases. The phases are monoclinic, tetragonal and non-stoichiometric ($Bi_2O_{2.33}$) phases of Bi_2O_3. The air as carrier gas, the deficiency of oxygen atoms may lead to the formation of $Bi_2O_{2.33}$ phase in the film. The nonstiochiometric phase can be removed by heat treatment [3]. Here the peak intensities are slightly increases with doping concentration.

From the XRD peak we can depict that the deposited films are more crystalline nature. The structural parameters like crystallite size (D), microstrain (ε), dislocation density (δ) and crystallite per unit area of (108) planes are calculated using equations (3.3), (3.4), (3.5) and (3.6), respectively. From the planes the crystallite size is about 22.72 nm for pure and after doping concentration the crystallite size is decreased at 3.0 at.% and then increases with further increasing doping concentrations. The dislocation density is decreased with doping concentration.
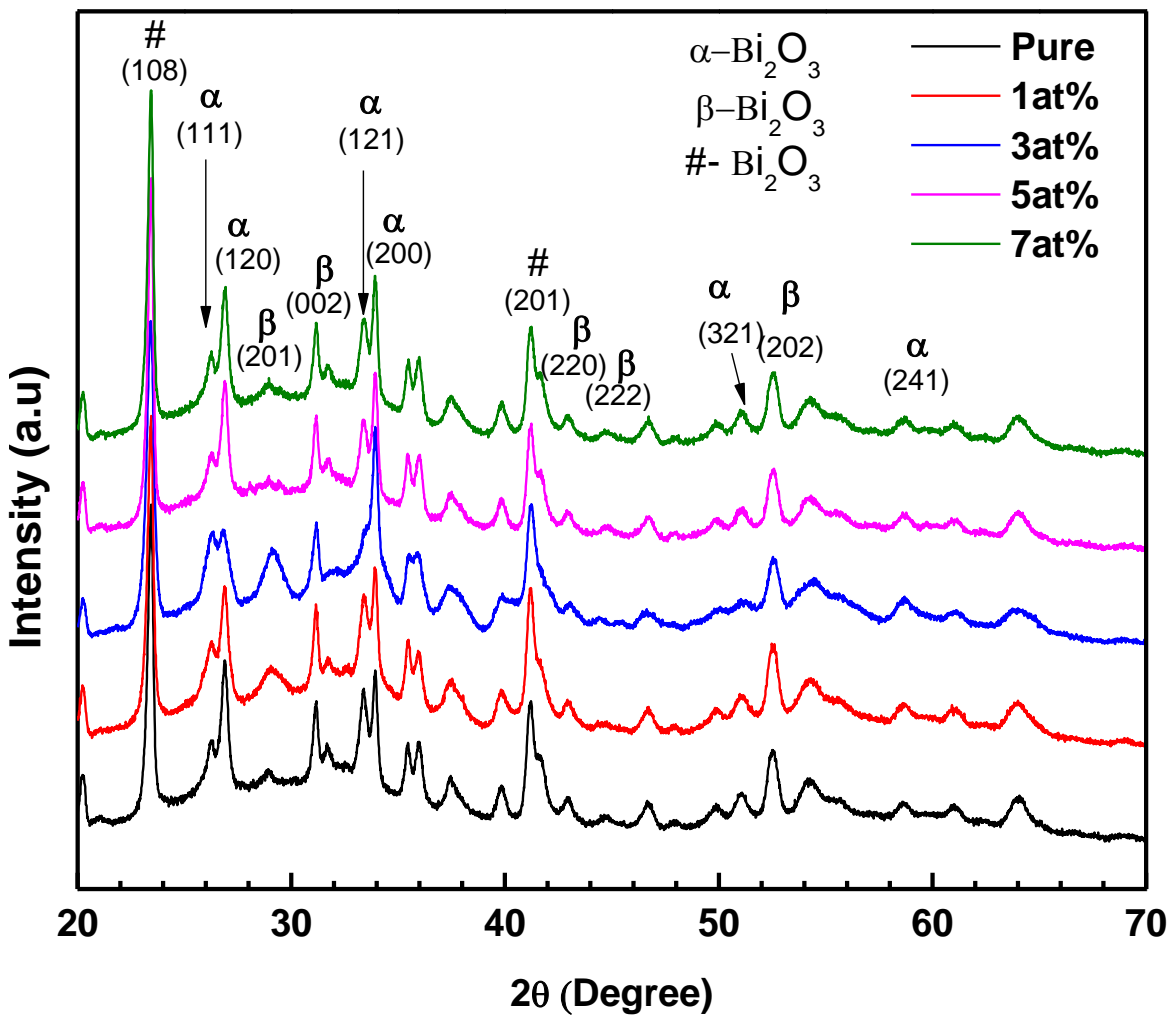

Figure 5.5: X-ray diffraction patterns of Bi_2O_3 thin films and B doped Bi_2O_3 thin films.

The dislocation density noticed that the presence of defects in the deposited films. More dislocation density indicates more defects. Here the dislocation density increases at 3.0 at.% and then decreasing with doping concentration. It implies that crystallization process improved and smaller crystallites agglomerated with increasing doping concentration. It is observed that the maximum value of D is about 28.40 nm and minimum values of ε and δ are about 77.41×10^{-3} and 1.23×10^{-3} line/nm^2 for 5 and 7.0 at.% of B concentration. Larger D indicates the less dislocation per unit area and minimum strain inside the crystallite. Decrease of ε and δ with B concentration indicates less deformation of the crystallites at higher B concentration [4]

Table 5.2: Structural parameters of Pure and B doped Bi_2O_3 thin films for (108) plane

Boron concentration (at%)	FWHM	Crystallite size, D (nm)	Dislocation density (δ) Line/nm^2	Microstain (ε)	Crystallite per unit area N (nm^{-2})
0	0.352	22.72	1.93×10^{-3}	86.39×10^{-3}	25.57×10^{-3}
1	0.340	23.54	1.80×10^{-3}	83.36×10^{-3}	22.99×10^{-3}
3	0.390	20.55	2.36×10^{-3}	95.51×10^{-3}	34.56×10^{-3}
5	0.316	25.35	1.55×10^{-3}	77.41×10^{-3}	18.41×10^{-3}
7	0.282	28.40	1.23×10^{-3}	69.12×10^{-3}	13.09×10^{-3}

5.5 Optical Properties

5.5.1 Transmittance

Figure 5.5 shows the transmittance (T %) of Bi_2O_3 thin films synthesized at T_s of 350 ^{0}C. The Figure 5.5 reveals that the transmittance of pure Bi_2O_3 is 39%. Gopinath et. al [5] found similar nature of transmittance. Here the transmittance for doping is varying with thickness. The transmittance of 1.0 at.% B doped is about 22% and the thickness is about 300 nm. Similarly for 3.0 at.%, 5.0 at.% and 7.0 at.% of boron the transmittance are 39%, 55% and 45% respectively.
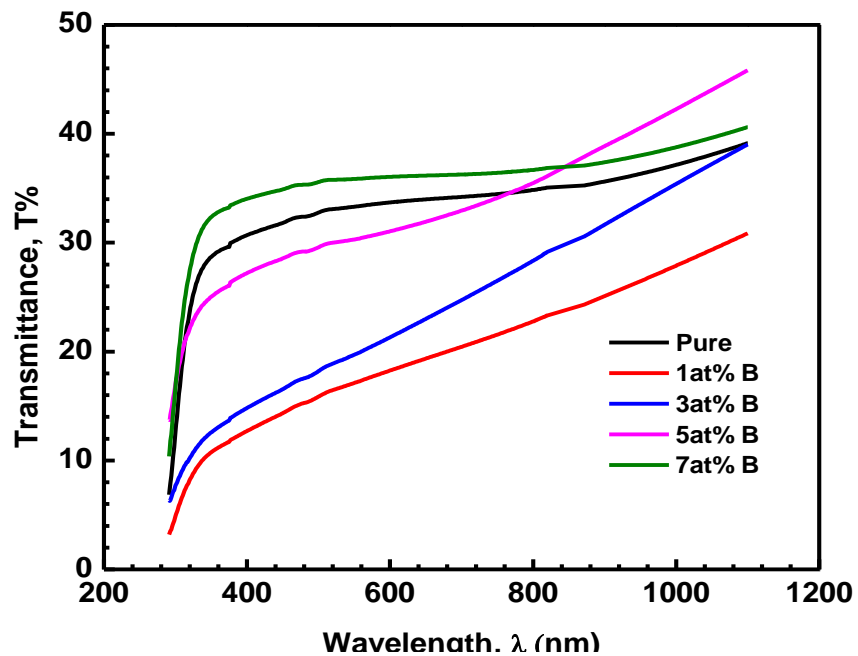
Figure 5.6: Transmittance vs. wavelength graph of Bi_2O_3 and Bi_2O_3: B thin films

5.5.2 Absorbance

Figure 5.6 shows the absorbance (A) for the pure Bi_2O_3 and B doped Bi_2O_3 thin films. The value of absorbance (A) is highest for the 1.0 at.% B doped Bi_2O_3 thin films in the wavelength range of 300-1100 nm as shown in Figure 5.6. The absorption starts at wavelength ~ 350nm. From the Figure 5.6, it is clear that A decreases for both types of films with the increase in wavelength. This decrease in the absorption indicates that the presence of optical band gap in the materials [6].
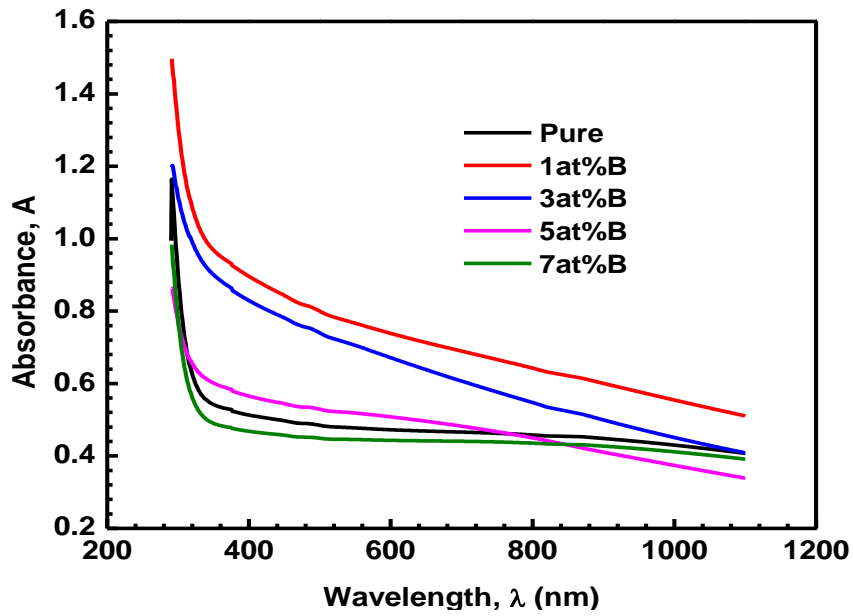
Figure 5.7: Absorbance vs. wavelength graph of Bi_2O_3 and Bi_2O_3: B thin films.

5.5.3 Absorption Coefficient

The absorption coefficient (α) was calculated from the transmission spectra using the

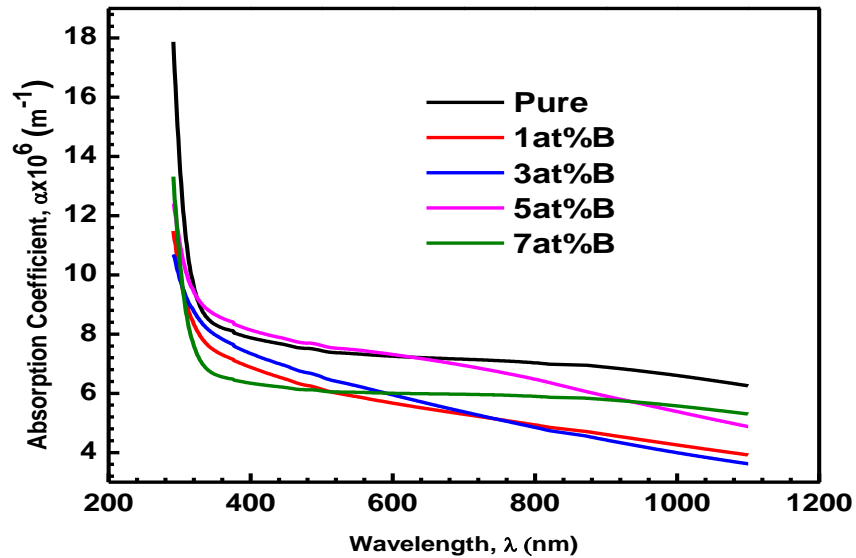relation, $\qquad \alpha = \dfrac{\ln(\frac{1}{T})}{t}$. Here t is the thickness of the deposited thin films.

Figure 5.8: Variation of absorption coefficient with wavelength for Bi_2O_3 and Bi_2O_3:B thin films deposited at T_s=350 ^0C

Variation of α with photon energy for different atomic concentration is shown in Figure. 5.7 for as deposited and B doped Bi_2O_3 films. From the figure it can be seen that the absorption coefficient first increases slowly in the low energy region i.e., in the high wavelength region and then increases sharply near the absorption edge. The absorption coefficients depend on the doping concentrations of the film. From the figure it is seen that the value of α is high for pure Bi_2O_3 thin film and α is minimum at lower energy region and increases with increasing photon energy.

5.5.4 Determination of Optical Band Gap

The optical transmittance spectra of the deposited film with respect to plain glass substrate were taken using double beam UV spectrophotometer in the wavelength range 200 to 1100 nm. From transmittance spectra, the absorption coefficient and optical band gap were calculated for different doping concentrations. The optical transmission data were analyzed using the classical relation for near edge of the optical absorption using the relation (for α $>10^4$ cm^{-1})

$$(\alpha h \nu) = A \left(h \nu - E_g \right)^n$$

Where A is a constant in the optical frequency range and E_g is the optical band gap, and n is an index related to the density of states for the energy band. This n is determined by the nature of the optical transition involved in the absorption process. Analyses of the data have been made using both n = 1/2. The energy gap in a semiconductor is responsible for the fundamental optical absorption edge [7-8]. A plot of $(\alpha h \nu)^2$ vs. hν for (direct transition) films of different doping concentrations B doped Bi_2O_3 thin films are shown in Figure.5.8. The direct band gap energy of the B doped Bi_2O_3 thin films have been obtained from intercept on the energy axis after extrapolation of the straight line section of $(\alpha h \nu)^2$ vs. hν curve. The optical band gap was determined in similar fashion as we did for direct transition. From the Figure it is seen that the band gap is decreasing from 3.99 to 3.70 eV with increasing lower concentration of B (upto 3.0 at%) and after that the band gap is further increasing under higher B concentrations.
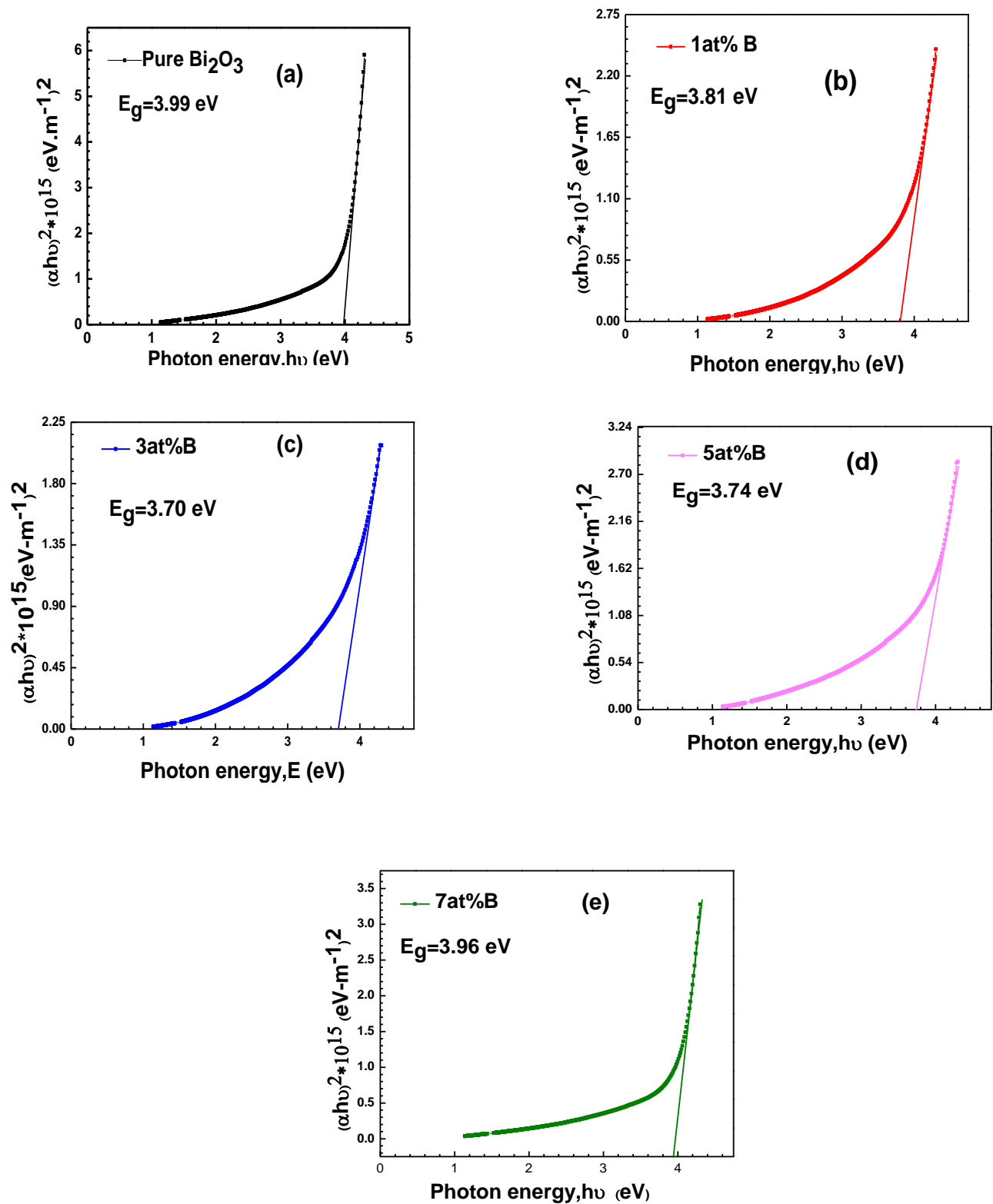
Figure 5.9: Plots of $(\alpha h\upsilon)^2$ vs. $h\upsilon$ of Bi_2O_3 and Bi_2O_3:B thin films deposited at T_s=350 ^{0}C . a) Pure Bi_2O_3, b) 1.0 at.% B, c) 3.o at.% B, d) 5.0 at.% B, e) 7.0 at.% B doped Bi_2O_3.

Increase of band gap (E_g) may be attributed the Burstein-Moss shift [9], i.e. due to increase in carrier concentration, the absorption edge shifts to higher energy level. Optical band gap obtained for direct transitions for film of different doping concentrations are given in the table 5.3.

Table 5.3: Variation of band gap with doping

Doping concentration (at. %)	Direct band gap energy E_g in eV
x = 0.00	3.99
x = 1.0	3.78
x = 3.0	3.70
x = 5.0	3.75
x = 7.0	3.96

5.5.5 Refractive Index

The refractive index or index of refraction n of a material is a dimensionless number that describes how light propagates through that medium. The refractive index (n) has been calculated using the equation

$$n = \left(\frac{1+R}{1-R}\right) + \sqrt{\left(\frac{4R}{(1-R)^2} - k^2\right)}$$

Where k is the extinction coefficient and R is the optical reflectance [10]. The variation of n with wavelength for Bi_2O_3 and Bi_2O_3: B thin films are shown in figure 5.9. The refractive is increased with wavelength. From the figure it is seen that the value of n is increasing with doping concentration and highest value of n is found 2.52 for 7.0 at.% B doping. Low

refractive index is found for 1.0 at.% B doping. Lower value of n reveals that light moves faster through the films.
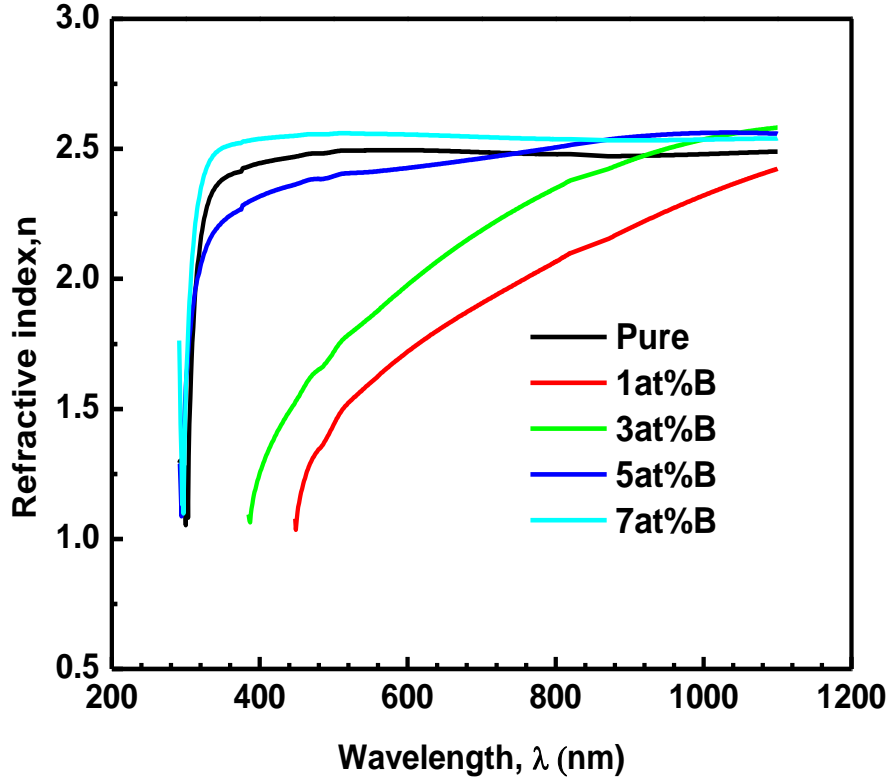

Figure 5.10: Variation of refractive index with wavelength for Bi_2O_3 and Bi_2O_3: B thin films

5.5.6 Extinction Coefficient

The extinction coefficient (also called molar absorptivity) is parameters defining how strongly a substance absorbs light at a given wavelength per mass density or per molar concentration respectively. The extinction coefficient (k) has been calculated using the equation

$$k = \frac{\alpha\lambda}{4\pi}$$

Where, α is the absorption coefficient and λ is the wavelength. The extinction coefficient is the imaginary part of the complex index of refraction, which also relates to light absorption [11-12]. The variation of k with wavelength for deposited thin films is shown in Figure 5.10.

It shows that k is increasing with increasing wavelength. The high value of k indicates the high surface roughness of the deposited samples. The rise and fall in k is directly related to the absorption of light. Since the extinction coefficient describes the attenuation of light in a medium and increase of k with wavelength indicates the probability of raising the electron transfers across the mobility gap with wavelength. Higher values of k represent the greater attenuation of light in a thin film and also the higher probability of raising the electron transfer across the mobility gap with the wavelength.
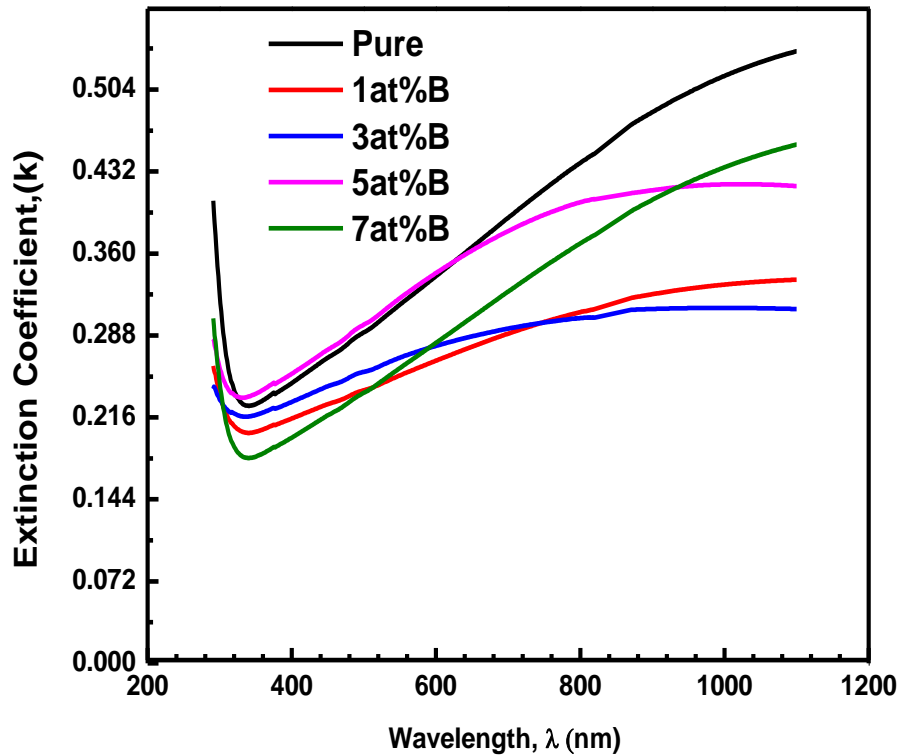

Figure 5.11: Variation of extinction coefficient with wavelength for Bi_2O_3 and Bi_2O_3: B

5.5.7 Optical conductivity

Optical conductivity refers that when on falling the light on the material surface, it shows conduction or transport of photons through a material. The optical conductivity (σ_{opt}) has been calculated using the equation

$$\sigma_{Opt} = \frac{\alpha \, n \, c}{4\pi}$$

Where, c is the velocity of light [13]. Figure 5.11 exhibits the variation of σ_{opt} with wavelength for the deposited thin films. It is increased at high wavelength due to the high absorbance in that region. This is may be due to the increase of band gap [14]. It is a frequency dependent quantity which is related to the E_g values.
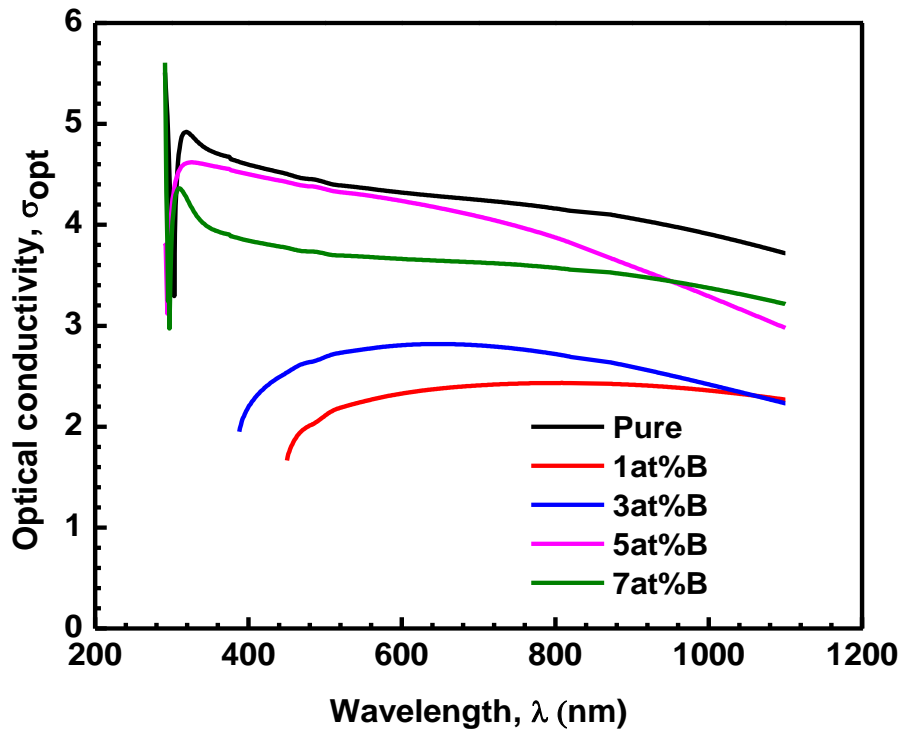
Figure 5.12: Variation of Optical conductivity with wavelength for Bi_2O_3 and Bi_2O_3: B thin films deposited at T_s=350 ^{0}C

5.5.8 Dielectric Constants

The dielectric constant is a fundamental intrinsic material property. The real ε_r and imaginary ε_I parts of the dielectric constant are determined using the relation [15]

$$\varepsilon_r = n^2 - k^2 \quad \text{and} \quad \varepsilon_I = 2nk$$

The variation of the real and imaginary parts of the dielectric constants for Bi_2O_3: B thin films are illustrated in Figure 5.12 and 5.13, respectively. ε_r represents the magnitude of polarization of a material i.e. it is associated with the property of slowing down the speed of light in the material. The variation of ε_r depends upon the frequency of the incoming light. ε_r shows the maximum value of about 6.4 at 400 nm wavelength for 7.0 at.% Bi_2O_3: B deposited $T_s=350\ ^oC$. ε_i shows the same behavior as that of the ε_r, the only difference is that their values seem to be very less as compared to that of ε_r values. The both part of the dielectric constant increase with increasing the wavelength value. The maximum imaginary part of the dielectric constant is 2.55 for pure Bi_2O_3 thin films.
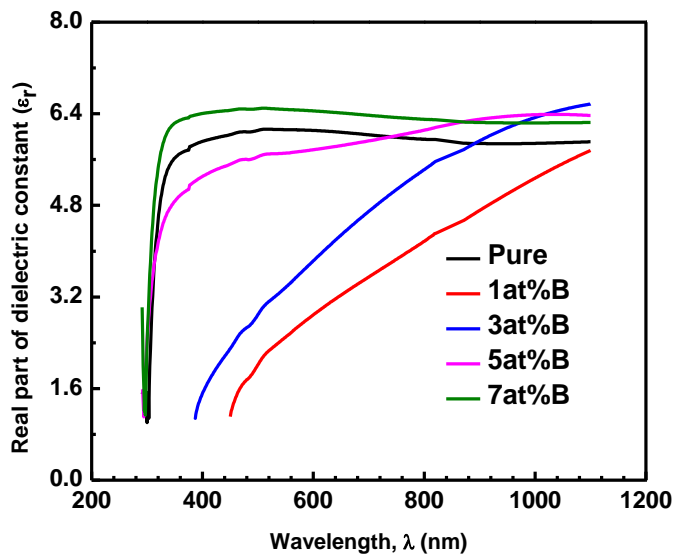

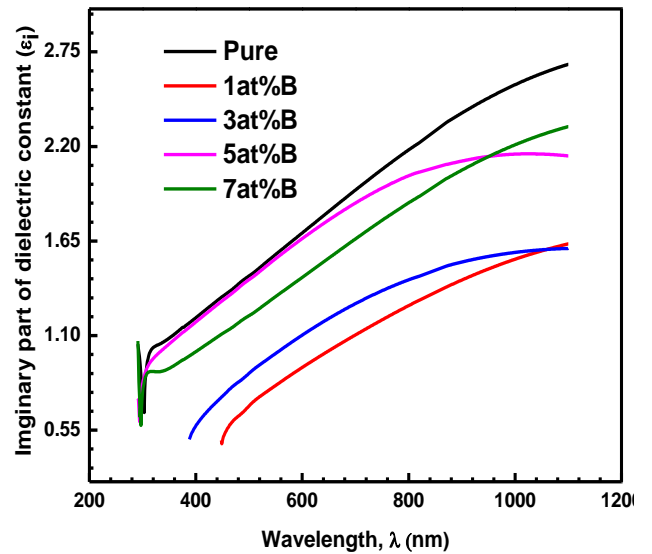Figure 5.13: Variation of real part of dielectric constant with wavelength for Bi_2O_3 and Bi_2O_3: B thin films.

Figure 5.14: Variation of imaginary part of dielectric constant with wavelength for Bi_2O_3 and Bi_2O_3: B thin films.

5.5.9 Dielectric Loss

Dielectric loss is a loss of energy that goes into heating a dielectric material in a varying electric field. The dielectric loss tangent (tanδ) has been calculated using the relation

$$\tan\delta = \frac{\varepsilon_i}{\varepsilon_r}$$

Where ε_r and ε_i are the real and imaginary parts of the dielectric constant [16].The variation of tanδ of Bi_2O_3: B thin films are plotted against wavelength in Figure 5.14. The tanδ for Bi_2O_3: B is decreased for 1.0 and 3.0 at% but for 5.0 and 7.0 at% increasing with the increase of B doping concentration. From tanδ vs. wavelength curves it is also observed that the values of tanδ are gradually increases with the increase of wavelength. Increase of tanδ indicates little loss of photon energy in the medium and vice versa.

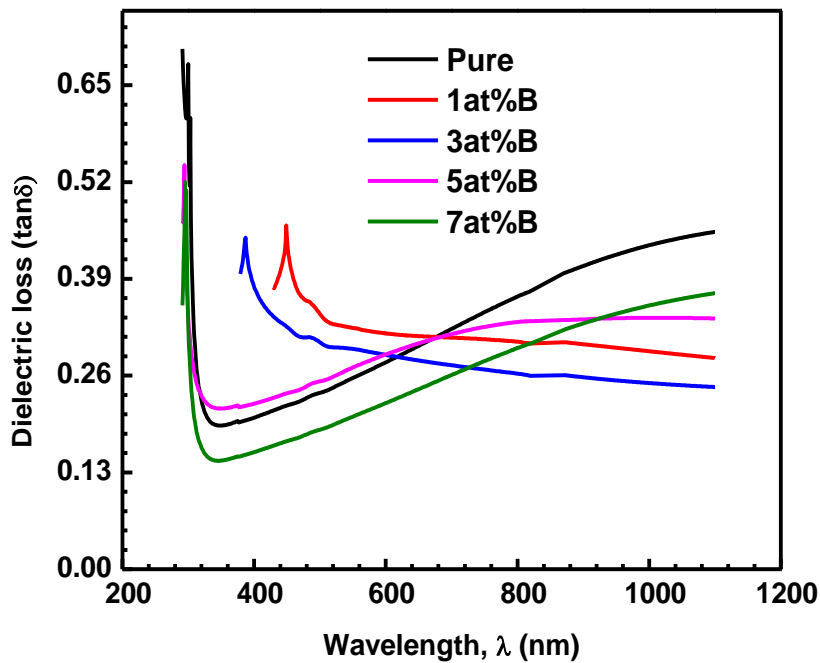Figure 5.15: Variation of dielectric loss with wavelength for Bi_2O_3 and Bi_2O_3: B thin films.

5.6 Electrical Properties

5.6.1 I-V Characteristics

Electrical resistivity of Bi_2O_3 and Bi_2O_3: B thin films are measured by in-line four point probe method. I-V characteristic curves of the Bi_2O_3: B thin films are shown in the Figure 5.16. The data for I-V characteristics are taken for the supply voltages in the range 0 - 20 V and the corresponding current and voltage drops are measured. I-V graphs are almost linear in nature and the conduction process is ohmic. The resistivities of the thin films are calculated using the I-V graphs. Resistivity is increasing with B doping. Resistivity is found between 1.24×10^3 Ω-m and 1.81×10^3 Ω-m.
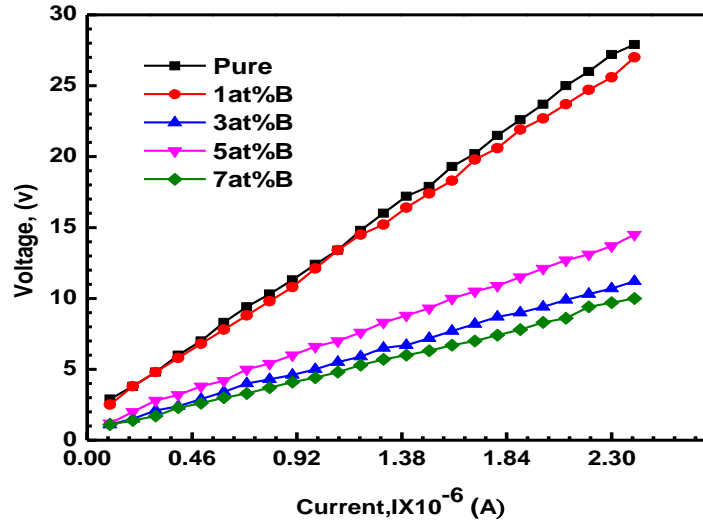
Figure 5.16: Plots of I-V characteristics of pure and boron
doped bismuth oxide thin films

5.6.2 Variation of Resistivity and Conductivity with Temperature

The resistivity (ρ) of undoped and B doped Bi_2O_3 thin films are measured by four point probe method [17] and data were taken by increasing the temperature slowly. The temperature dependence electrical resistivity calculated using equation (3.31). Figure 5.17 represents the variation of resistivity with temperature for undoped and B doped Bi_2O_3 thin films. It is observed that for pure Bi_2O_3 thin film the resistivity is decreased with increasing temperature that confirms the semiconducting nature of the samples. It is also seen that the

98

resistivity of the samples increases with increasing the doping concentration of B. The increase of resistivity with doping concentration may be due to decrease of carrier concentration with Boron doping. B is an acceptor and Bi is a donor, when B is added then it takes electron from Bi as a result resistivity is increases. The increase of resistivity with increase of B concentration may be due to decrease of donor electron by substitution of B at O lattice site forming solid solution. The resistivity of all the films is found to be in the order of 10^3 Ω-m.

The conductivity (σ) of all the deposited samples has been calculated from resistivity data. The plot of conductivity as a function of temperature for undoped and B doped Bi_2O_3 thin films are shown in Figure (5.18). From this figure it is clear that the conductivity is inversely related to the resistivity ($\sigma = 1/\rho$). The conductivity was found to decrease with increase of temperature and with increase of B concentration as well.
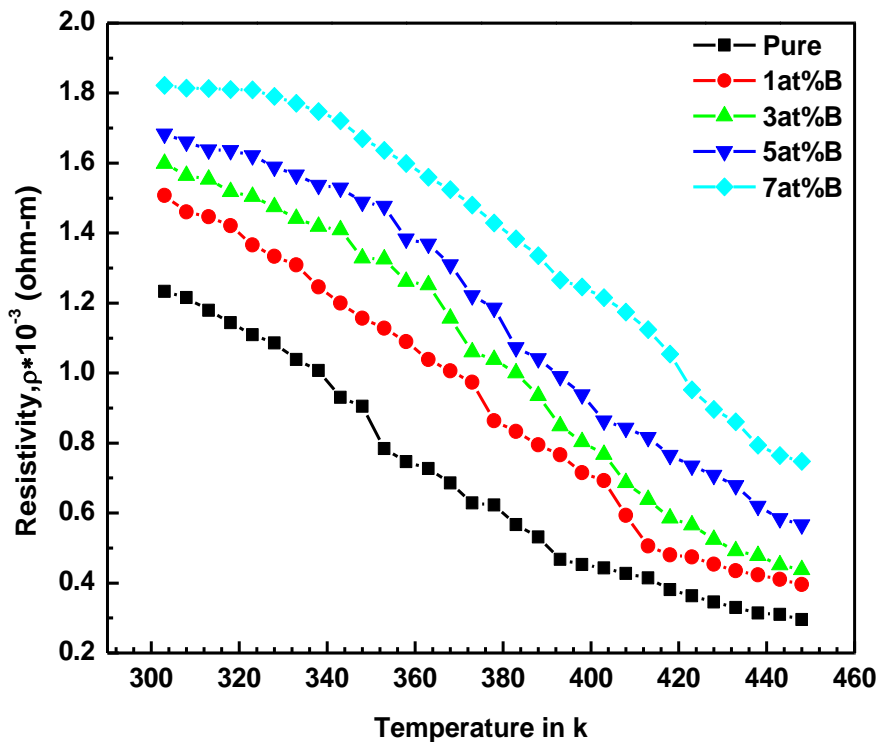
Figure5.17: Variation of resistivity with temperature for undoped and B doped Bi_2O_3 thin films.
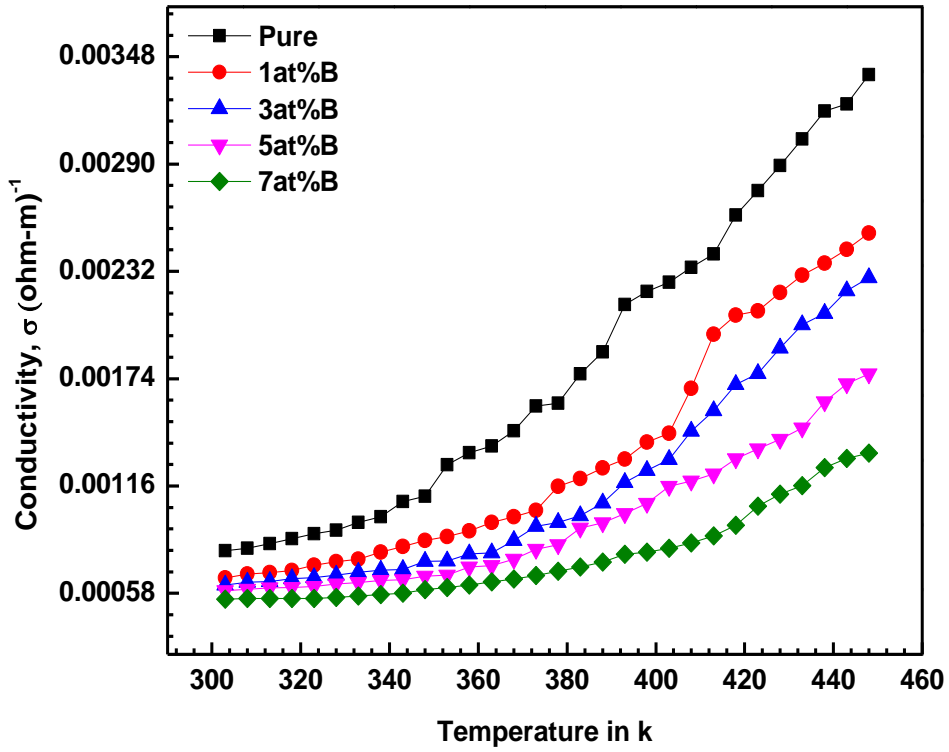
Figure 5.18: Variation of Conductivity with temperature for undoped and Bi_2O_3 thin films

5.6.3 Variation of Sheet Resistance with Temperature

Sheet resistance is a measure of resistance of thin films that are nominally uniform in thickness. Sheet resistance is applicable to two-dimensional systems in which thin films are considered two-dimensional entities. The sheet resistance can be calculated using the equation

$$R_S = \frac{\rho}{t}$$

Here ρ is the resistivity of the deposited thin films and t is the thickness. The sheet resistances of the deposited thin films are increases with increasing the B doping concentration. The sheet resistance of the deposited films is found of the order of 10^9 Ω/square.

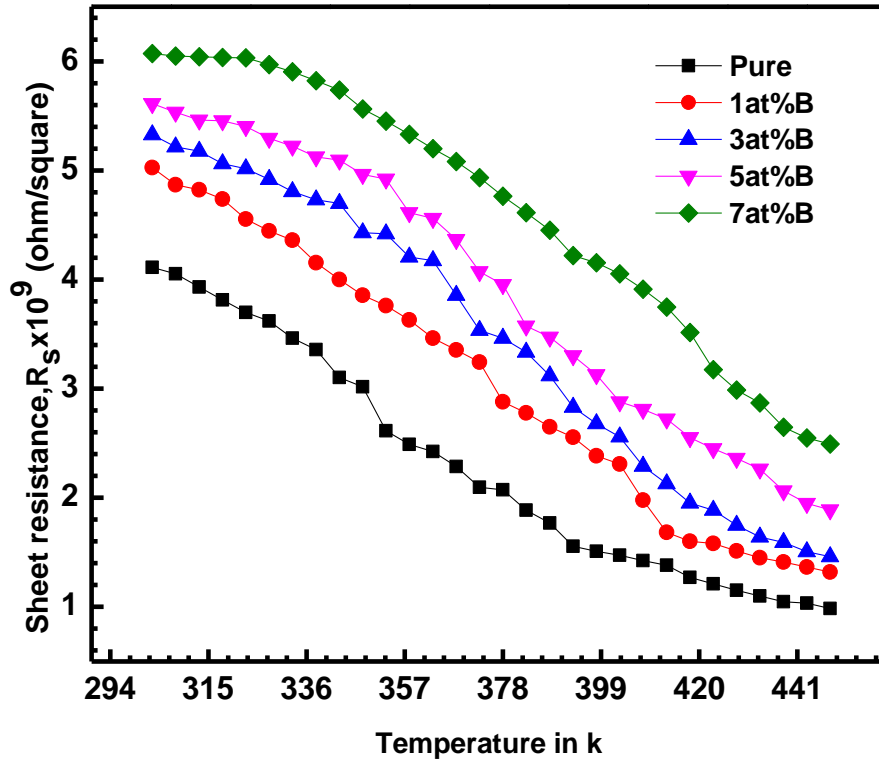Figure 5.19: Variation of sheet resistance with temperature for undoped and Bi_2O_3 thin films.

Table 5.4: Resistivity, Conductivity, and Sheet Resistance with B doping.

B Concentration in Bi$_2$O$_3$ (at %)	Resistivity, $\rho \times 10^3$ (Ω-m)	Conductivity, σ (Ω-m)$^{-1}$	Sheet Resistance, R$_S \times 10^9$(Ω/square)
0	1.23	0.00081	4.1
1	1.51	0.00066	5.02
3	1.60	0.00062	5.32
5	1.68	0.00059	5.61
7	1.82	0.00054	6.04

5.6.4 Activation Energy:

The activation energy ΔE can be calculated using the relation

$$\sigma = \sigma_o \exp\left(-\frac{\Delta E}{2k_B T}\right)$$

Where σ_0 is constant and σ is the electrical conductivity, k$_B$ is the Boltzmann constant and T is the absolute temperature [18].

For the calculation of activation energy the logarithmic variation of electrical conductivity with 1000/T was taken for undoped and B doped Bi$_2$O$_3$ thin films as illustrated in Figure (5.20). In this graph, if we look very carefully, we will find two regions with different slopes of the straight line separated at temperature 373 K as marked by vertical line in the graph. Therefore, the activation energies of 303 K to 370 K (ΔE_1) and 378 K to 448 K (ΔE_2).The ΔE_1 and ΔE_2 values are tabulated in Table (5.4). The activation energy (ΔE_1) in low temperature region varies from (0.1655 to 0.0447) eV and in the high temperature region the (ΔE_2) varies (0.2923 to 0.2466) eV, though these variations are inconsistent with doping concentration of B. In the lower temperature region, as the temperature is increased, the electrons are excited thermally from donor levels to conduction band. Thus more charge

carriers overcome the activation energy barrier causing the electrical conduction. In the higher temperature region, the trapped charge carriers induce the electrical conduction at the grain boundaries with donor electron. Figure (5.21) shows the variation of activation energy with B concentration as well as two temperatures region. It is also observed that the ΔE_2 activation energy is slightly greater than that of ΔE_1.
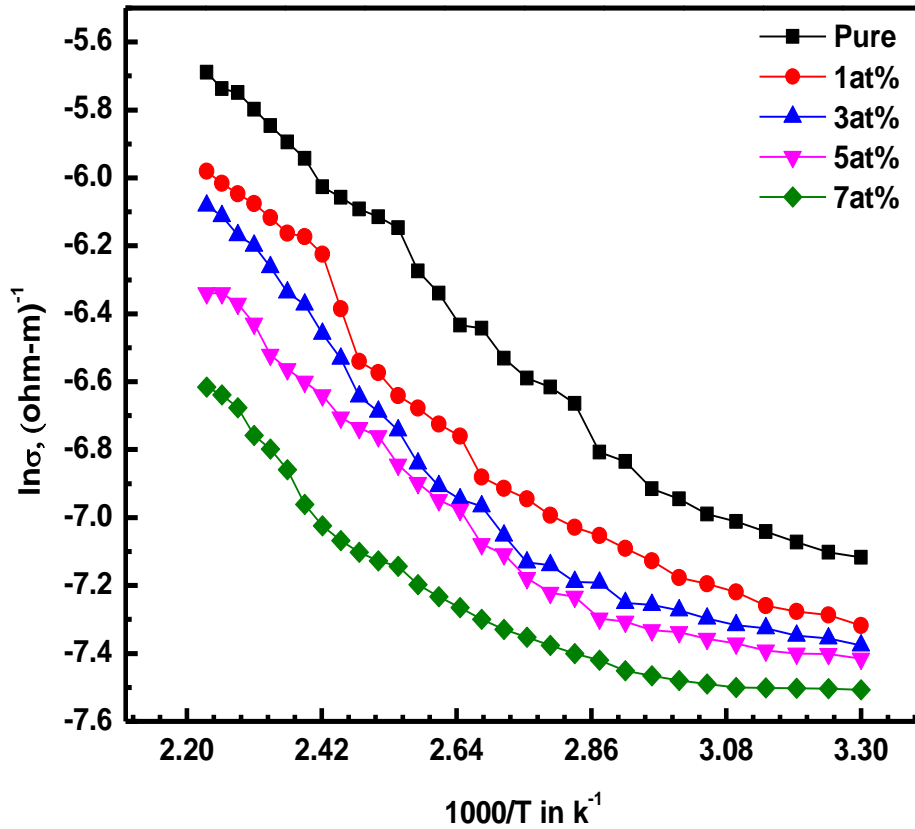
Figure 5.20: Variation of $\ln\sigma$ with 1000/T of pure and B doped Bi_2O_3 thin films.

Figure 5.21: Variation of activation energy of Bi_2O_3 thin films with different B concentration.
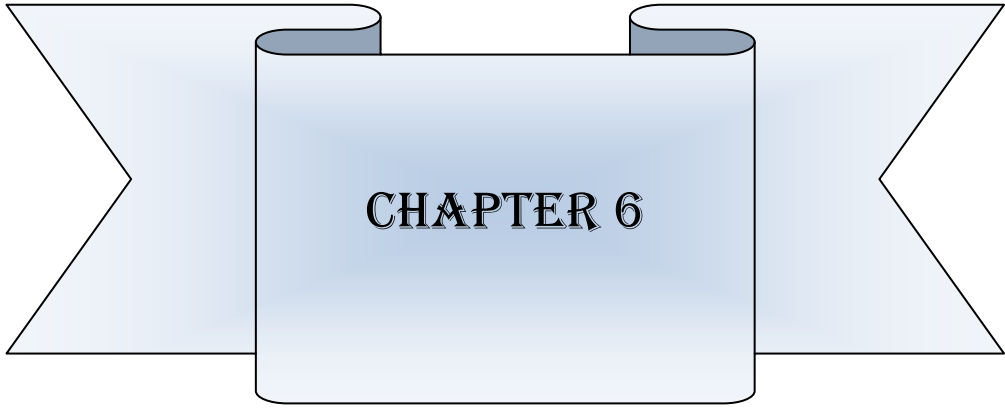
Table 5.5: Activation energy of undoped and B doped Bi_2O_3

B concentration in Bi_2O_3 (at %)	Activation Energy ΔE in eV	
	ΔE_1 (303-370)K (eV)	ΔE_2 (378-448)K (eV)
0	0.165	0.292
1	0.108	0.337
3	0.081	0.347
5	0.064	0.281
7	0.044	0.246

References

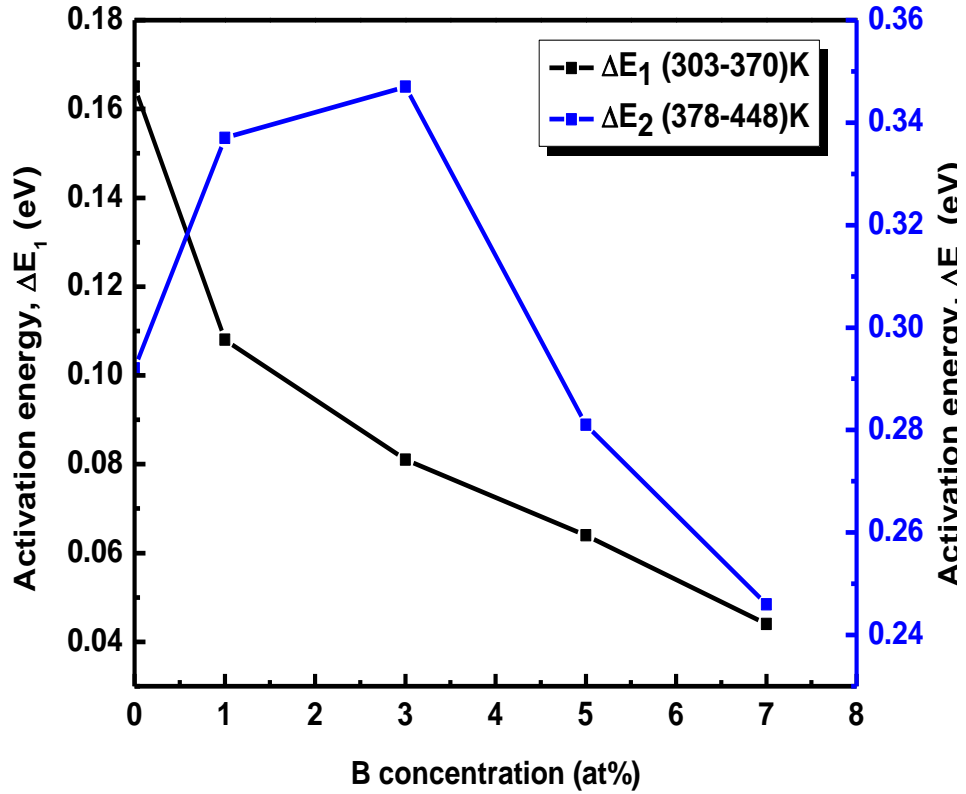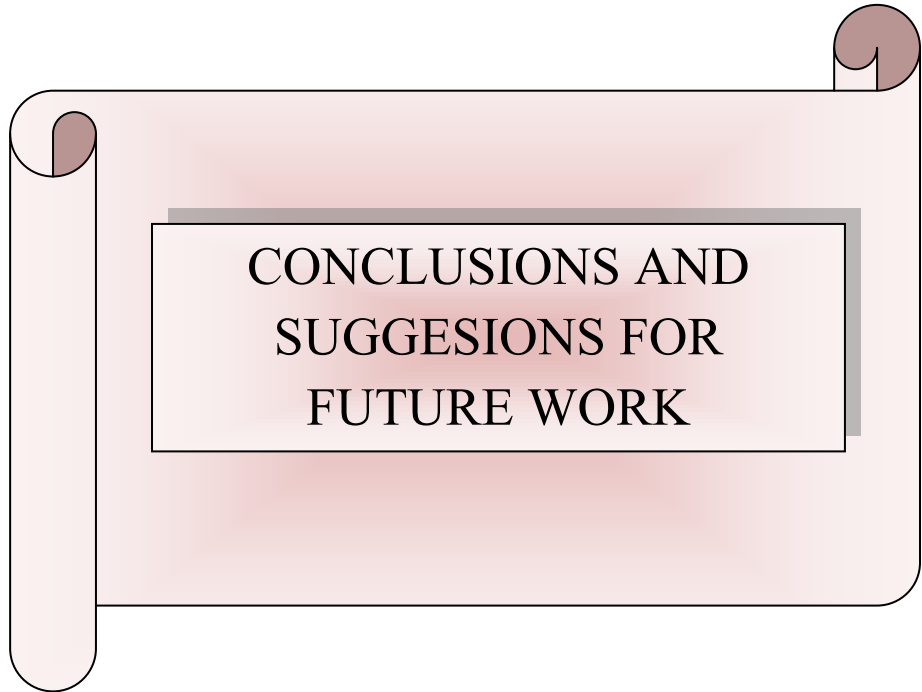[1]   Chen, D., Yang, D., Wang, Q., and Jiang, Z.,"Effects of Boron Doping on Photocatalytic Activity and Microstructure of Titanium Dioxide Nanoparticles", J. Ind. Eng. Chem. Res., Vol. 45, pp. 4110-4116, 2006.

[2]   Leontie, L., Caraman, M., Alexe, M., Harnagea, C.,"Structural and optical characteristics of bismuth oxide thin films", J. Surf. Scie., Vol. 507-510, issue 1-3, pp. 480-485, 2002.

[3]   Gujar, T. P., Shinde, V. R., Lokhande, C. D., "Spray pyrolysed bismuth oxide thin films and their characterization", J. Mater. Resea. Bulle., Vol. 41, pp. 1558–1564, 2006.

[4]   Jabbar, R. H., Elttayef, A. K., Jabor, A. A., and Hashim, A. H.,"Structural properties of boron doped zinc oxide films prepared by spray pyrolysis technique", Physics B., Vol. 302-303, pp.222-227, 2013.

[5]   Gopinath, P., Sriram, S., and Chandiramouli, R., "Influence of Zn doping on nanostructured Bi_2O_3 thin films". J. Inter. Chem. Tech. Resear., Vol. 5, pp. 2534-2539, 2013.

[6]   Rejit, S. G., and Krishnan, C., "Optical characterizations of Zn-doped CuO nanoparticles", Sciencia Acta Xaveriana, Vol. 4(1), pp. 91-98, 2013.

[7]   Park, Y., Rhee, S., "Low temperature silicon dioxide film deposition by remote plasma enhanced chemical vapor deposition: growth mechanism", J. Surf. Coat. Tech., Vol. 179, pp. 229-236, 2004.

[8]   Badera, N., Godbole, B., Srivastava, S. B., Vishwakarma, P. N., Sharath, C., Jain, D., Gangrade, M., Shripathi, T., Sathe, V. G., Ganesan, V., "Quenching of Photoconductivity in Fe doped CdS Thin films prepared by spray pyrolysis technique", J. Appl. Surf. Sci., Vol. 254, Issue 21, pp. 7042–7048, 2008.

[9]   Yousaf, S. A., and Ali, S., "The effect of fluorine doping on optoelectronic properties of tin-oxide ($F:SnO_2$) thin films", CODEN JNSMAC, Vol. 48(1&2), pp. 43-50, 2008.

[10]   Meth, J. S., Zane, S. G., Nunes, J. G., "Dual insulated-gate field-effect transistors with cadmium sulfide active layer and a laminated polymer dielectric", J. Appl. Phys. Lett., Vol. 84, No. 15, pp. 2922-2924, 2004.

[11]   Peter, C. R., Susan, B. B., "Deposition of cadmium sulfide films by decomposition of thiourea in basic solutions", J. Chem. Mater., Vol. 5(1), pp. 43-55, 1993.

[12]   Nandakumar, P., Vijayana, C., and Murti, Y. V. G., "Optical absorption and photoluminescense studies on CdS quantam dots in Nafion", J. Appl. Phys., Vol. 91, N0 3, pp. 1509-1514, 2002.

[13] Castillo, S. J., Mendoza, G. A., Ramlrez-Bon, R., Espinoza-Beltran, F. J., Sotelo-Lerma, M., Gonzale, H. J., Martinez, G., Martinez, G., "Structural, optical and electrical characterization of In:CdS glass thermally anneled system", Thin Solid Films, Vol. 373, pp. 10-14, 2000.

[14] Toshihiko, T., Hiroyuki, O., Kengo, M., and Hiroki, O., "Doping effects of dimethyl-tin-dichloride on material properties of CdS fims and on formation of CdS/CdTe heterostructures" , J. Appl. Phys., Vol. 98, pp. 013535-4, 2005.

[15] Jae-Hyeong, L., Woo-Chang, S., Jun-Sin, Y., Kea-Joon, Y., Wun-Dong, H., and Joon, H., "Growth and properties of the $Cd_{1-x}Zn_xS$ thin films by spray pyrolysis technique", Thin Solid Films, Vol. 431-432, pp. 349-353, 2003.

[16] Panta, J. P., Subedi, D. P., "Electrical characterization of aluminum (al) thin films measured by using four- point probe method", J. Sci. Eng. Tech., Vol. 8, No.2, pp. 31-36, 2012.

[17]   Varghese, S., and Iype, M., "Effect of Annealing on the Activation Energy of Thin Films of Manganese Sulphide, Copper Phthalocyanine and Multilayer Manganese Sulphide-Copper Phthalocyanine from their Electrical Studies", J. Chem., Vol. 27, No. (1), pp. 265-269, 2011.

[18] Hasnat, A., and Podder, j., "Optical and electrical characteristics of pure Cds thin films for different thickness" J. Bangladesh. Acad. Sci., Vol. 37, No. 1, pp. 33-41, 2013

CHAPTER 6

CONCLUSIONS AND
SUGGESIONS FOR
FUTURE WORK

CHAPTER 6

CONCLUSIONS AND SUGGESTIONS FOR FUTURE WORK

6.1 Conclusions

In this research work, Bi_2O_3 and Bi_2O_3:B thin films are deposited on glass substrate at substrate temperature $T_s = 350 \,^oC$ by spray pyrolysis technique. The concentration of B is varied from 1.0 at.% to 7.0 at.%. Thickness of the films is measured in the range of 150 to 300 nm. The effects of doping concentration on structural, optical and electrical properties of Bi_2O_3 and Bi_2O_3: B thin films are investigated. The results of the present work are summarized and the following noteworthy conclusions are drawn.

From FESEM micrographs multigonal or semi-circular particles are observed for both Bi_2O_3 and Bi_2O_3: B thin films. These show that the particles uniformly covered scanned area. Well –defined grain boundaries are observed. The FESEM micrographs show that the grain size is increasing with doping concentration. The EDX analysis reports that the all synthesized films are highly stoichiometric.

From the XRD patterns it showed that the films are polycrystalline nature. XRD patterns confirm that the films are mixed phases with monoclinic, tetragonal and non-stoichiometric. It is also observed that the intensity of peaks gradually increasing with doping concentration except 3.0 at.% of B concentration. The crystallite size is decreasing up to 3.0 at.% doping concentration and then increasing again. Minimum value of crystallite size is found to be about 20.55 nm and maximum value of crystallite size is found to be about 28.40 nm.

Form the UV-visible spectroscopy measurements it is seen that all the films synthesized at $Ts = 350 \,^oC$ are transparent in the near infra red region. The direct band gap is high as 3.99 eV for pure Bi_2O_3 and the band gap decreases with B concentration up to 3 at.% and after that it again increases. The refractive index n is increasing with doping concentration. The value of the extinction coefficient (k) for doping material is given lower value compare to the pure bismuth oxide thin films. The optical conductivity values of the deposited thin films shows that the optical conductivity is increased with increasing wavelength.

From the electrical data it is showed that the lowest resistivity is found for pure material. The resistivity for pure Bi_2O_3 is about 1.24×10^3 ohm-m. It is also observed that the resistivity is increasing with increasing doping concentration. It is also observed that the activation energy is decreasing with doping concentration in the high temperature regions.

In this study, the results obtained from surface, structural, optical and electrical characteristics of Bi_2O_3 are found to be in good agreement with the previous reported data by other researchers. Bi_2O_3 electrolyte is considered as one of the potential source materials for fuel cell fabrication. The essential characteristics of the precursor oxide based electrolyte materials for fuel cell should have high oxide ion conductivity, less porosity, low electrical conductivity, good mechanical strength, thermal shock resistance, phase stability, impermeable to gas etc. In this study, the role of B in Bi_2O_3 is found to provide the films with low porosity and low electrical conductivity. Boron can also reduce the processing temperature because of its low melting point. As a result the stable phase of Bi_2O_3 may be obtained at low temperature Bi_2O_3:B may be considered as a potential candidate for fuel cell application.

Finally, it can be concluded that the boron doped as deposited Bi_2O_3 films could be useful in fuel cell, gas sensors, solar cell, and optoelectronics devices.

6.2 Suggestions for Future Work

This is the first time that Bi_2O_3: B thin films have been prepared in our laboratory. We have deposited Bi_2O_3: B thin films on glass substrate at 350 °C substrate temperature and studied some of their structural, electrical and optical properties. More investigations are needed to explain different characteristics elaborately, which will help to reveal the suitable applications of Bi_2O_3 thin films, such as:

1. Measurements of Hall effect and temperature dependence of Hall mobility and carrier concentration
2. To measure the thermoelectric power.
3. To study the variation of the structural, optical and electrical properties of the Bi_2O_3: B thin films with annealing temperatures.
4. Study of the surface roughness by Atomic Force Microscopy.
5. To study the Bi_2O_3: B thin films at high temperature for thermal stability.